Republic of Iraq
Ministry of Higher Education
and Scientific Research
University of Diyala
College of Science

Effect of Aqueous Solution Molarity on Structural and Optical Properties of Nickel- Cobalt Oxide Thin Films Prepared by Chemical Spray Pyrolysis Method

A thesis

Submitted to the Council of the College of Science
University of Diyala in Partial fulfillment of
Requirements for the degree of M.Sc. in physics

By

Ahmed Mohammed Shano Al-Askari

(B.Sc. in Physics 2012)

Supervisor

Prof. Nabeel Ali Bakr , (Ph.D.)

2014 A.D 1436 A.H


بِسْمِ اللَّهِ الرَّحْمنِ الرَّحِيمِ
اللَّهُ نُورُ السَّمَاوَاتِ وَالأَرْضِ مَثَلُ نُورِهِ
كَمِشْكَاةٍ فِيهَا مِصْبَاحٌ الْمِصْبَاحُ فِي زُجَاجَةٍ
الزُّجَاجَةُ كَأَنَّهَا كَوْكَبٌ دُرِّيٌّ يُوقَدُ مِنْ شَجَرَةٍ
مُبَارَكَةٍ زَيْتُونَةٍ لا شَرْقِيَّةٍ وَلا غَرْبِيَّةٍ يَكَادُ
زَيْتُهَا يُضِيءُ وَلَوْ لَمْ تَمْسَسْهُ نَارٌ نُورٌ عَلَى
نُورٍ يَهْدِي اللَّهُ لِنُورِهِ مَنْ يَشَاءُ وَيَضْرِبُ
اللَّهُ الأَمْثَالَ لِلنَّاسِ وَاللَّهُ بِكُلِّ شَيْءٍ عَلِيمٌ
سورة النور
الأية (٣٥)

SUPERVISOR CERTIFICATION

I certify that this thesis is prepared by ***Ahmed Mohammed Shano*** under my supervision at the Department of Physics, College of Science, University of Diyala in partial fulfillment of requirements needed to award the degree of **Master of Science in Physics.**

Signature:
Name : Dr. ***Nabeel A. Bakr***
Title : Professor
(Supervisor)
Date : /10 / 2014

Head of the Department of Physics

In view of available recommendation, I forward this thesis for debate by the examining committee.

Signature:
Name : ***Dr. Ziad T. Khodair***
Title : Lecturer
Date : / 10 / 2014

Examination Committee Certificate

We certify that we have read this thesis entitled " **Effect of Aqueous Solution Molarity on Structural and Optical Properties of Nickel- Cobalt Oxide Thin Films Prepared By Chemical Spray Pyrolysis Method** " and, as an examining committee, we examined the student (Ahmed Mohammed Shano) on its content and in what is related to it, and that in our opinion it meets the standard of a thesis for the degree of Master of Science in Physics with an ( ) grade.

Signature
Name: **prof Dr. Sabah A. Salman**
Title: Professor
Address: University of Diyala
Data: / 1 / 2015
Chairman

Signature
Name: **Dr. Ali A. Yousif**
Title: Assistant Professor
Address: Al-Mustansiriyah University
Data: / 1 / 2015
Member

Signature
Name: **Dr. Hussein Kh. Rasheed**
Title: Assistant Professor
Address: University of Baghdad
Data: / 1 / 2015
Member

Signature
Name: **prof Dr. Nabeel A. Bakr**
Title: Professor
Address: University of Diyala
Data: / 1 / 2015
Supervisor

Approved by the Council of the College of Science.

(The Dean)

Signature:
Name: **Dr. Tahseen H. Mubarak**
Title: Assistant Professor
Date: / 1 / 2015

ACKNOWLEDGEMENT

First of all I thank the Almighty Allah, whose Grace enabled me to continue this work and overcome all difficulties and our prophet Mohammed (peace and blessings of Allah be upon him) who invites us to science and knowledge.

I would like to express my sincere gratitude to my supervisor ***Prof. Dr. Nabeel Ali Bakr*** who granted me the opportunity to do this research. I am indebted to him for his guidance, suggestions, valuable remarks and unfailing patience throughout my research work.

I would like to express my profound gratitude to ***Prof. Dr. Sabah Anwer Salman*** for his kind cooperation and constant support. I am highly indebted to ***Dr. Ziad Tariq Khodair*** for his constant encouragement throughout my M.Sc. study in the Department of Physics, College of Science, University of Diyala.

Special thanks are extended to the ***University of Diyala, College of Science*** and all the ***Staff of the Department of Physics*** for their assistance.

I would also like to thank the ***staff of the Library of College of Scienc***e, who continued to provide excellent service, tireless support and scientific resources to all students.

My greatest indebtedness goes to my ***Father*** and ***Mother*** for their valuable advice, and to my ***Friends*** for their endless support.

Dedication

To .....

The lights of my life

Father & Mother

The lights of my eyes

Brother, Sisters and My Friends

All faithful hearts who helped me
in the journey of my life.

Ahmed

Published and Accepted Research Articles

1- Nabeel A. Bakr, Sabah A. Salman and Ahmed M. Shano, "**Effect of Aqueous Solution Molarity on Structural and Optical Properties of Nickel Oxide Thin Films Prepared by Chemical Spray Pyrolysis Technique**", International Journal of Current Research, Vol. 6, Issue, 11, pp.9644-9652, November, (2014). ISSN: 0975-833X.

2- Nabeel A. Bakr, Sabah A. Salman and Ahmed M. Shano, "**Effect of Co Doping on Structural and Optical Properties of NiO Thin Films Prepared By Chemical Spray Pyrolysis Method",** International Letters of Chemistry, Physics and Astronomy, Vol. 2, pp. 15-30, (2015)**.** ISSN 2299-3843.

3- Nabeel A. Bakr, Ziad T. Khodair and Ahmed M. Shano**, "Effect of Aqueous Solution Molarity on Structural and Optical Properties of $Ni_{0.92}Co_{0.08}O$ Thin Films Prepared by Chemical Spray Pyrolysis Method",** International Journal of Thin Films Science and Technology, (communicated).

Abstract

In this study, Nickel-Cobalt Oxide ($Ni_{(1-x)}Co_xO$) thin films, where x = 0, 4, 6 and 8 % with different molarities (0.05, 0.1, 0.15 and 0.2 M) have been successfully deposited on glass substrates by chemical spray pyrolysis (CSP) technique at substrate temperature of (400 ±5^oC) and thickness of about 300 ±10 nm. The structural and optical properties of these films have been investigated using XRD, AFM, and UV-Visible spectroscopy. The XRD results showed that all films are polycrystalline in nature with cubic structure and preferred orientation along (111) plane. The crystallite size was calculated using Scherrer formula. The crystallite size of the samples was maximum (51.16nm) for the unopded NiO thin film prepared at molarity of 0.1M, and it was minimum (8.22nm) for the $Ni_{0.94}Co_{0.06}O$ thin film prepared at the same molarity, these results were qualitatively in agreement with the results of crystallite size obtained by Williamson-Hall method. The average grain size, average roughness and root mean square (RMS) roughness for Nickel-Cobalt Oxide were estimated from AFM. The absorbance and transmittance spectra have been recorded in the wavelength range of (300- 900) nm in order to study the optical properties. The transmittance for all thin films increases rapidly as the wavelength increases in the range (300- 350) nm, and then increases slowly at higher wavelengths.

The absorbance decreases rapidly at short wavelengths (high energies) corresponding to the energy gap of the film, (when the incident photon has an energy equal or more than the energy gap value). The absorption coefficient was estimated for all samples and due to its high values ($>10^4 cm^{-1}$), it was concluded that the thin films material has a direct band gap. The optical energy gap for allowed direct electronic transition was

calculated using Tauc equation. It was found that the band gap decreases when the molarity increases and the band gap values ranges between 3.71 eV and 3.54 eV. The Urbach energy increases as the molarity increases and the Urbach energy values range between 299 meV and 680 meV. The optical constants including (absorption coefficient, real and imaginary parts of dielectric constant) calculated as a function of photon energy, refractive index and extinction coefficient for all films were estimated as a function of wavelength.

Table of Contents

LIST OF FIGURES

List of Tables

List of Symbols

Symbol	Meaning	Unit
a_o	Lattice Constant	Å
FWHM	Full Width at Half Maximum	rad
D_{av}	The Crystallite Size	nm
d_{hkl}	Interplanner Spacing	Å
S	Micro Strain	%
N_0	Number of grains per unit area	cm^{-2}
T_C	Texture Coefficient	-
δ	Dislocation Density	cm^{-2}
I_o	Incident intensity	mW/cm^2
I_A	Absorbed light intensity	mW/cm^2
Eg	Energy Band gap	eV
E_u	Urbach energy	meV
E_d	Dispersion Energy	eV
E_v	Valence Band Energy	eV
E_c	Conduction Band Energy	eV
E_p	Assistant Phonon Energy	eV
λ	Wavelength of Incident Light	nm
λ_c	Cut off wavelength	nm
h	Planck's Constant	J.s
n	Refractive Index	-
n_o	Static Refractive Index	-
T	Transmittance	-
A	Absorbance	-

R	Reflectance	-
α	Absorption Coefficient	cm^{-1}
K_0	Extinction coefficient.	-
ε	Dielectric Constant	-
ε_1	Real Part of Dielectric Constant	-
ε_2	Imaginary Part of Dielectric Constant	-
θ	Diffraction Angle	Degree
t	Thickness	nm
hkl	Miller Indices	-
k_B	Boltzmann's Constant	J/k
$h\nu$	Photon Energy	eV
c	Speed of Light	m/s
A' and B	Constants Depending on Properties of Conduction and Valance Bands	-
ν	Frequency	s^{-1}
K_e	Wave Vector of Transmitted Electron	cm^{-1}
$\vec{K}_{ph}$	Photon Wave Vector	cm^{-1}
$\vec{K}$	Wave Vector	cm^{-1}
M	The Molar Concentration	mol/l
M_{wt}	Molecular Weight	g/mol
V	Volume of Distilled Water	ml
W_t	Weight of Material	g
A_s	Area of The Thin Film	cm^2
ρ_0	The Density of Material of The Thin Film	g/cm^3

List of Abbreviations

Symbol	Meaning
CSP	Chemical Spray Pyrolysis
AFM	Atomic Force Microscopic
UV	Ultra Violet
XRD	X- Ray Diffraction
RMS	Root Mean Square
W-H	Williamson-Hall
FAP	Fundamental Absorption Process
SRO	Short Range Order

Chapter One

Introduction

1.1. Introduction

The term "Thin Films" is used to describe a layer or several layers of atoms of a certain substance whose thickness ranges between (10 nm) and less than 1μm (1000 nm)[1]. Thin films technique is one of the most recent fully grown technologies that greatly contribute to develop the study of semiconductors and metals by giving a clear indication of their chemical and physical properties [1]. The properties of thin films are usually different from those of the bulk because of the two dimensions nature of thin films. In bulk “three dimensions” the particles are under the influence of forces at all directions, while in thin films the forces act upon the particles at the surface only [2]. Thin films are first made by (Busen & Grove) in 1852 by using (Chemical Reaction) and later in 1857; the scientist (Farady) had been able to obtain a thin metal film by means of (Thermal Evaporation) [3]. Spray pyrolysis was first used commercially more than half a century ago in 1947 as in U.S. patents registered for (H. A. McMaster and W. O. Lytle) to deposite conductive oxide films on heated glass substrate [4]. The film layer is deposited on certain plates chosen according to the nature of the study or the scientific need. Such plates could be glass slides, silicon wafers, aluminum, quartz and others [1]. There are already so many applications of thin films such as the electronic and optical applications**.** The applications of thin films in electronics have been grown steadily in importance during the last decades, because of their use in the electronic resistances, capacitances, transistors, integral circuits for digital computers and other electronic equipments [5]. Thin films are also particularly important for their use in great number of optical fields such as the manufacturing of ordinary and thermal mirrors, mirrors for high reflectance, semitransparent reflection coating which are used in optical devices such as filters in solar cells, and non absorbing materials which are used for interference phenomena [5].

1.2. Methods of Preparing Thin Films

The methods of preparing thin films can be divided essentially into two main groups, namely, physical and chemical methods [6]. These methods are shown in figure (1-1).

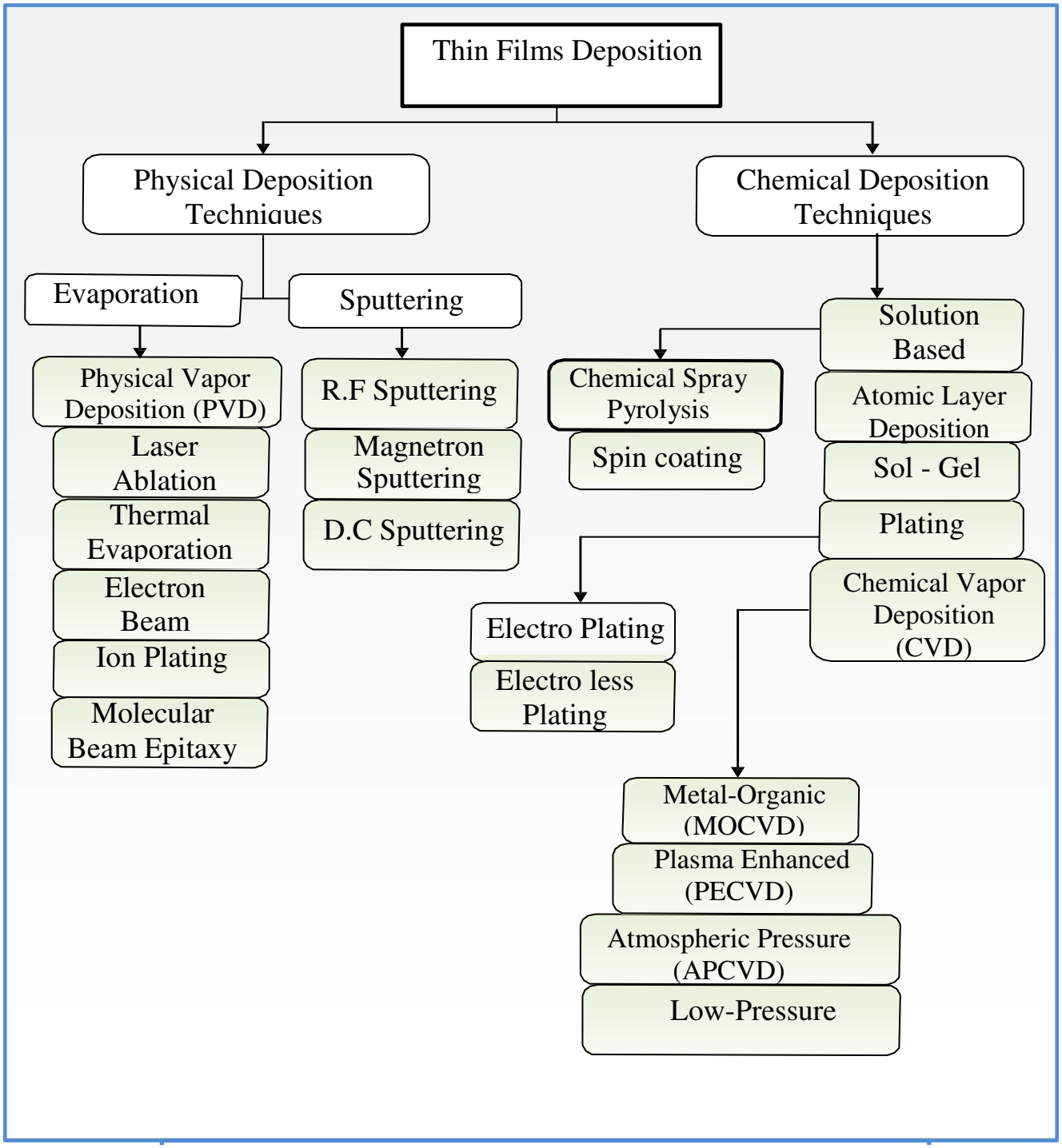

Figure (1-1): Classification of thin film deposition techniques [7].

1.2.1. Chemical Spray Pyrolysis Technique

Numerous materials have been prepared in the form of thin film because of their potential technical value and scientific curiosity in their properties. A number of techniques have been examined in the search for the most reliable and cheapest method of producing thin films [8]. Chemical spray pyrolysis (CSP) technique was initially suggested by Chamberlin and Skarman in 1966 to prepare CdS thin films on glass substrates. This method was used by many workers [9- 11]. Spray pyrolysis involves spraying of an aqueous solution containing soluble salts of the constituent atoms of the desired compounds to the heated substrates. The liquid droplets vaporize before reaching the substrate or react on it after splashing [12]. Doped and mixed films can be prepared very easily, simply by adding to the spray solution a soluble salt of the desired dopants or impurity.

1.2.2. Advantages of Chemical Spray Pyrolysis Technique

Chemical spray pyrolysis technique has a number of advantages as depicted in the following points [8, 13]:

1. It offers an extremely easy way to dope films with virtually any element in any proportion by merely adding it in some form to the spray solution.

2. Unlike closed vapor deposition method, CSP does not require high quality targets and/or substrates, and it does not require vacuum at any stage, which is a great advantage if the technique is to be scaled up for industrial applications.

3. The deposition rate and the thickness of the film can be easily controlled over a wide range by changing the spray parameters, thus eliminating the major drawbacks of chemical methods such as sol-gel method which produces films of limited thickness.

4. Operating at moderate temperatures (100 – 500 ^{o}C), CSP method can produce films on less robust material.

5. Unlike high – power methods such as radio frequency magnetron sputtering (RFMS), it does not cause local over – heating that can be detrimental for materials to be deposited.

6. By changing composition of the spray solution during the spray process, it can be used to make layered film and films having composition gradients throughout the thickness.

7. It is believed that reliable fundamental kinetic data are more likely to be obtained on particularly well characterized film surface, provided the film are quiet compact, uniform and that no side effects from the substrate occur. CSP offers such an opportunity.

8. Low cost comparing with other methods which require complex devices and instruments with high cost.

1.3. Mechanism of Thin Films Formation

Films growth may be divided into certain stages. These are as follows [14]:

1. Nucleation, during which small nuclei are formed that are statistically distributed (with some exceptions) over the substrate surface.
2. Growth of the nuclei and formation of larger islands, which often have the shape of small (crystallites).
3. Coalescence of the islands (crystallites) and formation of a more or less connected network containing empty channels.
4. Filling of the channels.

It is important to mention that after a certain concentration of nuclei is reached; additional particles do not form further nuclei but adhere to the existing ones or to the islands formed already.

1.4. Particular Considerations of the Chemically Sprayed Thin Films

Chemical reaction takes place when the falling drops reach the hot substrate thus the prerequisite material will follow the above stages to form thin film. Since there are many drops reaching the hot substrate, everyone will crystallize separately [13], and spotty film will form as shown in figure (1-2).

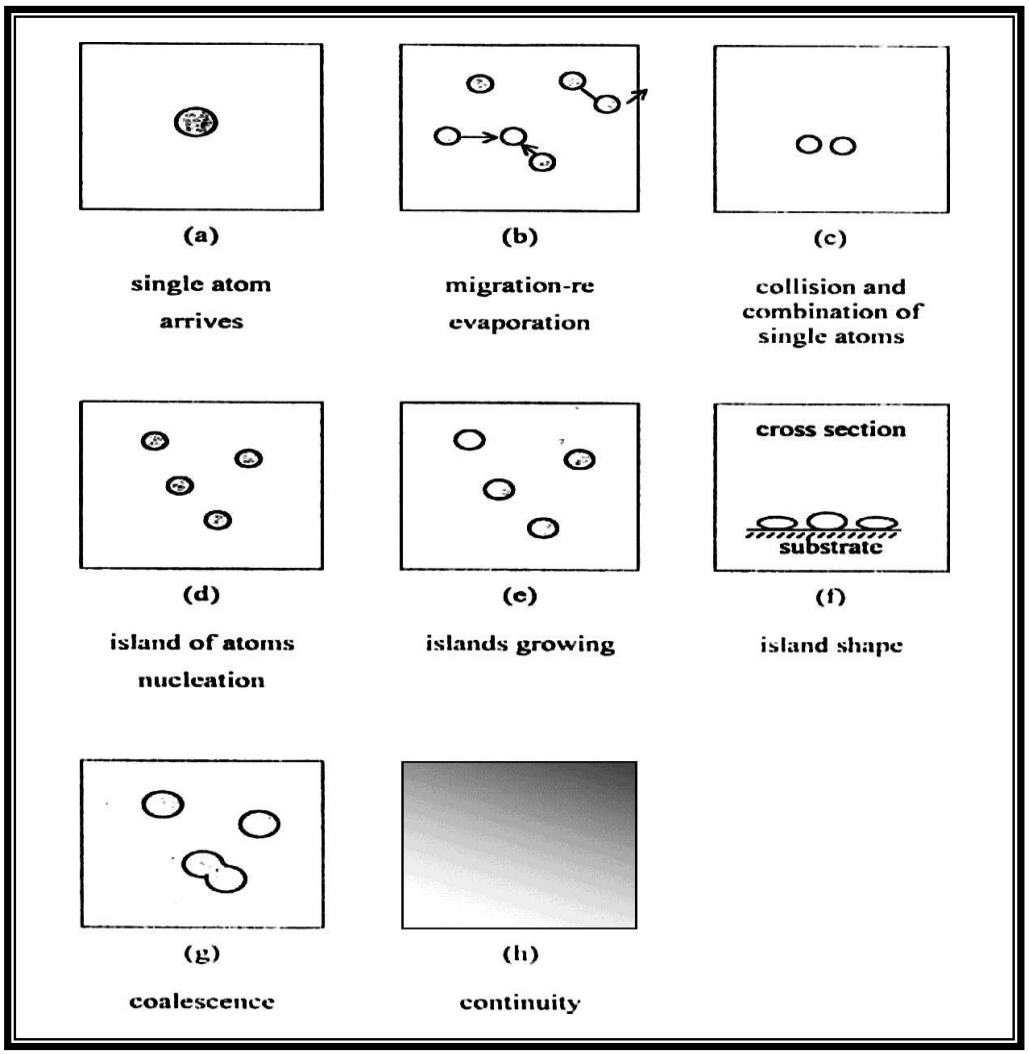

Figure (1-2)**:** Formation Stages of Thin Film [14]

1.5. Physical and Chemical Properties of Nickel Oxide

Nickel(II) oxide is the chemical compound with the formula NiO. It is notable as being the only well characterized oxide of nickel. The mineralogical form of NiO, bunsenite, is very rare. NiO can be prepared by multiple methods. Upon heating above 400 ^{o}C, nickel powder reacts with oxygen to give NiO. In some commercial processes, green nickel oxide is made by heating a mixture of nickel powder and water at 1000 ^{o}C, the rate for this reaction can be increased by the addition of NiO [15]. The simplest and most successful method of preparation is through pyrolysis of a nickel(II) compounds such as the hydroxide, nitrate, and carbonate, which yield a light green powder. Synthesis from the elements by heating the metal in oxygen can yield grey to black powders which indicates nonstoichiometry [16]. NiO adopts the NaCl structure, with octahedral Ni(II) and O_2^{-2} sites as shown in figure (1-3). The conceptually simple structure is commonly known as the rock salt structure. Like many other binary metal oxides, NiO is often non-stoichiometric, meaning that the Ni:O ratio deviates from 1:1. In nickel oxide this non-stoichiometry is accompanied by a color change, with the stoichiometrically correct NiO being green and the non-stoichiometric NiO being black. Nickel oxide (NiO) has a density of (6.67 g/cm^3) and molecular weight of (74.69 g/mol). Its melting point is (1955 ^{o}C) [17].

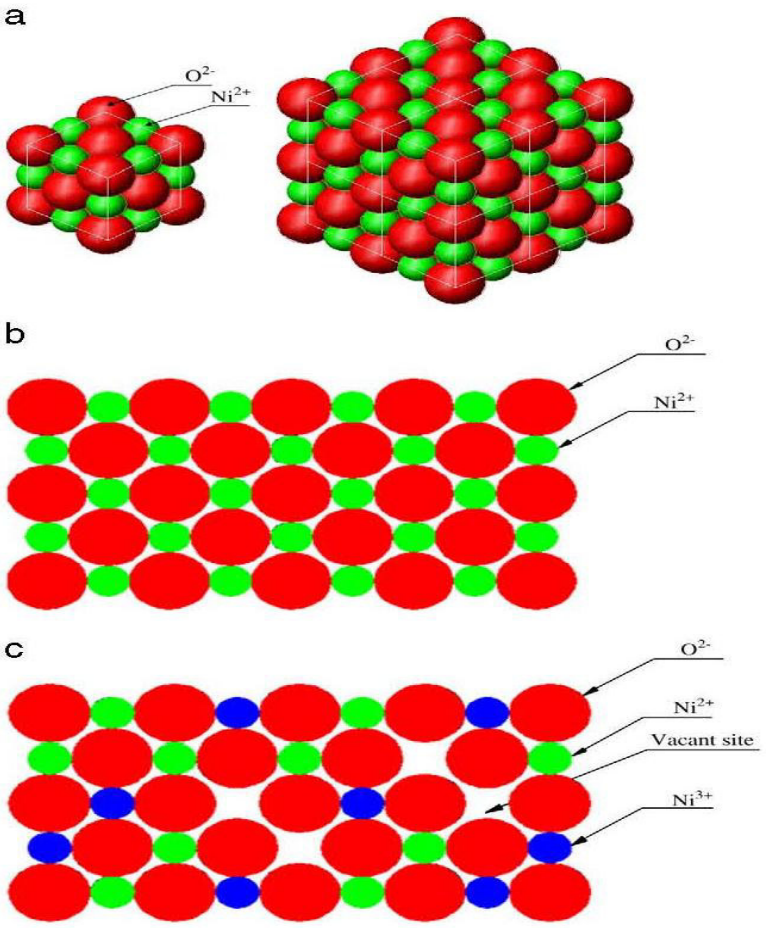

Figure (1-3): Structure of nickel oxide. [16]

a. Structure of nickel oxide in 3D
b. Structure of nickel oxide in 2D (Stoichiometric).
c. Structure of nickel oxide in 2D (Non-stoichiometric).

1.5.1. Different Applications of Nickel Oxide Thin Films

Nickel oxide thin films have been employed as:

1. An antiferromagnetic material [10].
2. p-type transparent conducting films [11].

3. Electro catalysis [18].

4. Positive electrode in batteries [19].

5. Fuel cell [20].

6. A material for electro-chromic display devices [21].

7. Part of functional sensor layers in chemical sensors [22].

8. Solar thermal absorber [23].

9. Photo electrolysis [24].

10. Promising ion storage material in terms of cyclic stability.

11. Resistive memories.

12. Electrochromic devices.

13. Giant magnetoresistive spin valve structures [25].

1.6. Physical and Chemical Properties of The Cobalt Oxide

Cobalt oxide is considered as a p-type semiconductor material. Although there are three different forms of cobalt oxides namely cobaltous oxide (CoO), cobaltic oxide (Co_2O_3) and cobaltite oxide (Co_3O_4), cobaltite oxide is the most widely used in electrochemical capacitor applications. The black tricobalt tetraoxide, Co_3O_4 is usually a product of thermal treatment of cobalt hydroxide, $Co(OH)_2$ at temperatures above 300^{o}C. Cobalt oxide is also a promising material in gas sensing and solar energy absorption as well as lithium ion battery electrodes. (CoO) has a density of (6.45 g/cm^3) and molecular weight of (74.9326 g/mol). Its melting point is (1933 ^{o}C) [26]

1.7. Previous Studies

In (2002), Patil and Kadam. [27] employed chemical spray pyrolysis (CSP) technique to deposit nickel oxide (NiO) thin films from hydrated nickel chloride salt solution on glass substrates. They studied the effect of the volume of sprayed solution on structural and optical properties by using X-ray diffraction (XRD), infrared (IR) and optical absorption. It was found that increase in the volume of sprayed solution leads to the increment in

film thickness and improvement of crystallinity of the film, consequently the band-gap energy varied from 3.58 to 3.4 eV.

In (2005), Chen et al. [28] studied the dependence of structural properties on the thickness of nickel oxide (NiO) films deposited on glass substrates by RF magnetron sputtering in a pure oxygen atmosphere at an RF power 200 W. The X-ray diffraction (XRD) and transmission electron microscope (TEM) analyses of nickel oxide films indicated that the films were polycrystalline. The thickness of the films varied in the range from 50 to 300 nm. The variations of the microstructural parameters, such as crystallite size, dislocation density, strain and density, with film thickness and substrate temperature were investigated. The results showed that the crystallite size increases as the thickness of the film increases, while the variation of the dislocation density and strain decrease as the thickness increases.

In (2007), Reguig et al. [29] studied NiO thin films grown on glass substrates by intermittent spray pyrolysis deposition of $NiCl_2 \cdot 6H_2O$ diluted in distilled water, using a simple "perfume atomizer". The effect of the solution molarity on their properties was studied and compared to those of NiO thin films deposited with a classical spray system. It was shown that NiO thin films crystallized after deposition. Whatever the precursor molarity, the grain size was around 25–30 nm. The crystallites were preferentially oriented along the (1 1 1) direction.

In (2007), Ghodsi and Khayatiyan. [30] prepared NiO thin films from $NiCl_2 \cdot 6H_2O$ precursor by using sol–gel route. The films were deposited on glass substrates using dip-coating technique. The optical and structural properties of the NiO thin films were investigated with respect to dipping

rate, number of layers, and annealing temperature. The microstructure of NiO thin films and powder were examined by X-ray diffraction (XRD). Various diffraction peaks of NiO powder were observed in the XRD patterns. The optical characteristics of the samples were determined by using UV–visible spectrophotometer. The results showed that the NiO thin films were transparent in the visible range. Optical constants like refractive index, extinction coefficient …etc. have changed by varying dipping rate, number of layers, and annealing temperature.

In (2008), Ezema et al. [31] deposited NiO_x thin film on glass slides from aqueous solutions of nickel chloride and ammonia. Ammonia was employed as complex agent in the presence of hydroxyl solution. The films were studied using X ray diffraction and photomicrograph for the structure and absorption spectroscopy for its optical properties. The optical characterization showed that the films have band gap that ranged between 2.10 eV and 3.90 eV, and thickness that ranged between 0.061 μm and 0.346 μm. The average transmittance of films was found to be between 50% and 91% in the UV-VIS-NIR regions. The films could be effective as optical coatings for poultry houses.

In (2008), Srivastava et al. [32] have prepared Nickel oxide thin films by spin coating on glass, silicon (111) and quartz substrates using a solution of nickel acetate tetrahydrate in 2-methoxyethanol and mono-ethanolamine and subsequent annealing at 300–600 ^{0}C for 2h in air. Those films have been characterized with regard to phase, microstructure and optical absorption using X-ray diffraction, atomic force microscopy and UV-visible spectrophotometry respectively. It was shown that NiO thin films have polycrystalline nature and possess an f.c.c. (NaCl-type) structure with lattice parameter varying with annealing temperature and solution molarity, typical value being a = 4.186 Å at 500 ^{o}C and molarity 0.5 M. The microstructure

clearly revealed the formation of ellipsoids with average projected major and minor diameters as ~58 and ~38 nm, respectively and nano-rods of average diameter ~12 nm with aspect ratio of ~5.2. On the other hand, thin films formed by dip coating with the same solution contain spherical particles of average diameter ~28 nm. NiO thin films exhibited (i) high optical transmittance (80–95%) in the wavelength range of 400–800 nm, (ii) sharp absorption in the interval 300- 400 nm like that of semiconductor/insulator, (iii) decrease of energy band gap, Eg (value lies in the range 3.66–3.83 eV, bulk value being 3.55 eV) with increase of both annealing temperature and molarity. The higher values of band gap have been attributed to the reduced average size of the crystallites.

In (2009), Igwe et al. [33] have prepared Nickel oxide thin films by chemical bath deposition technique on glass substrates using 3 mls of 1M of $NiSO_4$, 4 mls of 1M of KCl_4, and 1M of Ammonia as the complexing agent. The films were subjected to post-deposition annealing under various temperatures, 100, 150, 200, and 300 ^oC. The thermal treatment of $Ni(OH)_2$ thin film decomposes to NiO_x. The films were very prosperous materials with excellent electrochromic properties, firmly adhered to the substrate and resistant to chemicals. The transmittance was very high while the reflectance was low as the wavelength increases. The band gaps obtained under various thermal treatments were between 1.90 eV and 4.4 eV. The thickness achieved was in the range of 0.12-0.14 μm. These properties of the oxide film supports other important applications of NiO film such as preparation of alkaline batteries (as a cathode material) anti-ferromagnetic layers, P –type transparent conducting films.

In (2010), Saadati et al. [34] prepared NiO thin films by using the electron beam physical vapor method at room temperature on glass substrates for different thicknesses ranging from 285 to 645 nm. Nano-structures of the

films were investigated using X-ray diffraction (XRD) and atomic force microscopy (AFM). It was observed that NiO thin films have grown with (200) preferred orientation that increased with film thickness. In addition, crystallite size obtained from XRD results and grain size obtained from AFM analysis increased with film thickness. Transmittance spectra of NiO films were collected between 340 and 850 nm wavelength. Refractive indices and the thicknesses of these films were obtained using Swanepoel method. Optical functions of these films showed that films were of homogenous structure and the results agree with reported data obtained using different methods of film deposition.

In (2010), AL-Shammary [35] prepared nickel oxide (NiO) thin films on cleaned glass substrates at 498 K temperature using spray pyrolysis deposition technique of thickness (1451.8 Å). UV-VIS spectra of the film were studied by using the optical absorbance measurements which were taken in the spectral region from 300 nm to 1100 nm. Optical Constants such as optical allowed energy band gap of direct transition, absorption coefficient, extinction coefficient, refractive index and optical conductivity, were evaluated from these spectra. The films were found to exhibit high transmittance (~55-87%) and high absorbance values at ultraviolet region which they decrease rapidly in the visible / near infrared region. Optical allowed band energy for direct transition was (3.694eV).

In (2011), Patil et al. [36] employed Sol gel spin coating method for the deposition of nanocrystalline nickel oxide (NiO) thin films. The films were annealed at 400˚C - 700˚C for 1 h in air and the changes in the structural, morphological, and optical properties were studied. The structural properties of nickel oxide films were studied by means of X-ray diffraction (XRD), which showed that all the films were crystallized in the cubic phase

and present a random orientation. Surface morphology of the nickel oxide film consists of nanocrystalline grains with uniform coverage of the substrate surface with randomly oriented morphology. The decrease in the band gap energy from 3.86 to 3.47 eV was observed after annealing NiO films. It was concluded that the optical quality of NiO films was improved by annealing.

In (2011), Guziewicz et al. [37] fabricated NiO films by RF magnetron sputtering. Optical parameters of the films were characterized using transmittance measurements. P-type conductivity of as-deposited films and after annealing in oxygen or argon at the temperature range from 300 °C to 900 °C was verified. It was shown that the transmittance of NiO films strongly depends on deposition temperature and oxygen amount during sputtering. Films deposited at room temperature without oxygen had transmittance near 50% in the visible range and resistivity about 65 Ωcm. An increase in oxygen amount in deposition gas mixture resulted in higher conductivity, but transmittance decreased below 6%.

In (2011), Venter and Bothal [38] resistively deposited nickel (Ni) on glass substrates and oxidised at temperatures ranging from 300 ˚C to 600 ˚C. The oxidised Ni layers were subsequently characterized using scanning electron microscopy (SEM), X-ray diffraction (XRD) and UV-visible photospectrometry in the range 200 nm – 1000 nm. SEM results of the surface revealed a strong dependence of the surface texture and particle size on the oxidation temperature and time. XRD performed on the oxidised Ni indicated progressive transformation from nanograined polycrystalline Ni to NiO at elevated temperatures. Film thicknesses, particle sizes, energy band gap and refractive indices were determined from transmission and absorbance data.

In (2011), Thayumanavan et al. [39] developed an automated thin film formation technique to deposit NiO films at low temperatures using different molarities. The formed films were annealed at 310 ^{o}C to get better crystalline structure. The Structural and optical properties were studied for the grown thin films with the developed instrument. The band gap of the formed thin films was in the range of 3.73 eV to 3.35 eV. The optical studies revealed that the transmittance of the grown film is up to 80 % and decreases with increase of molarity of the solution

In (2011), Mahmoud et al**.** **[**40**]** prepared crystalline and non-crystalline nickel oxide (NiO) thin films by chemical spray pyrolysis technique using nickel acetate tetra hydrate solutions on glass substrates at different temperatures from 225 to 350°C. Structure of the as-deposited NiO thin films have been examined by X-ray diffraction (XRD) and atomic force microscope (AFM). The results showed an amorphous structure of the films at low substrate temperature (T = 225 °C), while at higher T ≥ 275 °C, a cubic single phase structure of NiO film was formed. The refractive index and the extinction coefficient have been calculated from the corrected transmittance and reflectance measurements over the spectral range from 250 to 2400 nm.

In (2012), Mallikarjuna et al. [41] prepared Nickel Oxide (NiO) thin films on Corning 7059 glass substrates at different oxygen partial pressures in the range of 1 x 10 $^{-4}$ to 9 x 10 $^{-4}$ mbar by using dc reactive magnetron sputtering technique. Structural properties of NiO films showed polycrystalline nature with cubic structure along (220) orientation. The optical transmittance and band gap values of the films increased with increasing the oxygen partial pressure from 1 x 10 $^{-4}$ to 5 x 10 $^{-4}$ mbar and decreased on further increasing the oxygen partial pressure. Using Scanning

Electron Microscopy (SEM), fine grains were observed at oxygen partial pressure of 5 x 10^{-4} mbar.

In (2012), Balu et al. [42] prepared NiO thin films with different molarities of nickel chloride on ultrasonically cleaned glass substrates kept at 350 ^{o}C by a simplified, economical spray technique using perfume atomizer. In this technique atomization was based on hydraulic pressure instead of compressor air pressure as in the conventional spray technique. The X-ray diffraction study revealed that the films were polycrystalline in nature with cubic structure. Micro structural parameters were calculated from the XRD data. Analysis of the absorption versus photon energy curves revealed an indirect transition and the band gap decreases with the increase in solution concentration.

In (2013), Ismail et al. [43] prepared transparent crystalline nanostructured nickel oxide (NiO) thin films by using a simple spray pyrolysis technique from hydrated nickel chloride salt solution ($NiCl_2.6H_2O$) on glass and silicon (n-type) substrates at different temperatures (280, 320, 360, and 400 ^{o}C) and with different solution concentrations (0.025,0.05, 0.075, and 0.1 M). Structural and morphological properties of the grown NiO films were studied using X-ray diffraction (XRD) and atomic force microscope. Optical properties of the films were characterized by UV–visible absorption spectra. The XRD results showed that the deposited films have an amorphous structure when deposited at temperature of T=280 ^{o}C and concentration of 0.025 M. At higher temperatures (T = 320, 360, and 400 ^{o}C) and solution concentrations of (0.05, 0.075, and 0.1 M), the deposited films had cubic polycrystalline structure formed with preferred orientation along (111) plane. The band gap of NiO film increased from 3.4 to 3.8 eV as the molarity decreased from 0.1 to 0.05 M.

In (2013), Sriram and Thayumanavan. [44] prepared Nickel Oxide (NiO) thin films by using spray pyrolysis technique. Structural and optical properties of two different films were studied. The structural studies showed that the film prepared from the aged solution had more grain size (60.3 nm) than the film prepared by fresh solution (21 nm). From the optical studies, it was found that the band gap of film from fresh solution was 3.6 eV while the band gap of film from aged solution was about 3.5eV. The refractive index was measured with the help of PUMA software and for the film from fresh solution it remained at 1.95 through visible region. However, for the film from aged solution, it varied from 2 to 1.78 in visible region. The calculated extinction coefficient values of the films showed no significant variation in visible and NIR range.

In (2013), Osuwa Onyejiuwa.[45] prepared Nickel oxide (NiO) thin films by using chemical bath deposition at room temperature of 30 ^{o}C and the films were then annealed in an oven at temperatures of 100 ^{o}C, 200 ^{o}C and 300 ^{o}C. Structural and properties of the thermally treated thin film samples were characterized using X-Ray Diffraction (XRD), Energy dispersive, Spectroscopy (EDS), and Surface Profiler. The results showed that the NiO thin film thickness decreased with annealing temperature from 1.40 μm for as grown sample to 0.75 μm for sample annealed at 300 ^{o}C. The XRD patterns revealed increasing amorphosity of the NiO thin films with increasing in annealing temperature.

In (2013), Patel et al. [46] prepared (NiO) thin films on glass and indium tin oxide coated glass substrates by e-beam evaporation technique at different substrate temperatures ranging from room temperature (27 ^{o}C) to (400 ^{o}C). The crystallization of the film was improved with increase in substrate temperature as inferred from the glancing incident X-ray diffraction

measurement. The increase in substrate temperature of the films caused an increase in the transmittance.

In (2013), Saleh [47] prepared NiO thin films on suitably cleaned quartz substrates by rapid thermal oxidation method for different oxidation time and 850 ^{o}C oxidation temperature. The structural properties of NiO thin films have been investigated. Polycrystalline nature of the material was confirmed by X-ray diffraction technique and various structural parameters were calculated. All the films showed most preferred orientation along (111), (200) and (220) planes. The grain size of prepared NiO films was within the range of 49 to 63 nm.

In (2014), Tareq [48] prepared Nickel oxide (NiO) thin films on quartz substrates using a pulsed 532 nm Q-Switched Nd: YAG laser. The X-ray diffraction (XRD) results showed that the deposited films were crystalline in nature. Furthermore, a higher annealing temperature resulted in a thicker NiO film, which was attributed to an increased grain size. The morphology of deposited films was characterized by scanning electron microscope (SEM) and atomic force microscope (AFM), with increasing annealing temperature, the grain size increase. The grain size value (10, 23 and 40 nm) for thin films annealing at 200, 300 and 400 ^{o}C respectively. UV–Vis spectrophotometric measurement showed high transparency (nearly 92 % in the wavelength range 400–900 nm) of the NiO thin film with a direct allowed band gap value lying in the range of 3.51–3.6 eV.

In (2014), Offiah et al. [26] employed chemical bath deposition (CBD) method for the growth of nanocrystalline nickel-cobalt oxides (NiO-CoO) thin films deposited on glass substrates. The XRD results showed that the average crystallite size of the thin films is about 2.2nm. The thin films

which were also characterized for AFM and SEM revealed randomly oriented nano-flake structures with absorbance greater than 45% in the UV region of the electromagnetic spectrum and band gap energy range between 2.75 eV and 2.95 eV. Characterization of the NiO-CoO composite thin films shows that they could possibly be useful in supercapacitive applications.

1.8. Objectives of the study

1. Preparation of undoped and Co doped Nickel Oxide thin films on glass substrates by chemical spray pyrolysis (CSP) technique at substrate temperature of (400 ±5 ^{o}C).

2. Studying the effect of aqueous solution molarity and cobalt concentration on the surface morphology, structural and optical properties of the deposited thin films.

Chapter Two

Theoretical Background

2.1. Introduction

This chapter includes general descriptions of the theoretical part of the current study, the physical concepts, relationships, and the laws used to interpret the obtained results.

2.2. Crystal Structure of Solids

Solid materials may be classified according to the regularity with which atoms or ions are arranged with respect to one another into two groups which are;

1. Crystalline Materials

Crystalline materials can be classified into two groups such as;

a. Single crystalline materials

The atoms in these types of materials are arranged in a three – dimensional periodic fashion as shown in figure (2-1a). The periodic arrangement of atoms in a crystal is called a lattice. In a crystal, an atom never strays far from a single and fixed position. The thermal vibrations associated with the atom are centered about this position. For a given semiconductor, there is a unit cell that is representative of the center lattice, by repeating the unit cell in three dimensions, the whole crystal can be generated, and such materials are said to have long range order [49].

b. Polycrystalline materials

The structure of polycrystalline materials consists of many tiny single crystals known as grains which are separated by grain boundaries, each of then contains a periodic array of atoms and is considered to pass long range order [50] as shown in figure (2-1b), while the grain in the polycrystalline state posses short range order [SRO] with random grain sites, shape, and orientational packing [49].

2. Non Crystalline (Amorphous) materials

Amorphous material is defined as the material in which its atomic sites are randomly arranged in three-dimensions as shown in figure (2-1c).

Amorphous material lacks the long range periodic ordering in their lattice network, but, they have short range order (SRO). Thus, such materials acquire variation in the interatomic distance and bond angles; however they are of covalently bonded atoms which are arranged in an open network. The atoms in the amorphous materials are linked by forces and oscillate to define equilibrium positions that are similar to those in crystals.

The properties of amorphous semiconductor thin films are very sensitive to the preparation technique and thermal history because there is no limit to the variation of bond lengths and angles in addition to the preparation defects [51].

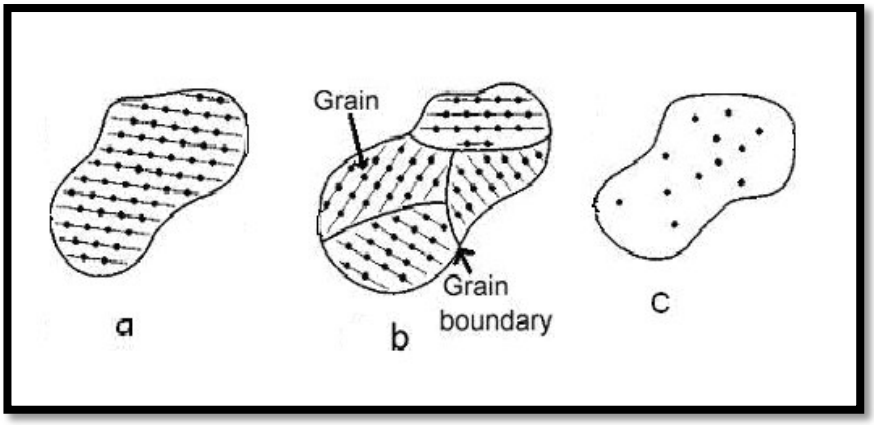

Figure (2-1): Schematics of the general types of materials**.**
a. single crystal, **b.** polycrystalline and **c.** amorphous [51].

2.3. Semiconductor Materials Groups

Semiconductors are the group of materials having conductivities between those of metals and insulators. Two general classifications of semiconductors are the elemental semiconductor materials, and the compound semiconductor materials, the two-elements, or binary compounds such as gallium arsenide. Compound semiconductor technology is not new. Devices based on GaAs, the most mature of the III-V technologies, have been used for more than forty years, mostly in aerospace and military applications. In the past twenty years or so, GaAs devices had been used in high-volume commercial applications such as cellular phones and other wireless

applications [53]. Three-elements, or ternary, compound semiconductor, for example AlGaAs can also be formed. More complex semiconductors can also be formed that provide flexibility when choosing material properties [53].

2.4. Crystal Defects

It is useful to classify crystal lattice defects by their dimension. The 0-dimensional defects affect isolated sites in the crystal structure, and are hence called point defects. An example is a solute or impurity atom, which alters the crystal pattern at a single point. The 1-dimensional defects are called dislocations. They are lines along which the crystal pattern is broken. The 2-dimensional defects are surfaces, such as the external surface and the grain boundaries along which distinct crystallites are joined together. The 3-dimensional defects change the crystal pattern over a finite volume. They include precipitates, which are small volumes of different crystal structure, and also include large voids or inclusions of second-phase particles [54].

The simplest imperfection is a lattice vacancy, which is a missing atom or ion also known Schottky defect. Schottky defect is created in a perfect crystal by transferring an atom from a lattice site in the interior to a lattice site on the surface of the crystal.

Another vacancy defect is the Frenkel defect in which an atom is transferred from a lattice site to an interstitial position, a position not normally occupied by an atom [55]. Figure (2-2) shows schematic of Schottky defect and the Frenkel defect.

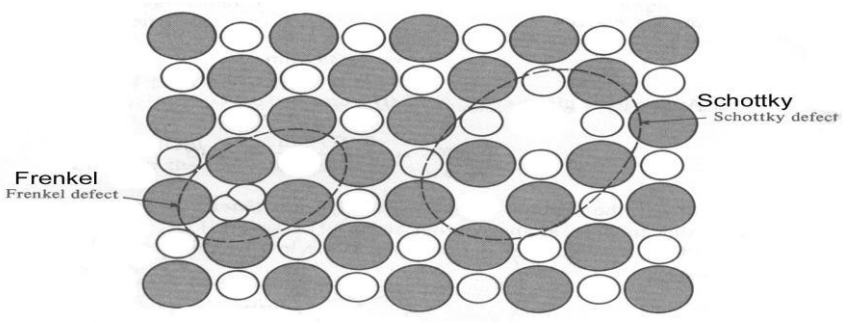

Figure (2-2): Schottky defect and Frenkel defect [55].

2.5. X-Ray Diffraction

X-rays is a form of electromagnetic radiation. Most X-rays have a wavelength in the range of (0.01 to 10 nm). X-ray wavelengths are shorter than those of UV rays and typically longer than those of gamma rays [56]. The wavelength must be equal to or roughly comparable to the lattice constant in order to investigate the structure of materials [57].

2.6. Structure of Thin Films

One of the most well known methods for studying the structure of bulk materials as thin films is the x-ray diffraction (XRD).

The analysis of the diffraction pattern may give information about the crystallization and interplanner spacing of substance examined. The Bragg's condition for the diffraction can be written as [58]:

$$m\lambda = 2d\sin\theta \qquad \ldots\ldots\ldots\ldots\ldots (2\text{-}1)$$

Where (m) is positive integer which represents the diffraction order, (λ) is the wavelength of the incident X-ray beam, (θ) Bragg diffraction angle of the XRD peak and the interplaner (d) can be determined. Fig (2-3) shows the (XRD) that satisfies Bragg's condition.

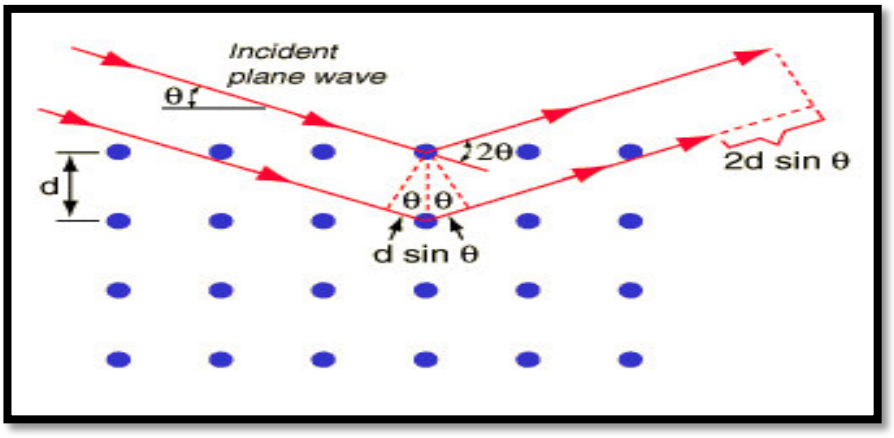

Figure (2-3)**:** Bragg's diffraction [59]**.**

According to the (XRD), in the case of polycrystalline films the (XRD) shows various peaks at different angles of diffraction and diffraction pattern as shown in figure (2-4) a. The single crystal material exhibits

sharpreflections (sharp peaks). as shown in figure (2-4)b [60]. For the amorphous films material, the diffraction does not exhibit any sharp peaks [60]. This can be simply represented in fig (2-4) c.

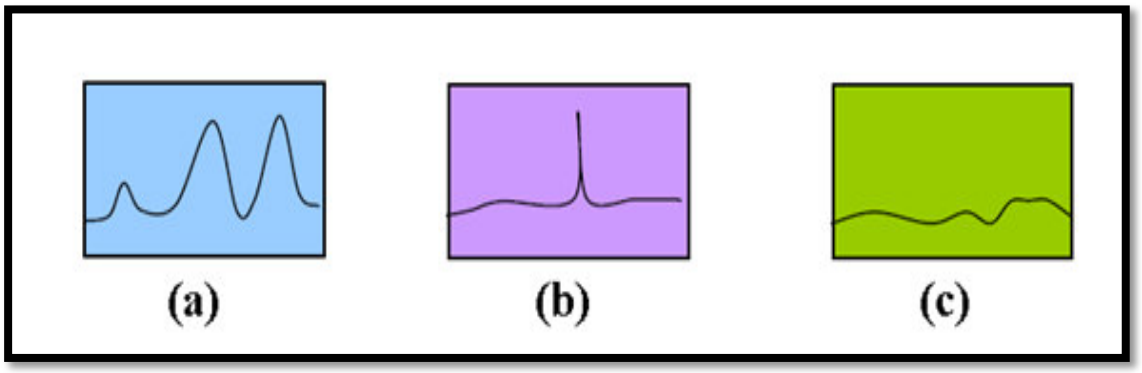

Figure (2-4): (XRD) of semiconductors.

(a) Polycrystalline (b) Single material (c) Amorphous material [61]**.**

2.7. Structural Parameters:

2.7.1. Lattice Constant (a_o)

Lattice Constant (a_o) can be calculated of a particular cubic system through the following relation [62]:

$$d_{hk\ell} = \frac{ao}{\sqrt{(h^2+k^2+\ell^2)}} \qquad \text{..... (2-2)}$$

2.7.2. Average crystallite size (D_{av})

The average crystallite size (D_{av}) can be estimated using two methods :

a. Scherrer method

Crystallite size can be calculated from peak broadening using XRD [63]. X-ray line broadening method was used to determine the particle size of NiO by using Scherrer equation [64]:

$$D_{av} = \frac{K\lambda}{\beta \cos\theta} \qquad \text{.....(2 -3)}$$

Where

K: is constant and was assumed to be equal to 0.9

λ: is the wavelength of incident X-ray radiation = (1.5406Å for CuK_α).

β: is the full width at half maximum of the peak (in radians).

θ: is Bragg diffraction angle of the XRD peak.

b. Williamson-Hall method

Crystal imperfections and distortion of strain-induced peak broadening are related by S ≈ βs/tanθ. Scherrer-equation follows a 1/cosθ dependency but not tanθ as the induced strain [65]. The following results are the addition of the Scherrer equation and S ≈ βs/tanθ [66].

$$\beta_{hk\ell} = \beta_D + \beta_S \qquad \text{…….....(2- 4)}$$

$$\beta_{hk\ell} = \left(\frac{K\lambda}{\beta \cos\theta}\right) + 4S\tan\theta \qquad \text{..…..…..(2-5)}$$

where S: is the microstrain

Rearranging equation (2-5) gives:

$$\beta_{hk\ell}\cos\theta = \left(\frac{K\lambda}{D}\right) + 4S\sin\theta \qquad \text{……(2- 6)}$$

If $\beta_{hk\ell}\cos\theta$ is plotted with respect to 4sinθ for the peaks, strain and crystallite size can be calculated from the slope and y-intercept of the fitted line respectively[67].

2.7.3. Texture Coefficient (Tc)

To describe the preferential orientation, the texture coefficient, $T_C(hkl)$ is calculated using the expression [68]:

$$T_C(hkl) = \frac{I(hkl)/I_0(hkl)}{N_r^{-1}\sum I(hkl)/I_0(hkl)} \qquad \text{…..……..(2-7)}$$

Where I(*hkl*) is the measured intensity, I_o (*hkl*) taken from the JCPDS data, (N_r) is the number of peaks and (*hkl*) is Miller indices. The texture coefficient $T_C(hkl)$ is a positive number and may have the values :

If $T_C(hkl)\approx1$ for all the *(hkl)* planes considered, then the films are with a randomly oriented crystallite, while values higher than 1 indicate the abundance of grains in a given *(hkl)* direction. Values $0<T_C(hkl)<1$ indicate the lack of grains oriented in that direction. As $T_C(hkl)$ increases, the preferential growth of the crystallites in the direction perpendicular to the *hkl* plane is the greater [69].

2.7.4. Dislocation density and number of grains

The dislocation density (δ) can be calculated as the following [70]:

$$\delta = 1/D_{av}^{2} \qquad \text{.....(2- 8)}$$

and number of crystallites can be calculated from the relation [71]:

$$N_o = t/D_{av}^{3} \qquad \text{.....(2- 9)}$$

Where t : is the thickness and N_o: is the number of crystallites.

2.8. Atomic Force Microscopy (AFM)

Atomic Force Microscopy (AFM) is a very high-resolution type of scanning probe microscopy, with demonstrated resolution on the order of fractions of a nanometer, more than 1000 times better than the optical diffraction limit. Binnig, Quate and Gerber invented the first atomic force microscope (also abbreviated as AFM) in 1986. The information is gathered by "feeling" the surface with a mechanical probe. Piezoelectric elements that facilitate tiny but accurate and precise movements on (electronic) command enable the very precise scanning [72]. Atomic Force Microscope (AFM) consists of probe, cantilever and imaging modes. Atomic force microscope (AFM) has three main modes of mapping topography: contact which was used in current morphology investigations, non-contact and intermittent contact or tapping. Figure (2-5) shows a schematic diagram of atomic force microscope. The most important part of an AFM is the tip with its nanoscale radius of curvature. The tip is attached to a micronscale cantilever which

reacts to the Van der Waals interaction and other forces between the tip and sample. In contact mode, the cantilever is deflected due to the force and this deflection is measured by reflecting a laser beam off the back of the cantilever. The microscope produces an image by recording the feedback signal from the control loop that maintains a constant amount of cantilever deflection. i.e., tip- sample force or tip-sample spacing. In non-contact and tapping modes, the cantilever is excited close to its resonant frequency, and the feedback loop maintains constant tip oscillation amplitude [73].

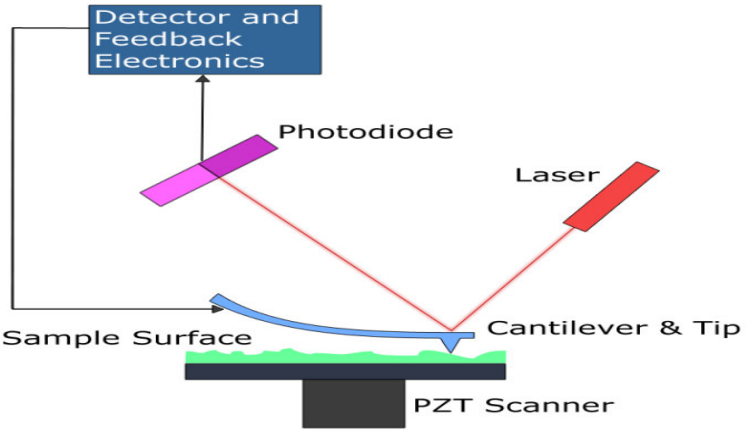

Figure (2-5): Schematic diagram of atomic force microscope [73].

2.9. Energy Bands in Crystalline Semiconductors

The detailed energy band structures of crystalline solids have been calculated using quantum mechanics. Figure (2-6) is a schematic diagram of the formation of silicon lattice crystal from isolated silicon atoms. Each isolated atom has its discrete energy levels (two levels are shown on the far right of the diagram). As the inter-atomic spacing decreases, each degenerate energy level splits to form a band. Further decrease in spacing causes the bands originating from different discrete levels to lose their identities and merge together, forming a single band. When the distance between atoms approaches the equilibrium inner atomic spacing of the diamond lattice (with a lattice constant of 5.43Å for silicon), this band splits

again into two bands. These bands are separated by region which designates that the electrons in the solid cannot be possessed. This region is called the forbidden gap, or band gap (E_g) [74]. The upper band is called the conduction band (C.B.), while the lower band is called valance band (V.B.) as shown on the far left of figure (2-6).

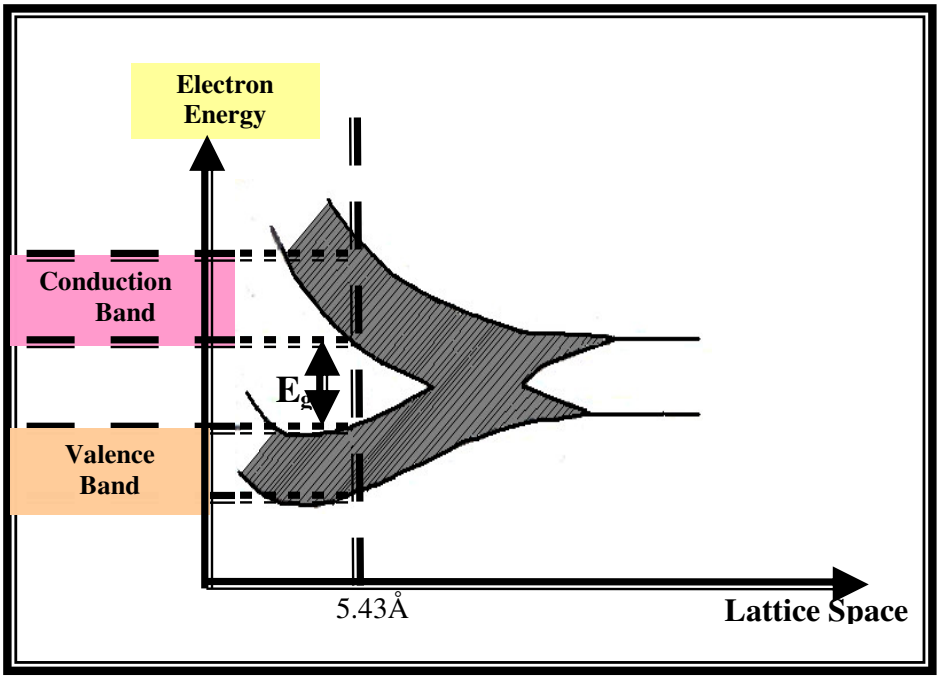

Figure (2-6): Formation of energy bands in silicon lattice crystal by bringing together isolated atoms [75].

The valance band is filled by electrons at temperature zero kelvin while conduction band is empty from electrons. At room temperature the energy is enough to some electrons in valance band to cross energy gap (E_g) to conduction band, after that, a hole will be left in valance band.

2.10. Electronic Transitions

Throughout the study of optical properties, two kinds of electronic transitions can be distinguished, direct and indirect, depending on the lower location point in conduction band, and upper point of valance band [76].

2.10.1. The Direct Transitions

The direct transition occurs when the upper point location is identified at the top of valance band (E_v) with lower point in conduction band bottom (E_c) in *(E-* $\vec{K}$ *)* curve at same value of wave vector ($\vec{K}$), the transition fulfilled vertically without any change in wave vector ($\Delta \vec{K}$ =0).

This means that photons with energy higher or equal to the forbidden energy gap ($hv \geq E_c - E_v$), so the direct optical absorption energy would be limited by the energy gap, that kind of transition is defined by allowed direct transition, as shown in figure (2-7-a).

That kind of transition is achieved by the conservation of energy and momentum as follows [74, 77]:

$$E_f = E_i + hv$$
$$\vec{K}_f = \vec{K}_i + \vec{K}_{ph} \qquad \text{…….. (2-10)}$$

Where:

E_f, E_i: final and initial energies of conduction and valance bands, respectively.

$\vec{K}_f$, $\vec{K}_i$: the final and initial wave vectors of transited electron.

$\vec{K}_{ph}$: photon wave vector .

It should be mentioned here that the electron wavelength is at the range of the distance between the atoms, thus the electron wave vector ($|Ke| = \frac{2\pi}{\lambda}$) is very high compared with the photon wave vector ($\vec{K}_{ph}$) e.g, ($\vec{K}_{ph} << \vec{K}_e$), so , ($\vec{K}_{ph}$) is neglected and equation (2-10) becomes as follows:

$$\vec{K}_f = \vec{K}_i \qquad \text{……... (2-11)}$$

There is an important relationship between forbidden energy gap (E_g) and photon energy (hv), which is expressed by the following equation [78, 79]:

$$\alpha hv = A'(hv - E_g)^r \qquad \text{…..……..(2-12)}$$

Where

A' : is constant depending on properties of conduction and valance bands

r : is constant and its value depends on the transition nature, where *r=1/2* for allowed direct transitions , *r=3/2* for forbidden direct transitions [78].

At a forbidden direct transition condition, the excited electron transition will occur vertically, but from an adjacent region of allowed direct transition, i.e., from a region which is adjacent to the upper point of valance band to points which are adjacent to the lower point of conduction band on condition that the wave vector should stay the same, e.g. $(\Delta \vec{K} = 0)$ before and after transition, as shown in figure (2-7-b). It is worth to mention here that each of the two transitions does not depend on temperature [76].

2.10.2. The Indirect Transitions

Semiconductors in which these kinds of transitions may occur are called indirect semiconductors, and these have indirect energy gap, while semiconductors in which direct transitions occur are called direct semiconductors and these have direct energy gap [55].

Indirect transitions occur when the location of the valance band top energy is not quite under the lower point of the conduction band bottom in (E- $\vec{K}$) curve. Electrons transition will be non-vertical from the valance band to conduction band, so that transition demands change in transited electron momentum. e.g. ($\Delta \vec{K} \neq 0$). Momentum of each electron and photon is not conserved. To achieve the momentum conservation, a third particle is needed and this particle is called phonon. This phonon awards the system the required momentum, either by absorbing phonon with momentum $[-h(\vec{k}_f - \vec{k}_i)]$ or by emission of phonon with momentum $[+h(\vec{k}_f - \vec{k}_i)]$, thus, the conservation of momentum law is achieved as follows [56]:

$$h\vec{k}_i + h\vec{k}_{ph} = h\vec{k}_f + h\vec{k}_p \qquad \text{.....(2-13)}$$

Where $\vec{k}p$: is phonon wave vector.

The required energy for transition can be expressed by the following formula:

$$h\nu = E_g \pm E_p \qquad \text{..... (2-14)}$$

Where E_p : represents the absorbed (– sign) or emitted (+ sign) phonon energy.

The following equation shows absorption coefficient of this kind of transitions [80]:

$$\alpha h\nu = B(h\nu - E_g \pm E_p)^r \qquad \text{.....(2-15)}$$

Where

B : is constant depends on valance and conduction bands properties, and on temperature

r: is exponential coefficient equals 2 in allowed indirect transition and equals 3 in forbidden indirect transition .

E_p : is the phonon energy.

The indirect transition occurred as shown in figure (2-7-c) when the electrons transition is not vertical and from the upper point in top valance band to the lower point in conduction band bottom, associated with changing in wave vector ($\vec{K}$) before and after transition, e.g. $(\Delta \vec{K} \neq 0)$. When the transition be also not vertical but from the adjacent points to the upper point in valance band to point in conduction band with changing in the value of wave vector ($\vec{K}$) before and after transition, the transition is called the forbidden indirect transition, as shown in figure (2-7-d).

Temperature plays an important role in indirect electron transitions as they increase with the increase in temperature. It should be noticed that in low temperatures there is a decrease in the probability of photon absorption because there are no phonons. Increasing the phonon emission accompany the electron transition process at high temperature, such transitions distinguished by their occurrence in all energies in conduction and valance

bands on condition that the conservation of energy and momentum laws are fulfilled [76].

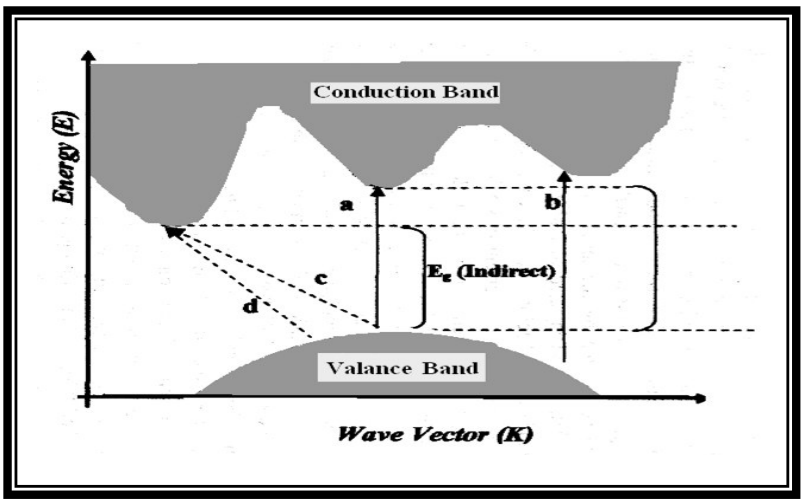

Figure(2-7): Types of electronic transitions[78].

(a) allowed direct transition (c) allowed indirect transition

(b) forbidden direct transition (d) forbidden indirect transition.

2.11. Optical Properties of Crystalline Semiconductors

The study of the optical properties of a material is interesting for many reasons. Firstly, the use of materials in optical applications such as interference filters, optical fibers and reflective coating requires accurate knowledge of their optical constants over a wide range of wavelengths. Secondly, the optical properties of all materials may be related to their atomic structure, electronic band structure, and electrical properties.

2.12. Transmittance (T)

Transmittance (T) is given by ratio of the intensity of the rays (I_T) transmitting through the film to the intensity of the incident rays (I_o) as follows [78]:

$$T = I_T / I_o \qquad \text{..... (2-16)}$$

2.13. Reflectance (R)

Reflectance can be obtained from absorption and transmission spectrum in accordance to the law of conservation of energy by the relation [49]:

$$R + T + A = 1 \qquad \text{.....(2-17)}$$

R is related to the refractive index and extinction coefficient of the material as follows [78]:

$$R = \frac{(n-1)^2 + k_o^2}{(n+1)^2 + k_o^2} \qquad \text{.....(2-18)}$$

R: reflectance

n : Refractive Index

K_o **:** Extinction Coefficient

When $K_o = 0$

$$R = \frac{(n-1)^2}{(n+1)^2} \qquad \text{.....(2-19)}$$

2.14. Absorbance (A)

Absorbance can be defined as the ratio between absorbed light intensity (I_A) by material and the incident intensity of light (I_o) [78]:

$A = I_A / I_o$ .....(2-20)

2.15. Absorption coefficient (α)

When light proceeds from one medium into another (e.g. from air into a solid substance), some of the light radiation may be transmitted through the medium, some will be absorbed, and some will be reflected at interface between the two media.

Absorption coefficient .may be defined as the decreasing ratio in incident ray energy in distance unit toward wave propagation inside the medium. Absorption coefficient is characteristic of the particular semiconductor material; furthermore, it varies with the incident photon energy (*hv*) and semiconductor property [60].

When incident photon energy is less than the energy gap, photon will transmit and the transmittance for thin film is given by the relation [78]:

$T=(1-R)^2e^{-\alpha t}$ .....(2-21)

Where:

T**:** is transmittance, R**:** is Reflectance and t**:** is the thickness.

The absorption coefficient can be estimated from the absorbance using the formula :

$$\alpha = (2.303 \times A)/t \qquad \text{..... (2-22)}$$

2.16. Fundamental Absorption

The absorption of light by intrinsic semiconducting material takes place by fundamental absorption process (FAP).

The fundamental absorption refers to transition from band-to-band or to excitation transitions of an electron from the valance band to the conduction band. The fundamental absorption, which manifests itself by a rapid rise in absorption, can be used to determine the energy gap of the semiconductor [80].

The cut off wavelength λ_c is the fundamental absorption edge, that occurs when incident photon energy equals the forbidden gap energy (Eg) and it is given by the relation [79]:

$$\lambda_c\,(nm) = \frac{1240}{Eg\,(eV)} \qquad \text{..... (2-23)}$$

Figure (2-8) shows the variation of the absorption coefficient of the semiconductor as a function of wavelength.

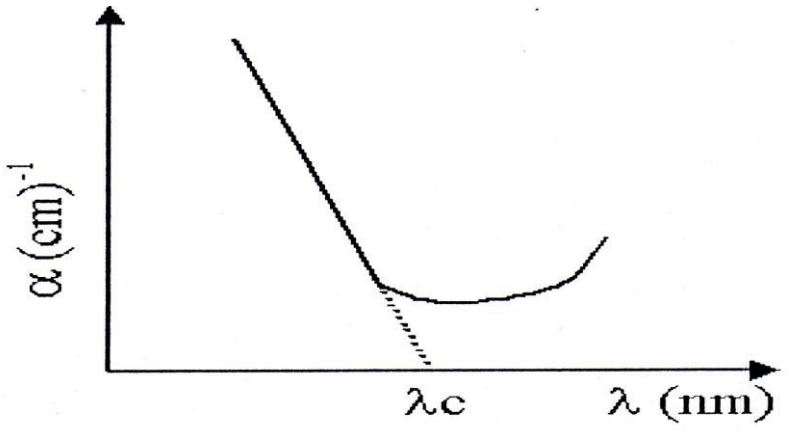

Figure (2-8): Fundamental absorption edge of crystal semiconductor [79].

2.17. Optical Properties of Amorphous Semiconductors

The optical properties of amorphous semiconductors study have big importance for knowing the composition of energy bands and its properties. As a result to have short range order and existence of the local levels and their tails inside the energy gap, the amorphous semiconductors absorption edge varies from that of crystalline, this can divide the fundamental absorption edge into three distinguished regions [79, 80] which are:

2.17.1. High Absorption Region

The absorption coefficient in this region is more or equal to ($\alpha \geq 10^4 cm^{-1}$). This high absorption refers to electronic transitions from extended levels in valance bands to extended levels in conduction bands, as shown in part A of figure (2-9), as throughout this region, the forbidden energy gap (E_g) can be recognized. The absorption coefficient (α) is given at this region by the following relationship [79, 81]:

$$\alpha h\nu = \alpha_o (h\nu - E_g)^r \qquad \text{..... (2-24)}$$

Where α_o**:** is constant depends on the type of transitions and hν : is the photon energy.

2.17.2. Exponential Region

Absorption coefficient value in this region ranges ($1 < \alpha < 10^4$) cm^{-1}. The electronic transitions in this region are from tail state of valance band to the extended states in the conduction band [80].

Absorption coefficient can be expressed according to Urbach relation [79]:

$$\alpha = \alpha_o \exp\left(\frac{h\nu}{Eu}\right) \qquad \text{..... (2-25)}$$

Where E_u : is urbach energy for localized states.

Part B of figure (2-9) represents this region.

2.17.3. Low Absorption Region

Absorption coefficient in this region is very small (α <1cm^{-1}). The transitions occur between local states inside the forbidden energy gap (E_g) [54], as shown in part C of figure (2-9).

This region depends on the nature of the material depending on its preparation and purity.

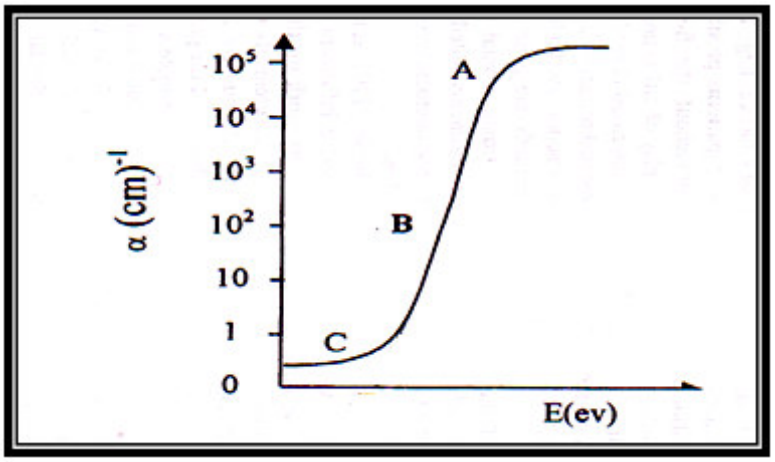

Figure (2-9): The fundamental absorption edge and absorption regions [59].

2.18. Optical Energy Gap (g)

The term "band gap" refers to the energy difference between the top of the valence band to the bottom of the conduction band. Electrons are able to jump from one band to another. In order for an electron to jump from a valence band to a conduction band, it requires a specific minimum amount of energy for the transition, the band gap energy. Measuring the band gap is important in the semiconductor and nanomaterial industries. The band gap energy of insulators is high (> 4eV), but lower for semiconductors (< 3eV). The energy band gap in some semiconductors tends to decrease as the temperature is increased [82].

The energy gap for allowed direct transition materials can be estimated by plotting a graph between $(\alpha h\nu)^2$ and $(h\nu)$ in eV, a straight line is obtained

and the extrapolation of this line to $(\alpha hv)^2 = 0$ gives the value of the direct band gap of the material [83].

2.19. Some Optical Parameters

2.20.1. Refractive Index (n)

It is the ratio of light velocity in vacuum (c) to its velocity in material (v) [84].

$$n = c / v \qquad \text{.....(2-26)}$$

The refractive index can be calculated using the relation [1]

$$n = \left[\frac{(1+R)^2}{(1-R)^2} - (k_o^2 - 1)\right]^{1/2} + \frac{(1+R)}{(1-R)} \qquad \text{..... (2-27)}$$

Where n: is the refractive index, R: is the reflectance and K_o**:** is the extinction coefficient.

The static refractive index (n_o) can be estimated by applying the dispersion relation proposed by Cauchy to the obtained n - λ data. Cauchy's equation is an empirical relationship between the refractive index and wavelength. The most general form of Cauchy's equation is:

$$n(\lambda) = B + \frac{C}{\lambda^2} + \frac{D}{\lambda^4} + \cdots, \qquad \text{..... (2-28)}$$

Where n is the refractive index, λ is the wavelength, B, C, D, etc., are coefficients that can be determined for a material by fitting the n-λ data to equation (2-28) [85].

The static refractive index n_o (the refractive index at zero photon energy) can be obtained by taking the limit of $n_{(\lambda)}$ as $\lambda \rightarrow \infty$ and it is found to be equal to B in equation (2-28)

2.19.2. Extinction Coefficient (K_o)

This represents the extinction occurring in the electromagnetic wave inside the material; it is also represented by the imaginary part of the complex

refraction index and is related to the absorption coefficient by the following relation [78]:

$$K_0 = \frac{\alpha\lambda}{4\pi} \qquad \text{..…….. (2-29)}$$

Where:

K_o **:** is the **e**xtinction coefficient and λ : is the wavelength of incident photon.

2.19.3. Dielectric Constant (ε)

When light is incident on the atoms in the material, a reaction between incident radiation and the charges of the material will happen. This will lead to a polarization of the charges of the material [86].

The dielectric constant can be represented by the flowing equation:-

$$\varepsilon = \varepsilon_1 - i\varepsilon_2 \qquad \text{…….(2-30)}$$

Where ε_1 : is the real part of the complex dielectric constant and ε_2 : is the imaginary part of it. For the calculation of the dielectric constant in its two parts one can use the following expressions:

$$\varepsilon_1 = n^2 - k_o^2 \qquad \text{……. (2-31)}$$

$$\varepsilon_2 = 2nk_o \qquad \text{……. (2-32)}$$

Chapter Three

Experimental Work

3.1. Introduction

This chapter involves the description of all the instruments and devices that were employed in the current study, the deposition parameters and the preparation of chemical solutions used in the study. It starts with the detailed description of the chemical spray pyrolysis system followed by the cleaning procedure and preparation of glass substrates, the discussion of various deposition parameters that may affect the films properties, the chemical reactions involved in the study, and finally the characterization techniques used in order to study the structural and optical properties of the deposited films.

3.2. System of Chemical Spray Pyrolysis:

Figure (3-1) illustrates a schematic diagram of the chemical spray pyrolysis system used in the preset work. The system consists of many simple parts as follows:

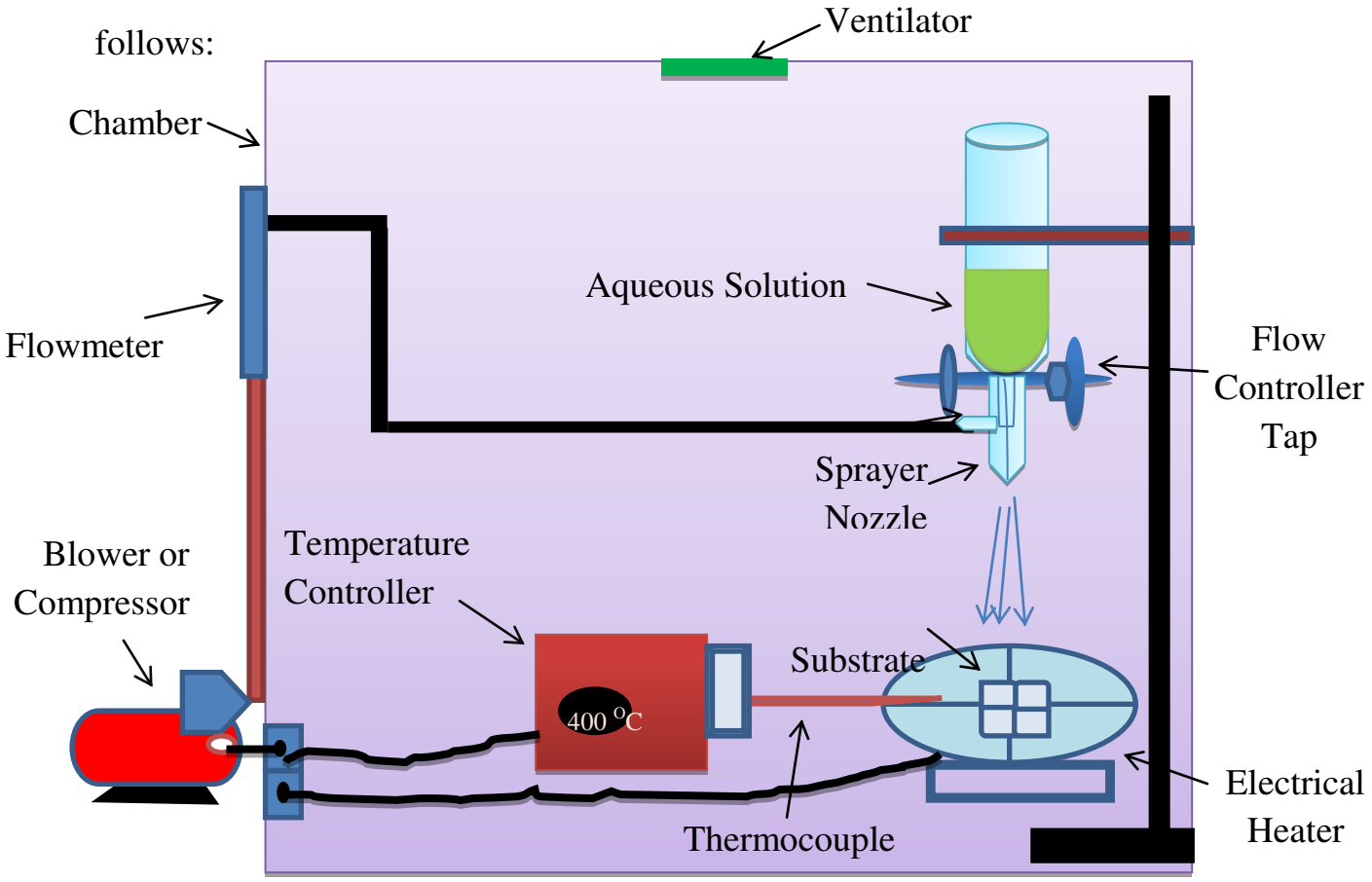

Figure (3-1): Schematic diagram of the chemical spray pyrolysis system used in the preset work.

3.2.1. Sprayer Nozzle

One of the basic advantages of the apparatus used is its simplicity in preparing thin films because it can be made mostly in any glass workshop with a relatively low cost.

The apparatus consists of small bulb of about 100 ml in volume opened from above in circular aperture of 1.5 cm in radius; the small bulb has a height of about 8 cm. The bulb is used as a tank for solutions to be deposited on the substrates. In the bottom of the bulb there is a valve used to control the descending solution to a capillary tube of (0.1 cm) diameter and (6 cm) length.

The glass room is closed from the upper side because it joins the capillary, and it is opened from the bottom surrounding the capillary tube. The glass room has a side opening for the passage of the compressed air which goes out from the bottom opening, thus the out – coming solution is mixed with the compressed air and it will be in a spray form in a direction toward the substrate which the thin film is deposited on it. Figure (3-2) shows the schematic diagram of the sprayer nozzle used in our work.

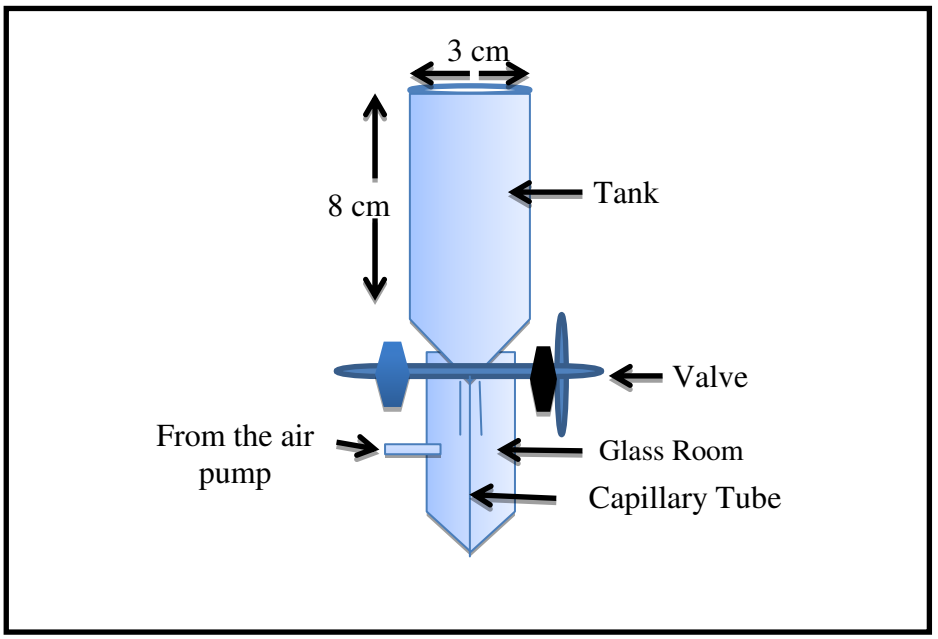

Figure (3-2): Schematic diagram of the spray nozzle.

3.2.2. Electrical Heater

The heater is used for heating the plate on which the glass substrate is placed, to deposit the thin film. In this study the temperature used was 400 ±5 ^{o}C.

3.2.3. Thermocouple

This includes a sensitive thermal wire; it is attached to the hot plate and joined to the digital temperature controller which fixes the temperature of the surface of the plate to the desired value.

3.2.4. Air compressor

The compressor pushes the pressurized air inside the glass room; this leads to make the solution flows from the capillary tube to the glass substrates, as soft spray.

3.2.5. Chamber

The system is placed inside a homemade chamber connected to ventilator to evacuate the hazardous gases.

3-.2.6. Flowmeter

A flowmeter is device used to measure and control the flow rate or quantity of a gas in pipe to sprayer nozzle . It consists of three parts, control valve, nipple pipe and float ball. Figure (3-3) shows the flowmeter device used in the system of the current study.

Figure (3-3): Flowmeter device.

3.3. Parameters Affect The Films Deposition:

3.3.1. Substrate Temperature

The substrate temperature is one of the important parameters in preparing thin films. It has a significant effect upon the homogeneity of the prepared films, because it is responsible for the variation of the crystal structure of the material that affects the physical properties of the materials.

3.3.2. Spraying Rate

This parameter affects the homogeneity and thickness of the prepared films. One can control this parameter via nozzle valve, taking into account that the increment in sprayer rate might cause a significant decrease in substrate temperature and lead to substrate crush.

The spraying rate of the films in this study was kept at (5 ml/min) to ensure a good stoichiometry and obtain a homogenous film.

3.3.3. Spraying Time

Spraying operation should be uniform, thus it is important to control the time period between every spraying. The spraying time period was 10 sec with 2 minutes wait between any two successive sprayings.

3.3.4. Nozzle Distance From The Substrate

The normal distance from the end of the capillary tube to the substrate is one of the important parameters to obtain uniform film. In the present experiment the best height for the nozzle spray was (30) cm, any excess in this distance causes scattering of the atomized solution away from the substrate, also any decrease in this distance will cause the collection of solution drops in one spot and this will affect film homogeneity.

3.3.5. Air Pressure

The air pressure inside the glass room was adjusted to obtain fine atomizes in order to avoid the rapid decrease in substrate temperature which will cause the glass substrate to be broken. In this study the air pressure was kept at (1.5 bar) to get uniform films.

3.3.6. The Drops Size Effect

The size of drops has an important effect to obtain best deposition processes. Figure (3-4) shows the drops size effect on the preparation of homogenous thin films [87]:

Case A:

In this case, the drops size is large; therefore, the absorbed heat is not enough for solution evaporation. So, when the drop collides with the substrate it produces solid precipitate after solvent evaporation with a high decreasing rate in substrate temperature which causes the formation of inner potentials and leads to obtain a heterogeneous thin film and this affects the physical properties of the thin film.

Case B:

This represents the chemical spray pyrolysis operation, which gives the perfect properties for the thin film. In this case, the fine drops will evaporate in a short time before they reach the substrate, i.e. the particles reach the heated substrate as vapor phase, thus it can get enough heat to elevate its temperature, and therefore, the reaction on the substrate will take place.

Case C:

In this case, the drops are dried before they reach the substrate and become as powder on the substrate, which is distributed and condensed as smooth grains on the substrate surface, it can easily be removed because its adhesion to the substrate is weak, this case happens when the spray distance is large.

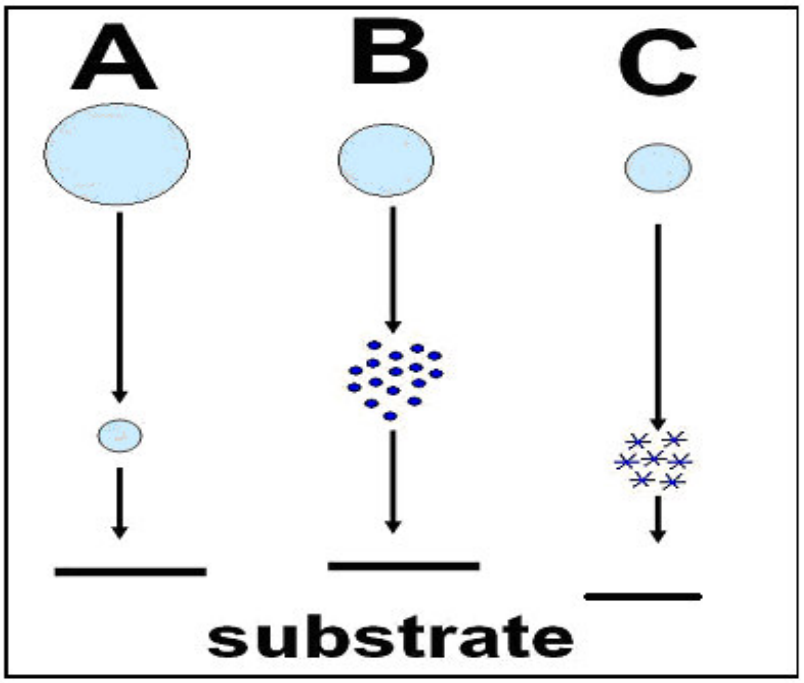

Figure (3-4): The drops size effect.

3.4. Substrates Cleaning

Glass substrates on which $Ni_{(1-x)}Co_xO$ thin films were deposited are soda-lime glass made in china (China National Machinery) of the dimensions of (2.5×2.5) cm^2 and thickness of (0.1) cm. The slides are high-quality glass with low iron content, no green tint is observed and their transparency is high.

The cleaning of the substrate is very important because it has a great effect on the properties of the films. The process can be summarized by the following steps[88]:

1. Cleaning the glass slides by using a cleaning solution to remove any oil or dust that might be on the surface of the substrate and then they are placed in distilled water for ten minutes.

2. Immersing the substrates in a pure alcohol solution which reacts with contamination such as grease and some oxides, this process is fulfilled accurately by rewashing the substrates in the Ultrasonic Bath (Bran sonic 220) for 10 minutes.

3. Placing the glass slides in a clean beaker containing distilled water and then rinsing them in an Ultrasonic Bath for 10 minutes.

4. Drying the slides by wiping them with soft paper or use electrical oven.

3.5.The Raw Materials

The materials used in the present study are:

3.5.1. Nickel Nitrate

Nickel nitrate hexahydrate is a green monoclinic system crystal. table (3-1) shows the physical and chemical properties of Nickel nitrate.

Table (3-1): The physical and chemical properties of Nickel nitrate

Chemical name	Nickel Nitrate
Molecular formula	$Ni(NO_3)_2.6H_2O$
Molecular weight	290.811 g/mol
Color	Green
Density	2.05 g/cm^3
Melting point	56.7°C

3.5.2. Cobalt Nitrate

Superior quality cobalt nitrate which is derived from reacting metallic cobalt or one of its oxides, hydroxides, or carbonate with nitric acid. This cobalt nitrate is commonly used in dyes and inks as well as a common source of cobalt in metal organic frameworks [89]. Table (3-2) shows the physical and chemical properties of Cobalt nitrate.

Table (3-2): The physical and chemical properties of Cobalt nitrate

Chemical name	Cobalt Nitrate
Molecular formula	$Co(NO_3)_2.6H_2O$
Molecular weight	291.03 g/mol
Color	Red
Density	1.87 g/cm^3
Melting point	55°C

3.6. Preparation of The Spray Solution

The $Ni_{(1-x)}Co_xO$ thin films were prepared by spraying aqueous solution of nickel nitrate $Ni(NO_3)_2.6H_2O$ [Shenyang Meiyao Chemical Co, Ltd, China, Purity 99.9% make] and cobalt nitrate $Co(NO_3)_2.6H_2O$ [Shenyang Meiyao Chemical Co, Ltd, China, Purity 99.9% make]. where x= (0, 4, 6, and 8)%. precursor salt with different molarities (0.05M, 0.1 M, 0.15M and 0.2 M). This solution was prepared by dissolving appropriate amount of $Ni(NO_3)_2.6H_2O$, which is a powder of white green with molecular weight of 290.811g/mol, in distilled water and appropriate amount of $Co(NO_3)_2.6H_2O$, which is a powder of red color with molecular weight of 291.03 g/mol, in distilled water too. The appropriate weight (W_t) of the materials $Ni(NO_3)_2.6H_2O$ and $Co(NO_3)_2.6H_2O$ were determined by using the following equation [90]:

$$M = (W_t / M_{wt}) * (1000 / V) \quad \text{.....(3-1)}$$

Where M : is the molar concentration, taken to be equal to (0.05 M-0.2M) for [$Ni(NO_3)_2. 6H_2O$] and [$Co(NO_3)_2. 6H_2O$]

M_{wt} : is the molecular weight of the material (g/mol) .

V : is the volume of distilled water (ml).

W_t: is the weight (g)

The weights of $Ni(NO_3)_2.6H_2O$ and $Co(NO_3)_2.6H_2O$ were measured by sensitive electronic balance (Mettler, AE -160) with four digits (10^{-4} g) sensitivity. Mixing the solutions was carried out by using (Magnetic Stirrer) and leaving the solution for 30 minutes to make sure that no residues were left and to ensure the homogeneity of the resultant solution. The resultant solution was sprayed on glass substrate kept at (400 ±5ºC). When the solution is sprayed, the reaction takes place at the surface of the heated

substrate. The resultant films were stable and have good adhesive properties. Film thickness was estimated by employing the Gravimetric method. The formation of nickel oxide thin films was achieved according to the following chemical reaction [91]:

$$2(Ni(NO_3)_2.6H_2O) \xrightarrow[400^{\circ}C]{\Delta} 2NiO\downarrow + 4NO_2\uparrow + O_2\uparrow + 12(H_2O)\uparrow \quad .....(3\text{-}2)$$

Table (3-3) shows the volumetric ratios of the solutions used in the preparation of thin films.

Table (3-3): Volumetric ratios of the solutions used in the preparation of thin films

Percentage	Solution of $Ni(NO_3)_2.6H_2O$	solution of $Co(NO_3)_2.6H_2O$
Undoped	100	0
(4)%	96	4
(6)%	94	6
(8)%	92	8

3.7. Thickness Measurement

Thickness is one of the most important thin film parameters since it largely determines the properties of the film. The thickness of the films is usually measured by monitoring the rate of the deposition during the coating process. However there are several methods used for measuring thickness of the film, such as gravimetric, optical, electrical and other methods. In the current experiment the thickness of the thin films was measured by the gravimetric method.

The Gravimetric Method

This method is done by using sensitive electronic balance (Mettler, AE - 160) with four digits sensitivity (10^{-4} g). The substrates are weighted before and after deposition. From the weight difference and the area of substrate, the thin film thickness (t) can be measured, according to the following equation [92]:

$$t = \frac{\Delta m}{\rho_0 A_s} \qquad \text{.....(3-3)}$$

Where:

Δm: is the weight difference of substrate. This means that it is the mass of the thin film (g).

A_s: area of the thin film (cm^2), ρ_0: the density of material of the thin film (6.67 g/ cm^3) for nickel oxide and (6.45 g/ cm^3) for cobalt oxide, the density of material calculated from:

Total density(ρ_o)=density of NiO x its percentage in the solution + density of CoO x its percentage in the solution . .....(3-4)

3.8. Structural Measurements

X-ray diffraction (XRD) analysis was used to investigate the crystal structure of ($Ni_{(1-x)}Co_xO$) thin films. When incident (X-ray) beam of mono wavelength diffracts on film surface this will exhibit peaks on specific angles for each material because of Bragg's reflection on parallel crystalline surface. The X-ray diffraction instrument used in this study (Shimadzu 6000) having the following properties:

1. Source: Cu k_α radiation of λ=1.5406 Å .
2. Current: 30 mA.

3. High voltage: 40 kV.

4. Speed : 5 deg / min

5. Incident angle from 20 to 70 degrees.

3.9. Atomic Force Microscope (AFM)

Atomic Force Microscopy studies were made by using (Scanning probe Microscope type (SPM- AA3000), contact mode, supplied by Angstrom Advanced Inc.2008, USA.

3.10. Optical Measurements

The optical transmission and absorption spectra of the ($Ni_{(1-x)}Co_xO$) thin films in the visible and NIR regions (300 -900 nm) have been recorded using (UV–Visible1800 Double beam spectrophotometer) made by (Shimadzu), Japanese company. Substrate transmission was recorded by placing an identical glass substrate in the reference beam. The data from transmission spectrum can be used in the calculation of the optical constants. A computer program (Origin) was employed to obtain the optical constants, absorption coefficient (α), extinction coefficient (K_o) and refractive index (n) of ($Ni_{(1-x)}Co_xO$) thin films.

Chapter Four

Results and Discussion

4.1. Introduction

This chapter includes the description and the analysis of the measurements and the discussion of the results. It focuses on the structural and optical properties of Nickel-Cobalt Oxide ($Ni_{(1-x)}Co_xO$) thin films, where x = 0, 4, 6 and 8 % with different molarities (0.05, 0.1, 0.15 and 0.2 M). These films have been deposited on glass substrates by chemical spray pyrolysis (CSP) technique at substrate temperature equal to (400 ±5 ^oC) and thickness of about 300 ±10 nm.

Figure (4-1) shows the photo images of Nickel-Cobalt Oxide ($Ni_{(1-x)}Co_xO$) thin films, where x = 0, 4, 6 and 8 % with different molarities (0.05, 0.1, 0.15 and 0.2 M). It is reported that the stoichiometrically correct NiO thin films are expected to have green color [16]; however, the undoped NiO thin films deposited in the present study have black-grey color which can be attributed to non-stoichiometry of the deposited material. It can also be observed that the Co-doped NiO thin films are accompanied by a color change from black to orange. This change of color is attributed to the cobalt doping. It can be noticed also that the color density of the deposited films increases as Co-concentration and molarity increase.

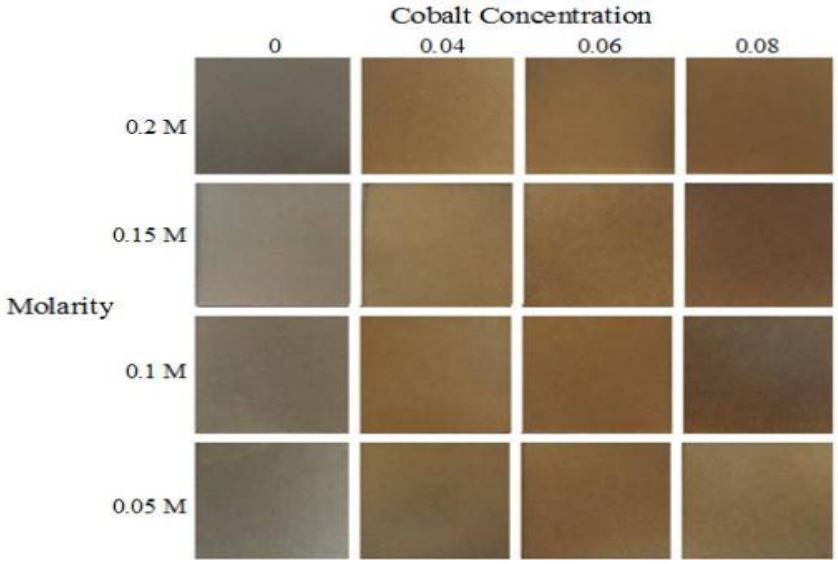

Figure (4-1): Photo image of Nickel-Cobalt Oxide thin films deposited in the present study.

4.2. Structural Analysis

XRD patterns of all the deposited samples of Nickel-Cobalt Oxide thin films are shown in figures (4-2), (4-3), (4-4) and (4-5). From the figures, it can be noticed that all the patterns exhibit diffraction peaks around (2θ~37^o, 43^o and 63^o) referred to (111), (200), and (220) favorite directions respectively which is in agreement with the Joint Committee of Powder Diffraction Standards (JCPDS) card number 04-0835 as shown in figure (4-6). The strongest peak occurs at 2θ~37^o which is referred to (111) plane. The positions of the peaks and the presence of more than one diffraction peak lead to the conclusion that the films are polycrystalline in nature with a cubic crystalline structure, which is in agreement with other reports [42, 43].

Figure (4-2) shows the XRD patterns of the undoped (NiO) thin films at different molarities. It can be observed that the films are polycrystalline in nature with cubic structure. The intensity of the peak corresponding to (111) plane increases as the molarity increases except for the sample deposited at 0.1 M. It can be noticed that 2θ for (111) direction decreases with molarity increasing, which is in agreement with other studies [44], as shown in table (4-1). The average crystallite size of the films was estimated for (111) direction by Scherrer formula and it was maximum (~51nm) for the film prepared at 0.1 M.

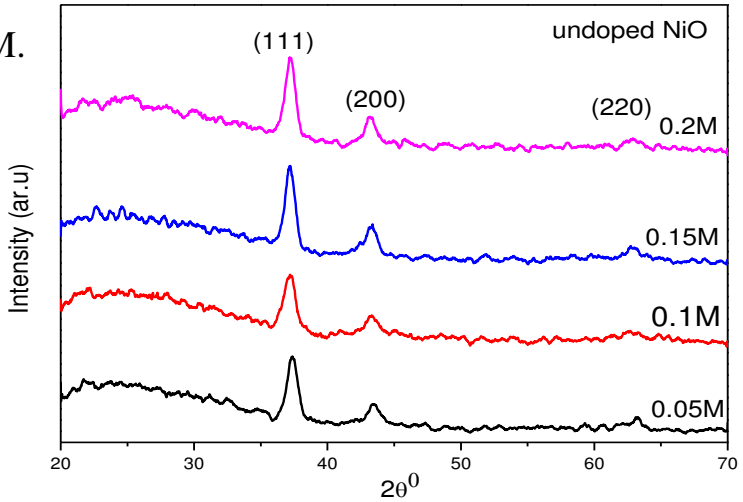

Figure (4-2): XRD patterns of undoped (NiO) thin films at different molarities.

Table (4-1): X-ray diffraction data of undoped NiO thin films at different molarities.

	Molarity (M)	2Θ (deg)	d (Å)	*hkl*
Undoped NiO	0.05	37.3854	2.40347	(111)
		43.4816	2.0796	(200)
		63.2233	1.46959	(220)
	0.1	37.2539	2.41167	(111)
		43.3017	2.08782	(200)
		62.2283	1.46949	(220)
	0.15	37.2260	2.41341	(111)
		43.2617	2.08966	(200)
		62.5935	1.48286	(220)
	0.2	37.1826	2.41613	(111)
		43.1818	2.09334	(200)
		62.8834	1.47672	(220)

Table (4-2) shows the lattice constant (a_o) and texture coefficient (T_c) for the undoped NiO thin films.

Table (4-2): XRD results of the undoped NiO thin films at different molarities.

undoped NiO				
Molarity (M)	0.05	0.1	0.15	0.2
2Θ (deg)	37.3854	37.2539	37.2260	37.1826
hkl	(111)	(111)	(111)	(111)
d (Å)	2.40347	2.41167	2.41341	2.41613
(FWHM) (rad)	0.0136	0.0028	0.0118	0.0134
(D_{av}) nm	10.76	51.16	12.33	10.84
Lattice Constants a_o (Å)	4.1629	4.1771	4.1802	4.1848
T_c	1.92	1.72	1.89	2.18

It is clear that the texture coefficient T_c values are >1 for all films indicating that there are numerous grains in the (111) favorite direction. It can be noticed also that the lattice constant (a_o) increases as the molarity increases. It should be mentioned here that the standard a_o value for NiO is 4.176 Å as shown in figure (4-6) which indicates that the film prepared at 0.1M has the nearest a_o value to the standard lattice constant.

Figure (4-3) shows XRD patterns of ($Ni_{0.96}Co_{0.04}O$) thin films at different molarities. Ones can observe that there is a little shift of 2θ location. The shift in peak position is may be due to the variation of the ionic radius of the Co dopant (Ni= 0.69Å, Co=0.745Å). It can be observed that no peaks correspond to the Co dopping exist in the XRD patterns. In fact, doping with low concentration impurities does not result in the appearance of new XRD peaks, but instead leads to a shift in the lattice parameters of the host material. This shift may arise from the strain induced when the dopant is incorporated into the crystal lattice [93]. The intensity of the (111) plane increases as the molarity increases. The average crystallite size of the films was estimated for (111) direction by Scherrer formula and it was maximum (~ 44.94nm) for the film prepared at 0.05 M.

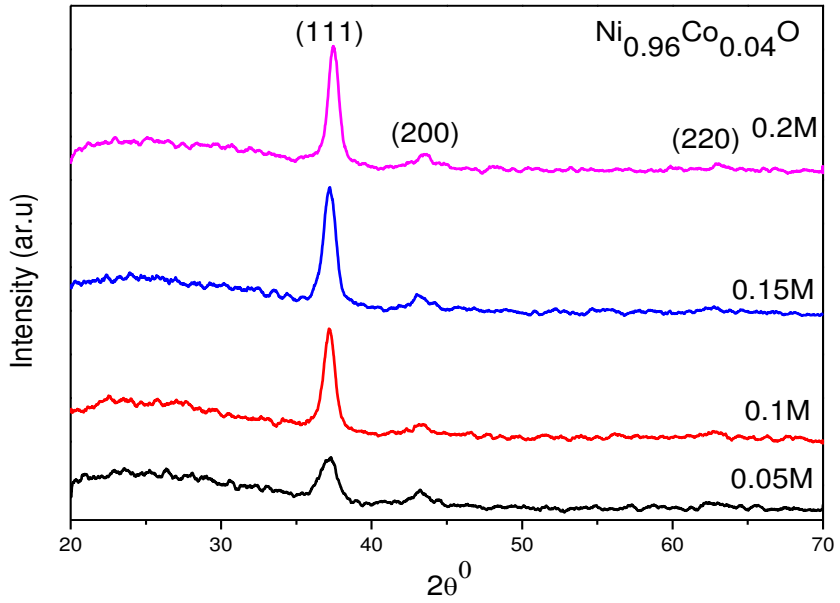

Figure: (4-3): XRD patterns of ($Ni_{0.96}Co_{0.04}O$) thin films at different molarities.

Table (4-3): X-ray diffraction data of $Ni_{0.96}Co_{0.04}O$ thin films at different molarities.

	Molarity (M)	2Θ (deg)	d (Å)	*hkl*
$Ni_{0.96}Co_{0.04}O$	0.05	37.4024	2.40244	(111)
		43.0884	2.09766	(200)
		63.5082	1.46368	(220)
	0.1	37.1893	2.41571	(111)
		43.4816	2.07960	(200)
		62.7234	1.48010	(220)
	0.15	37.2093	2.41446	(111)
		43.2318	2.09103	(200)
		62.8134	1.47819	(220)
	0.2	37.4608	2.39883	(111)
		43.5416	2.07687	(200)
		62.9234	1.47587	(220)

Table (4-4) shows the lattice constant (a_o) and texture coefficient (T_c) for the $Ni_{0.96}Co_{0.04}O$ thin films.

Table (4-4): XRD results of $Ni_{0.96}Co_{0.04}O$ thin films at different molarities.

$Ni_{0.96}Co_{0.04}O$				
Molarity (M)	0.05	0.1	0.15	0.2
2Θ (deg)	37.4024	37.1893	37.2093	37.4608
hkl	(111)	(111)	(111)	(111)
d (Å)	2.40244	2.41571	2.41446	2.39883
(FWHM) (rad)	0.0054	0.0134	0.0155	0.012
(D_{av}) nm	44.94	10.85	9.38	12.13
Lattice Constants a_o (Å)	4.1586	4.1896	4.1884	4.1548
T_c	1.58	2.46	1.85	2.56

It is clear that the texture coefficient T_c values are >1 for all films indicating that there are numerous grains in the (111) favorite direction. The film prepared at 0.15M has the nearest a_o value to the standard lattice constant (4.176 Å).

Figure (4-4) shows the XRD patterns of $(Ni_{0.94}Co_{0.06}O)$ thin films at different molarities. It can be noticed that 2θ for (111) direction decreases with molarity increasing, as shown in table (4-5). The intensity of the peak corresponding to (111) plane increases as the molarity increases except for the sample deposited at 0.1 M. The average crystallite size of the films was estimated for (111) direction by Scherrer formula and it was maximum (~ 12nm) for the film prepared at 0.05 M.

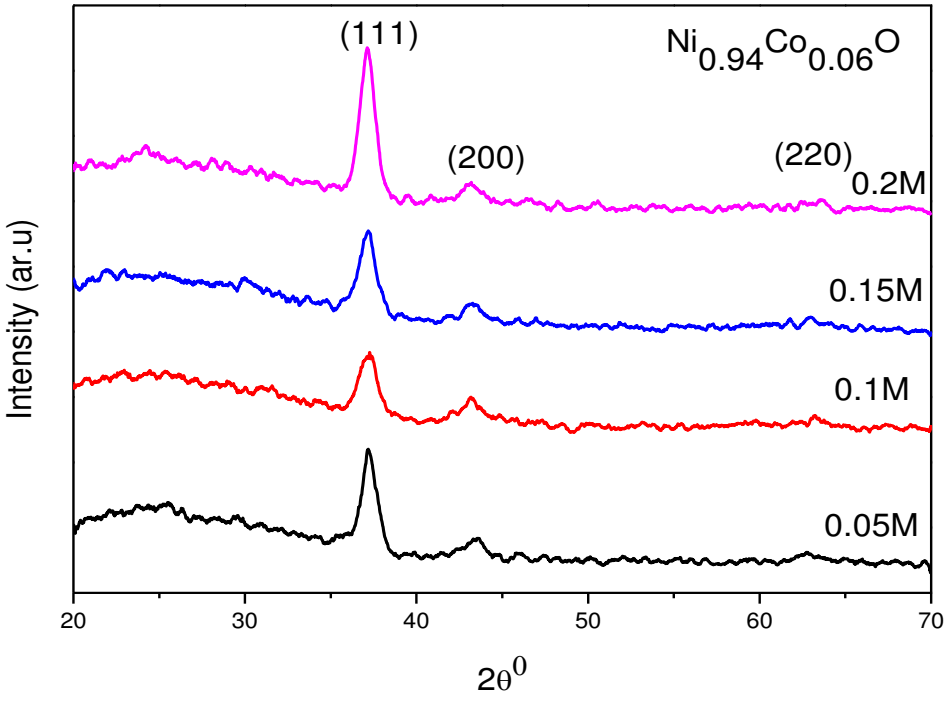

Figure (4-4): XRD patterns of $(Ni_{0.94}Co_{0.06}O)$ thin films at different molarities.

Table (4-5): X-ray diffraction data of $Ni_{0.94}Co_{0.06}O$ thin films at different molarities.

	Molarity (M)	2Θ (deg)	d (Å)	*hkl*
$Ni_{0.94}Co_{0.06}O$	0.05	37.2459	2.41217	(111)
		43.5216	2.07778	(200)
		62.7834	1.47883	(220
	0.1	37.146	2.41843	(111)
		43.2118	2.09195	(200)
		63.2133	1.46980	(220)
	0.15	37.126	2.41969	(111)
		42.852	2.10868	(200)
		62.9534	1.47524	(220)
	0.2	37.116	2.42031	(111)
		43.2218	2.09149	(200)
		63.6431	1.46091	(220)

Table (4-6) shows the lattice constant (a_o) and texture coefficient (T_c) for the $Ni_{0.94}Co_{0.06}O$ thin films.

Table (4-6): XRD results of $Ni_{0.94}Co_{0.06}O$ thin films at different molarities.

$Ni_{0.94}Co_{0.06}O$				
Molarity (M)	0.05	0.1	0.15	0.2
2Θ (deg)	37.2459	37.1460	37.126	37.116
hkl	(111)	(111)	(111)	(111)
d (Å)	2.41217	2.41843	2.41969	2.42031
(FWHM) (rad)	0.0115	0.0177	0.016	0.0163
(D_{av}) nm	12.71	8.22	9.11	8.91
Lattice Constants a_o (Å)	4.178	4.1841	4.1921	4.191
T_c	2.18	1.68	2.31	2.57

It is clear that the texture coefficient T_c values are >1 for all films indicating that there are numerous grains in the (111) favorite direction. It can be noticed also that the lattice constant (a_o) increases rabidly as the molarity increases. It should be mentioned here that the standard a_o value for NiO is 4.176 Å as shown in figure (4-6) which indicates that the film prepared at 0.05M has the nearest a_o value to the standard lattice constant.

Figure (4-5) shows the XRD patterns of ($Ni_{0.92}Co_{0.08}O$) thin films at different molarities. It can be observed that the films are polycrystalline in nature with cubic structure. It can be noticed that 2θ for (111) direction increases with molarity decreasing, as shown in table (4-7). The intensity of the peak corresponding to (111) plane decreases as the molarity increases. The average crystallite size of the films was estimated for (111) direction by Scherrer formula and it was maximum (~ 49nm) for the film prepared at 0.2 M.

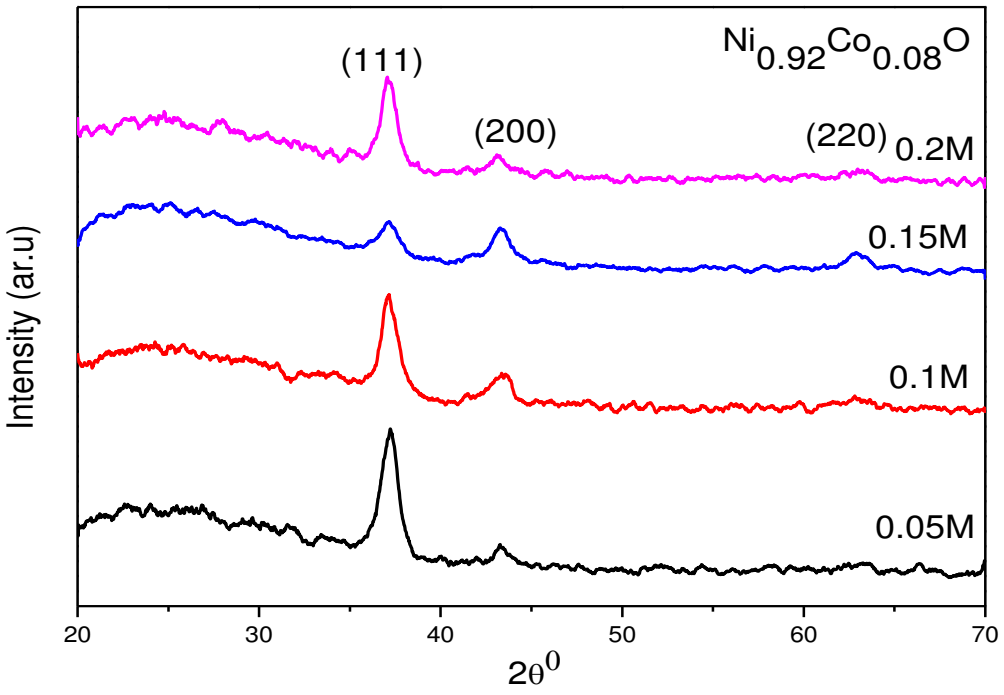

Figure (4-5): XRD pattern of ($Ni_{0.92}Co_{0.08}O$) thin films at different molarities.

Table (4-7): X-ray diffraction data of $Ni_{0.92}Co_{0.08}O$ thin films at different molarities.

	Molarity (M)	2Θ (deg)	d (Å)	*hkl*
$Ni_{0.92}Co_{0.068}O$	0.05	37.1760	2.41655	(111)
		43.411	2.08278	(200)
		63.2533	1.46897	(220)
	0.1	37.1810	2.41623	(111)
		43.7015	2.06964	(200)
		62.7634	1.47925	(220)
	0.15	37.236	2.41279	(111)
		43.3317	2.08644	(200)
		62.9134	1.47608	(220)
	0.2	37.4265	2.40094	(111)
		43.1543	2.09461	(200)
		62.8384	1.47766	(220)

Table (4-8) shows the lattice constant (a_o) and texture coefficient (T_c) for the $Ni_{0.92}Co_{0.08}O$ thin films.

Table (4-8): XRD results of $Ni_{0.92}Co_{0.08}O$ thin films at different molarities.

$Ni_{0.92}Co_{0.08}O$				
Molarity (M)	0.05	0.1	0.15	0.2
2Θ (deg)	37.1760	37.1810	37.236	37.4265
hkl	(111)	(111)	(111)	(111)
d (Å)	2.41655	2.41623	2.41579	2.41438
(FWHM) (rad)	0.0167	0.0144	0.0052	0.003
(D_{av}) nm	8.75	10.1	27.97	49.51
Lattice Constants a_o (Å)	4.1855	4.1850	4.1788	4.1585
T_c	1.8	2.18	1.08	1.93

It is clear that the texture coefficient T_c values are >1 for all films indicating that there are numerous grains in the (111) favorite direction. It can be noticed also that the lattice constant (a_o) decreases as the molarity increases. The film prepared at 0.15M has the nearest a_o value to the standard lattice constant.

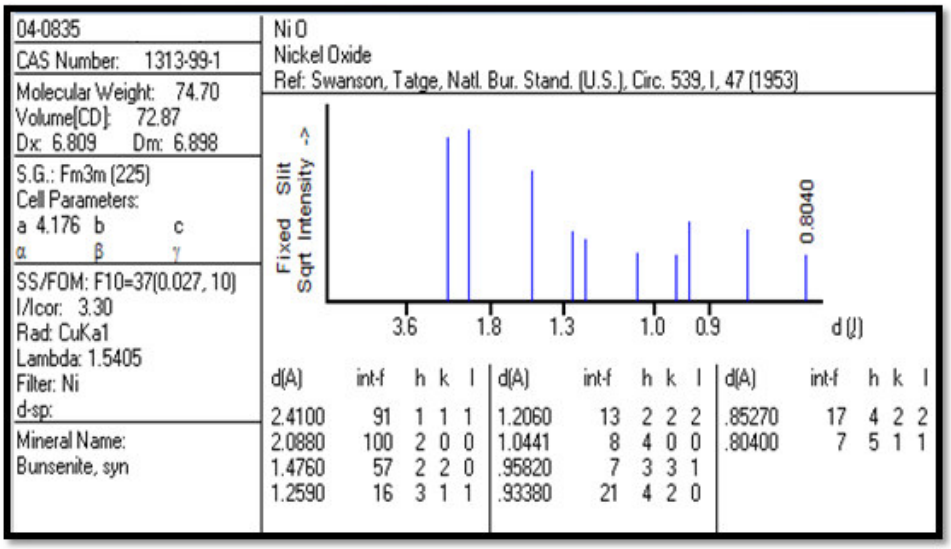

Figure (4-6): (JCPDS) card number 04-0835**.**

4.2.1. The crystallite size (D_{av})

I. Calculation of crystallite size using Scherrer formula:

The crystallite size of Nickel-Cobalt Oxide ($Ni_{(1-x)}Co_xO$) thin films, where x = 0, 4, 6 and 8 % prepared with different molarities (0.05, 0.1, 0.15 and 0.2 M) can be calculated by using Scherrer formula (2-3) for the (111) plane. Figure (4-7) shows the crystallite size as a function of molarity values for all samples. It is observed that the crystallite size for the undoped NiO thin films increases as the molarity increases from 0.05M to 0.1M to reach its maximum value of (51.16nm). The crystallite size then decreases as the molarity increases further to reach its minimum value of (10.84nm) at 0.2M as shown in figure (4-7). The crystallite size for the ($Ni_{0.96}Co_{0.04}O$) thin films decreases from (44.94 nm) as the molarity increases from 0.05M to 0.15M to reach its minimum value of (9.38nm). The crystallite size then

increases slowly as the molarity increases further to reach the value of (12.13nm) at 0.2M as shown in figure (4-7). The ($Ni_{0.94}Co_{0.06}O$) thin films decrease as the molarity increases from 0.05M to 0.1M to reach the value of (8.22 nm). The crystallite size then increases as the molarity increases further to reach the value of (8.91nm) at 0.2M as shown in figure (4-7). The ($Ni_{0.92}Co_{0.08}O$) thin films increase as the molarity increases from 0.05M to 0.2M to reach its maximum value of (49.51nm)[42]. The larger crystallite size values indicate better crystallization of the films. as shown in figure (4-7).

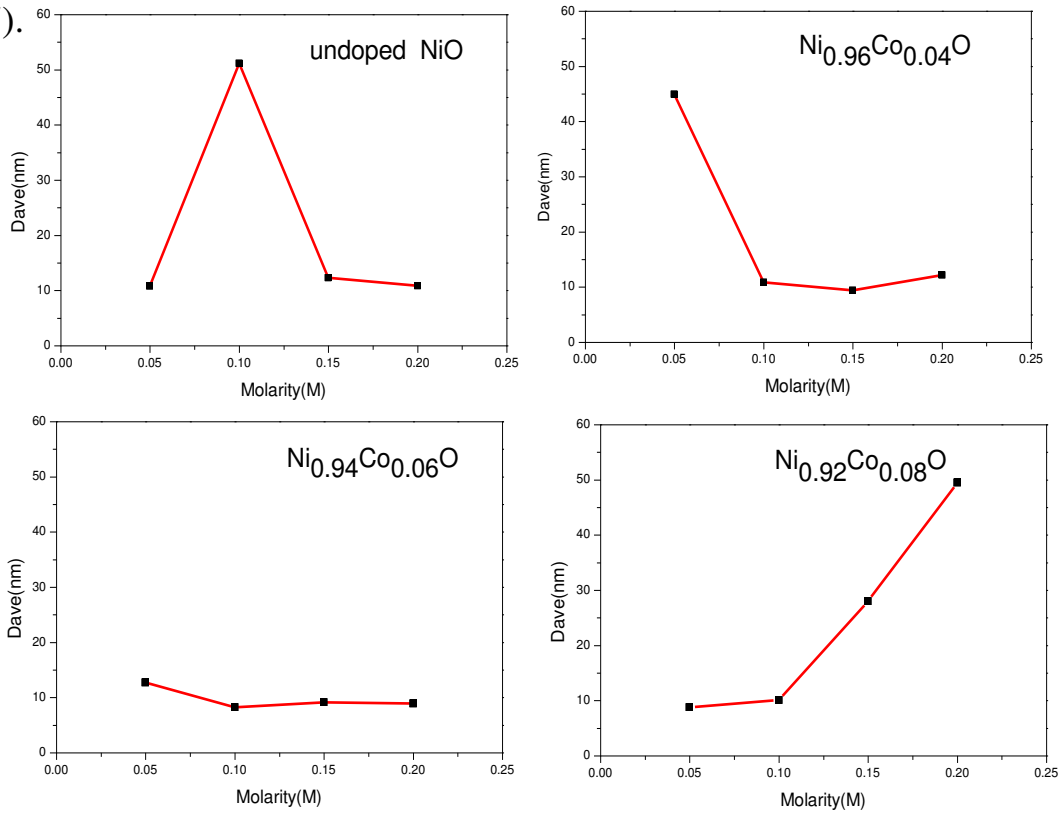

Figure(4-7): The crystallite size (D_{av}) of ($Ni_{(1-x)}Co_xO$) thin films, where x = 0, 4, 6 and 8 % at different molarities.

II. Calculation of crystallite size by Willamson-Hall analysis:

The crystallite size can be estimated using W-H equation (2-6) for (111), (200) and (220) planes. A plot is drawn with ($4\sin\theta$) along the x-axis and ($\beta_{hkl}\cos\theta$) along the y-axis for ($Ni_{(1-x)}Co_xO$) thin films as shown in figures (4-8), (4-9), (4-10) and (4-11). From the linear fit of the data, the crystallite size was estimated from the y-intercept, and the microstrain S, from the

slope of the fit. The micro strains are induced during the growth of thin films, and will be raised from stretching or compression in the lattice. The strain broadening is caused by varying displacements of the atoms with respect to their reference lattice positions [47, 66]. From the results, it was observed that the strain value decreased but the particle size increased [67, 94, 95]. Figures (4-8), (4-9), (4-10) and (4-11) show the W-H plots for all samples and table (4-9) summarizes the results obtained from W-H analysis. The crystallite size values calculated by scherrer formula were depicted in table (4-9) for comparison.

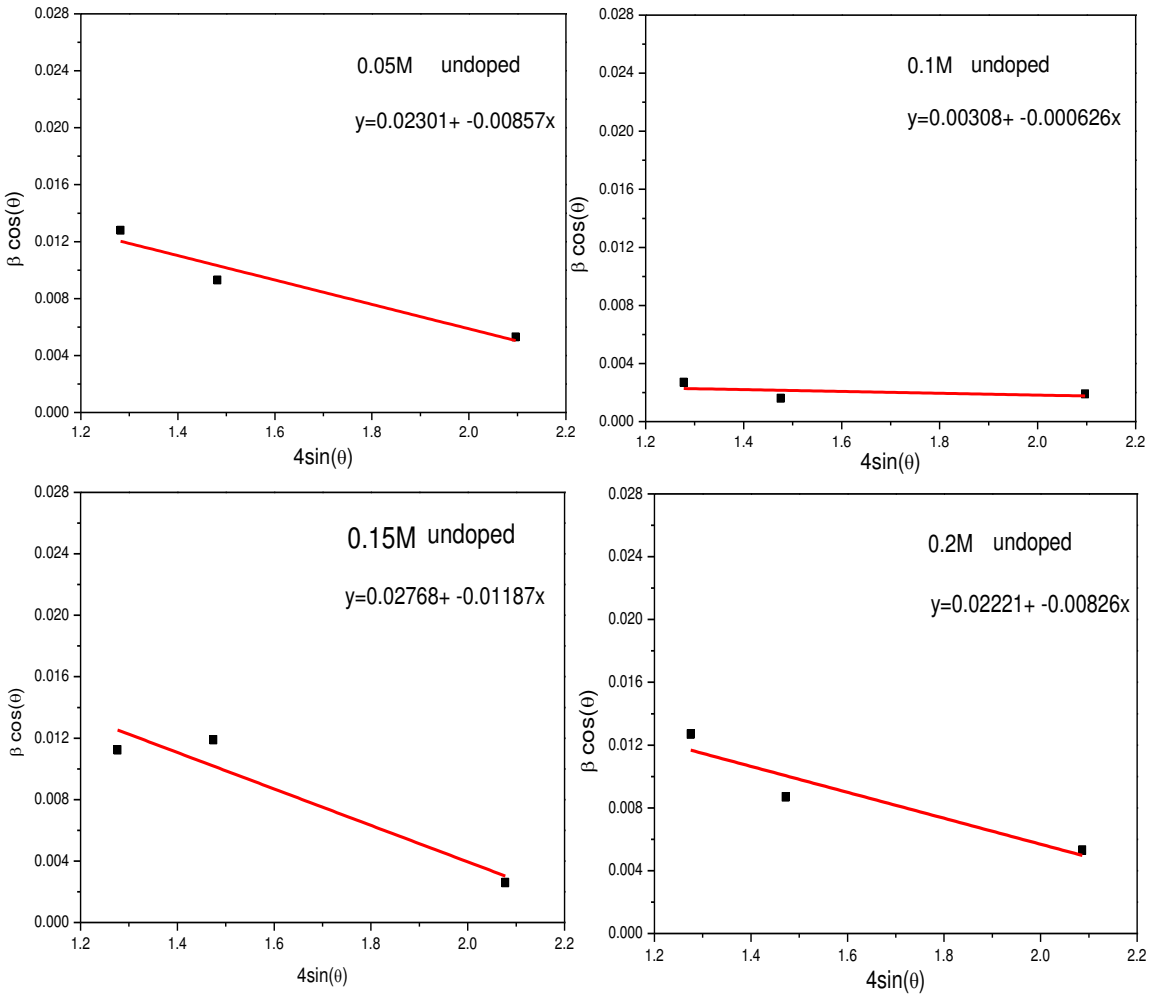

Figure (4-8): The W-H analysis of undoped NiO thin films at different molarities.

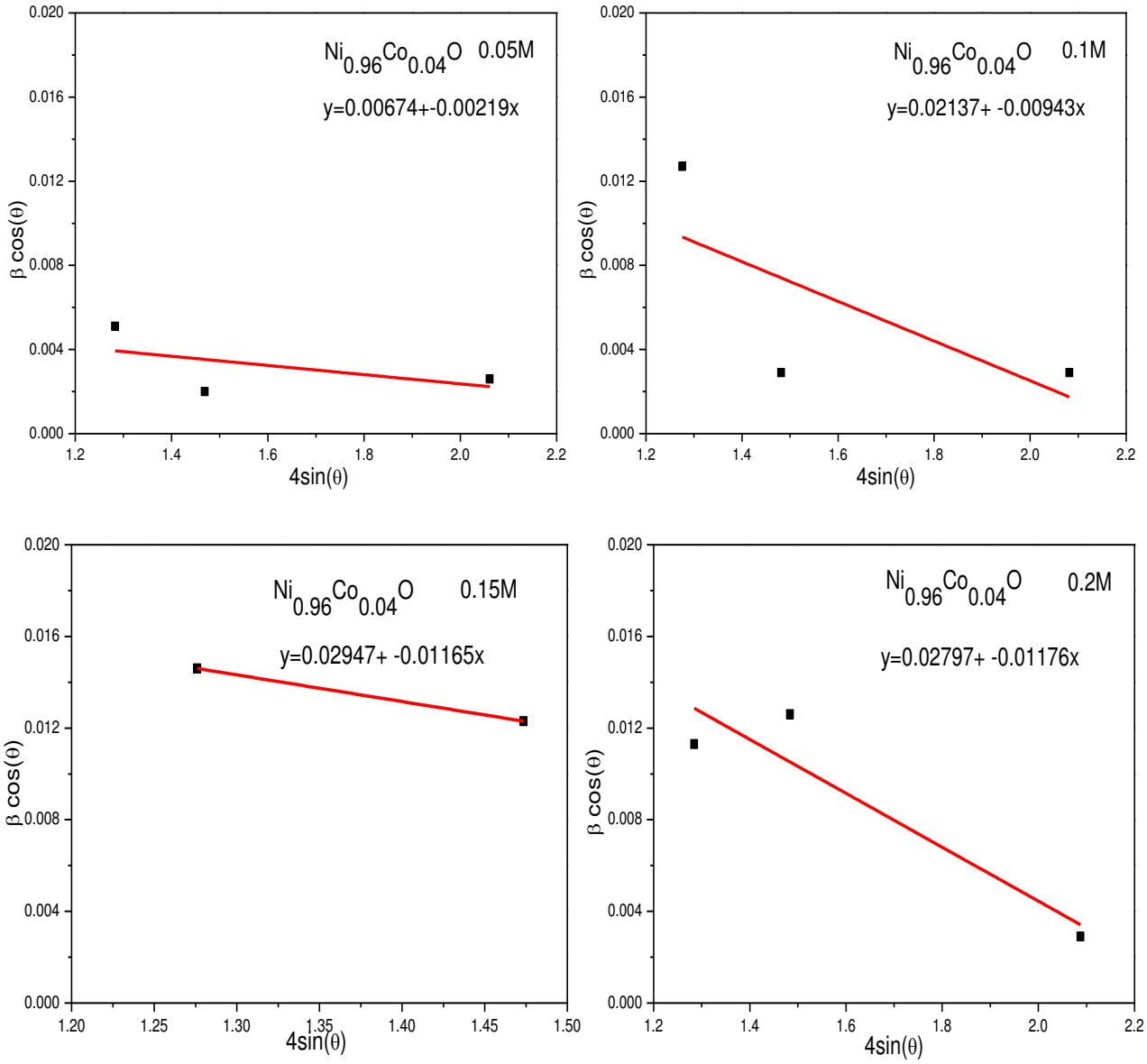

Figure (4-9): The W-H analysis of $Ni_{0.96}Co_{0.04}O$ thin films at different molarities.

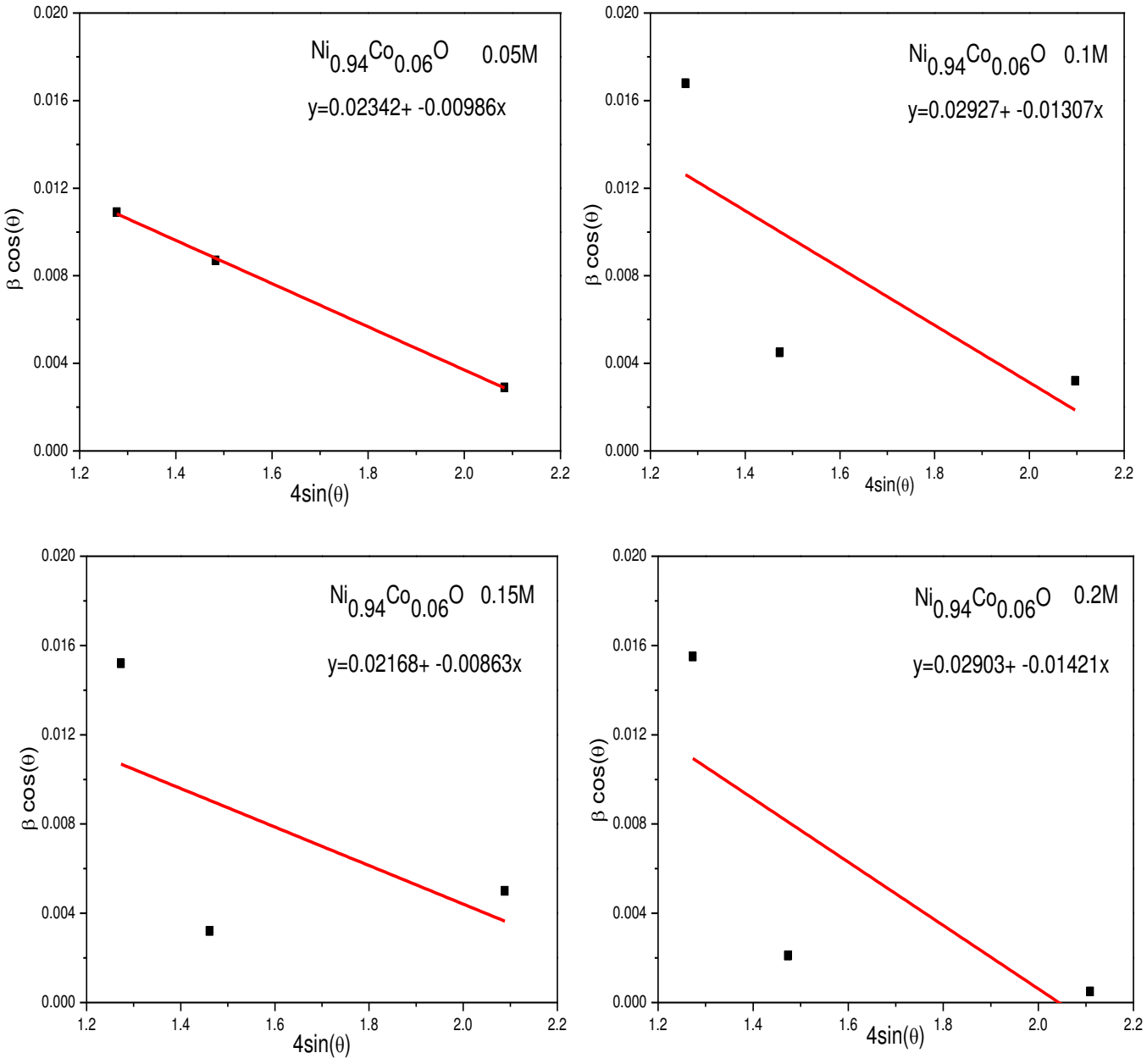

Figure (4-10): The W-H analysis of $Ni_{0.94}Co_{0.06}O$ thin films at different molarities.

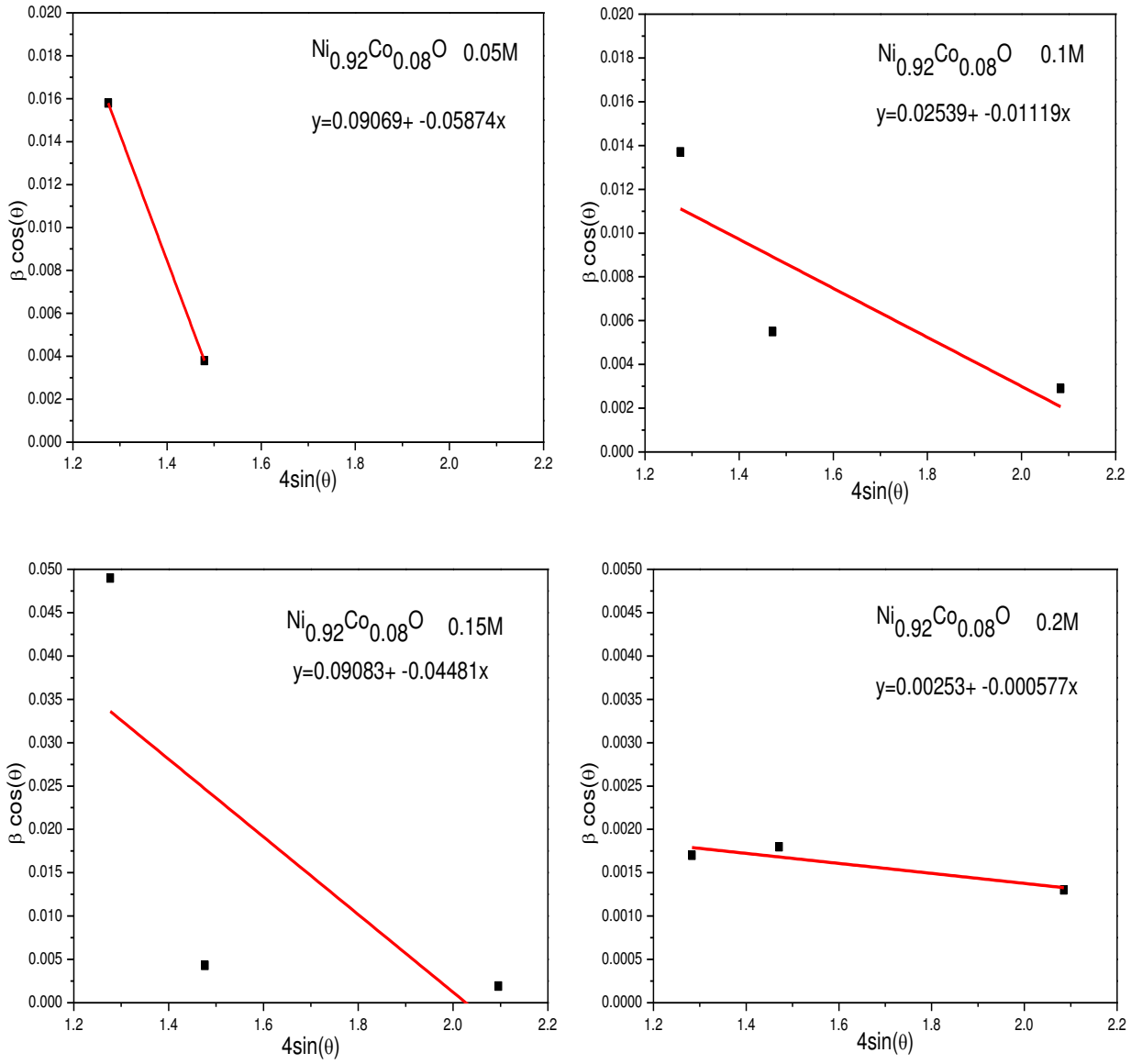

Figure (4-11): The W-H analysis of $Ni_{0.92}Co_{0.08}O$ thin films at different molarities.

The values of microstrains were negative for all samples which indicates the occurrence of compression in the lattice.

Table (4-9): Crystallite size by using Scherrer formula and Williamson-Hall methods and the microstrain induced in the prepared films.

Molarity (M)	undoped NiO			$Ni_{0.96}Co_{0.04}O$		
	D(nm) Scherrer	D(nm) W-H	Micro strain S $*10^{-3}$	D(nm) Scherrer	D(nm) W-H	Micro strain S $*10^{-3}$
0.05	10.76	6.02	-8.57	44.94	20.57	-2.19
0.1	51.16	45.01	-0.62	10.85	6.48	-9.43
0.15	12.33	5	-11.87	9.38	4.7	-11.65
0.2	10.84	6.24	-8.26	12.13	4.95	-11.76
	$Ni_{0.94}Co_{0.06}O$			$Ni_{0.92}Co_{0.08}O$		
	D(nm) Scherrer	D(nm) W-H	Micro strain S $*10^{-3}$	D(nm) Scherrer	D(nm) W-H	Micro strain S $*10^{-3}$
0.05	12.71	5.92	-9.86	8.75	1.52	-58.74
0.1	8.22	4.73	-13.07	10.1	5.46	-11.9
0.15	9.11	6.39	-8.63	27.97	1.52	-44.81
0.2	8.91	4.77	-14.21	49.51	5.48	-0.57

4.2.2. Dislocation Density (δ)

The dislocation density is the measure of amount of defects in a crystal. The small value of dislocation density obtained in the present work confirmed good crystallinity of the Nickel-Cobalt Oxide thin films fabricated by employing spray pyrolysis technique. It can be seen that the dislocation density of prepared films have values in the range of (0.3 to 14.8)10^{-17} cm^{-2}, as shown in table (4-10). which is in agreement with other studies [42],

4.2.3. The Number of crystals (N_o)

The number of crystals per unit area was calculated using equations (2-9), It can be seen that the number of crystals of prepared films have values in the range of (2.4 to 540.1)$10^{-17}$$cm^{-2}$ as shown in table (4-10).

Table (4-10): Dislocation density (δ) and number of crystallites (N_o) for the Nickel-Cobalt Oxide thin films.

undoped NiO					$Ni_{0.96}Co_{0.04}O$			
Molarity (M)	0.05	0.1	0.15	0.2	0.05	0.1	0.15	0.2
$\delta *10^{-17}$ $(cm)^{-2}$	8.6	0.3	6.5	8.5	0. 4	8.4	11.3	6.7
N_o*10^{-17} $(cm)^{-2}$	240.5	22	160	235.2	3.3	234.7	363.5	168
$Ni_{0.94}Co_{0.06}O$					$Ni_{0.92}Co_{0.08}O$			
Molarity (M)	0.05	0.1	0.15	0.2	0.05	0.1	0.15	0.2
$\delta *10^{-17}$ $(cm)^{-2}$	6.1	14.8	12	12.5	13	9.7	1.2	0.4
N_o*10^{-17} $(cm)^{-2}$	146.11	540.1	396.7	242	447.8	291.1	13.4	2.4

4.3.Results of Atomic Force Microscope (AFM)

The morphological investigation of Nickel-Cobalt Oxide ($Ni_{(1-x)}Co_xO$) thin films, where x = 0, 6 and 8 % with different molarities (0.05M, 0.1 M, 0.15M and 0.2 M), deposited on glass substrates at 400 ±5 ^oC was accomplished by using AFM. The size of the scanned area was (2x2) μm^2. Figure (4-12) shows the AFM images of undoped NiO thin films synthesized at different molarities. The average grain size, average roughness and root mean square (RMS) roughness for undoped NiO, estimated from AFM, are given in Table (4-11). The samples prepared at molarity of 0.1M has highest average grain size, average roughness and RMS roughness of the film. The increasing of the grain size may be caused by columnar grain growth in the structure, which is in agreement with other studies [43].

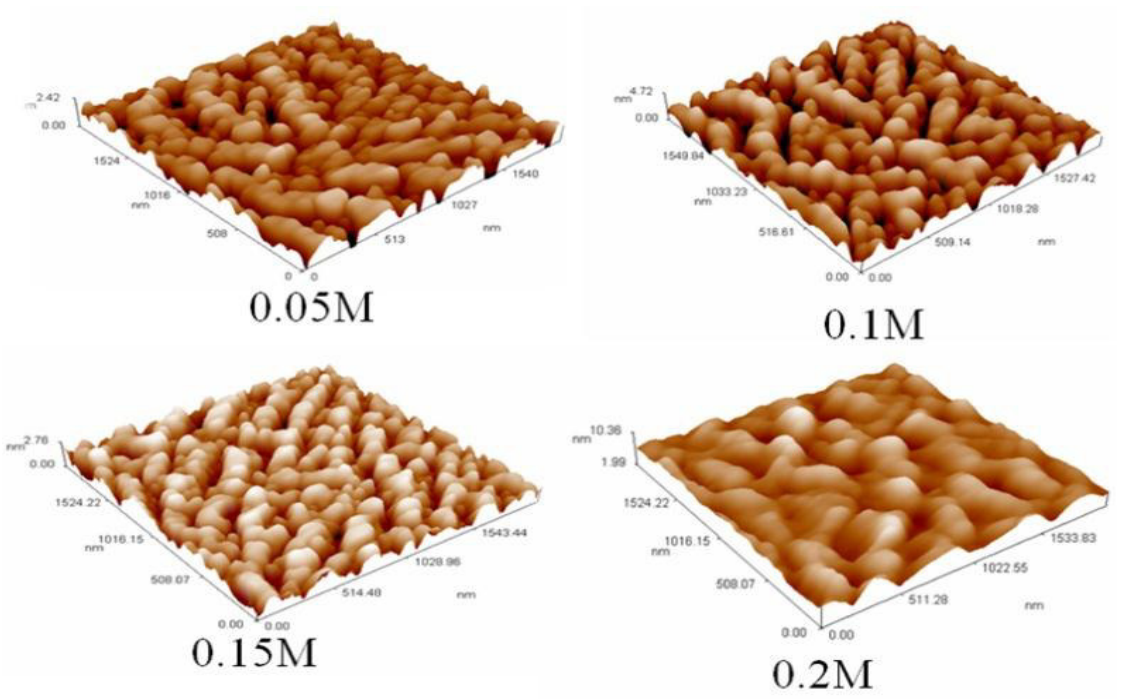

Figure (4-12): 3D AFM images of undoped NiO thin films at different molarities.

The grain size values shown in table (4-11), (4-12) and (4-13) are estimated from the granularity report which is generated by the AFM instrument through a special computer program.

Table (4-11): Surface roughness, root mean square (RMS) and grain size of undoped NiO thin films at different molarities.

undoped NiO			
Molarity (M)	Surface roughness (nm)	RMS (nm)	Grain size (nm)
0.05	0.378	0.459	83.84
0.1	0.89	1.05	133.8
0.15	0.517	0.615	98.77
0.2	0.864	1.1	98

Figure (4-13) shows the AFM images of $Ni_{0.94}Co_{0.06}O$ thin films synthesized at different molarities. The average grain size, average roughness and root mean square (RMS) roughness for $Ni_{0.94}Co_{0.06}O$, estimated from AFM, are given in Table (4-12). The sample prepared at molarity of 0.05M has highest grain size, average roughness and RMS roughness of the film. The results of grain size obtained from AFM investigation are qualitatively in agreement with those obtained from XRD analysis shown in Table (4-6).

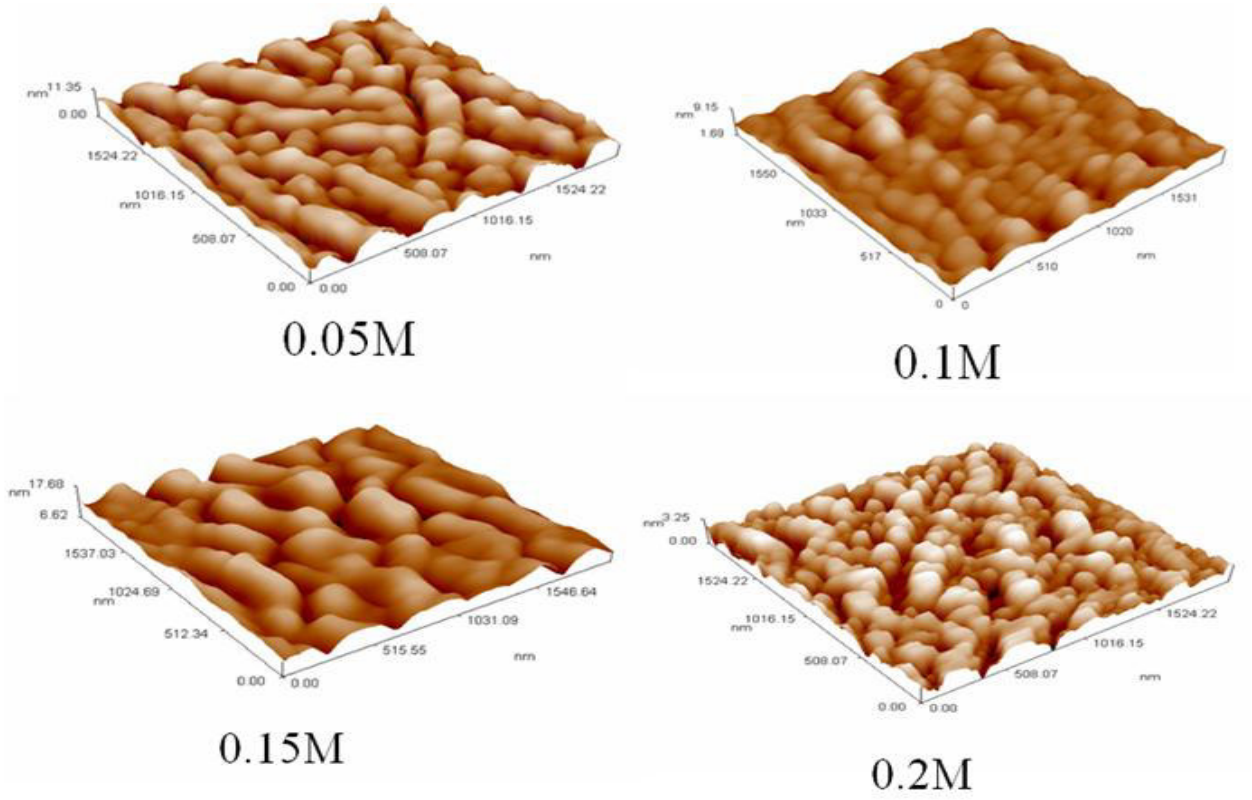

Figure (4-13): 3D AFM images of $Ni_{0.94}Co_{0.06}O$ thin films at different molarities.

Table (4-12): Surface roughness, root mean square (RMS) and grain size of $Ni_{0.94}Co_{0.06}O$ thin films at different molarities.

$Ni_{0.94}Co_{0.06}O$			
Molarity (M)	Surface roughness (nm)	RMS (nm)	Grain size (nm)
0.05	1.88	2.26	139.38
0.1	0.634	0.829	131.15
0.15	1.4	1.77	132.93
0.2	0.577	0.697	91.08

Figure (4-14) shows the AFM images of $Ni_{0.92}Co_{0.08}O$ thin films synthesized at different molarities. The average grain size, average roughness and root mean square (RMS) roughness for $Ni_{0.92}Co_{0.08}O$, estimated from AFM, are given in Table (4-13). The average grain size, average roughness and RMS roughness of the film increased with increasing the molarity. The sample prepared at molarity of 0.2M has highest average grain size, average roughness and RMS roughness of the film.

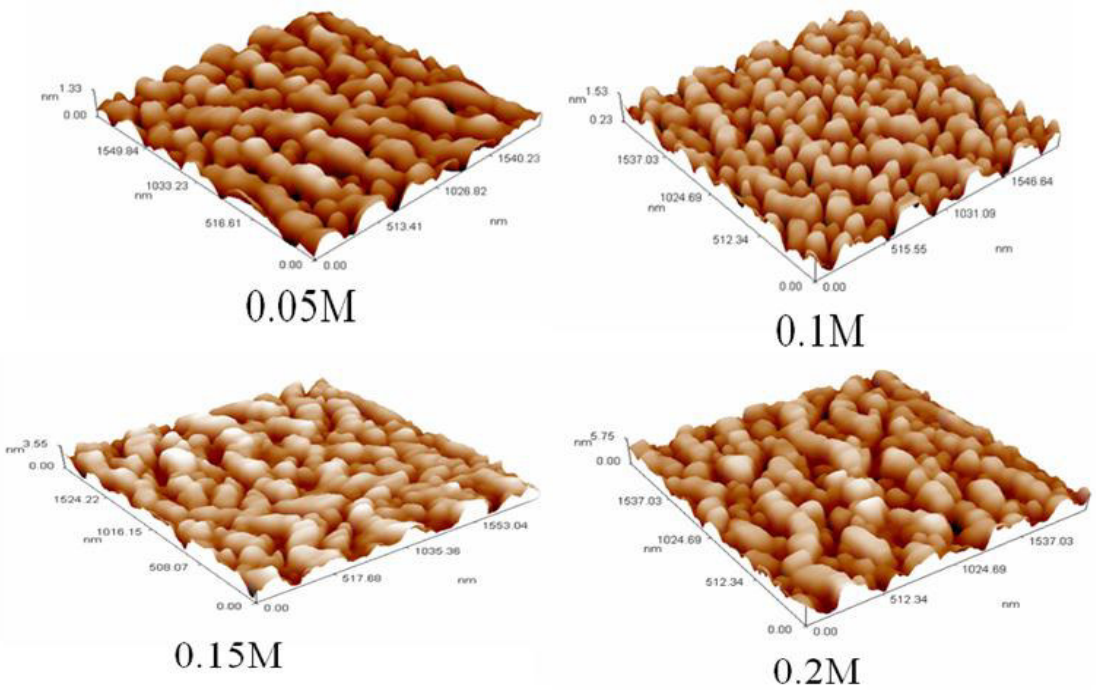

Figure (4-14): 3D AFM images of $Ni_{0.92}Co_{0.08}O$ thin films at different molarities.

Table (4-13): Surface roughness, root mean square (RMS) and grain size of $Ni_{0.92}Co_{0.08}O$ thin films at different molarities.

$Ni_{0.92}Co_{0.08}O$			
Molarity (M)	Surface roughness (nm)	RMS (nm)	Grain Size (nm)
0.05	0.243	0.29	85.23
0.1	0.247	0.293	88.84
0.15	0.63	0.756	96
0.2	1	1.21	111.18

4.4. Optical Properties

The optical measurement results include relations of the transmittance and absorbance with wavelength for Nickel-Cobalt Oxide ($Ni_{(1-x)}Co_xO$) thin films, where x = 0, 4, 6 and 8 % with different molarities (0.05, 0.1, 0.15 and 0.2 M) and computing some optical parameters like absorption coefficient, refractive index, extinction coefficient, real and imaginary part of dielectric constant, optical energy gap and Urbach energy.

4.4.1. Transmittance (T)

Figure (4-15) shows the relation between transmittance and wavelength in the range of (300 - 900 nm) for Nickel-Cobalt Oxide thin films. The transmittance for all thin films increases as the wavelength increases in the range of (300- 350 nm), and then increases slowly at higher wavelenghts. The spectrum shows high transmittance in the visible and infrared regions, and low in the ultraviolet region. Also, ones can observe in this figure that the fundamental absorption edge (absorption edge which separates the high absorption region and the low absorption region or the window region) is sharp in the visible region at the wavelength (680 nm) of the spectrum.

Figure (4-15a) shows the transmittance with wavelength of undoped NiO thin films. The maximum transmittance observed of undoped NiO thin films was about 85% at 0.1M. Figures (4-15b) and (4-15c) show the transmittance as a function of wavelength of $Ni_{0.96}Co_{0.04}O$ and $Ni_{0.94}Co_{0.06}O$ thin films. The transmittance decreases with increase in the molarity of the solution. The molarity 0.05M has a maximum transmittance of nearly equal to 85%. Figure (4-15d) shows the transmittance as a function wavelength for $Ni_{0.92}Co_{0.08}O$ thin films. The transmittance increases with increase in the molarity of the solution and the molarity 0.2M has a maximum transmittance of nearly equal to 85%, these results are in agreement with other studies [39, 42, 43].

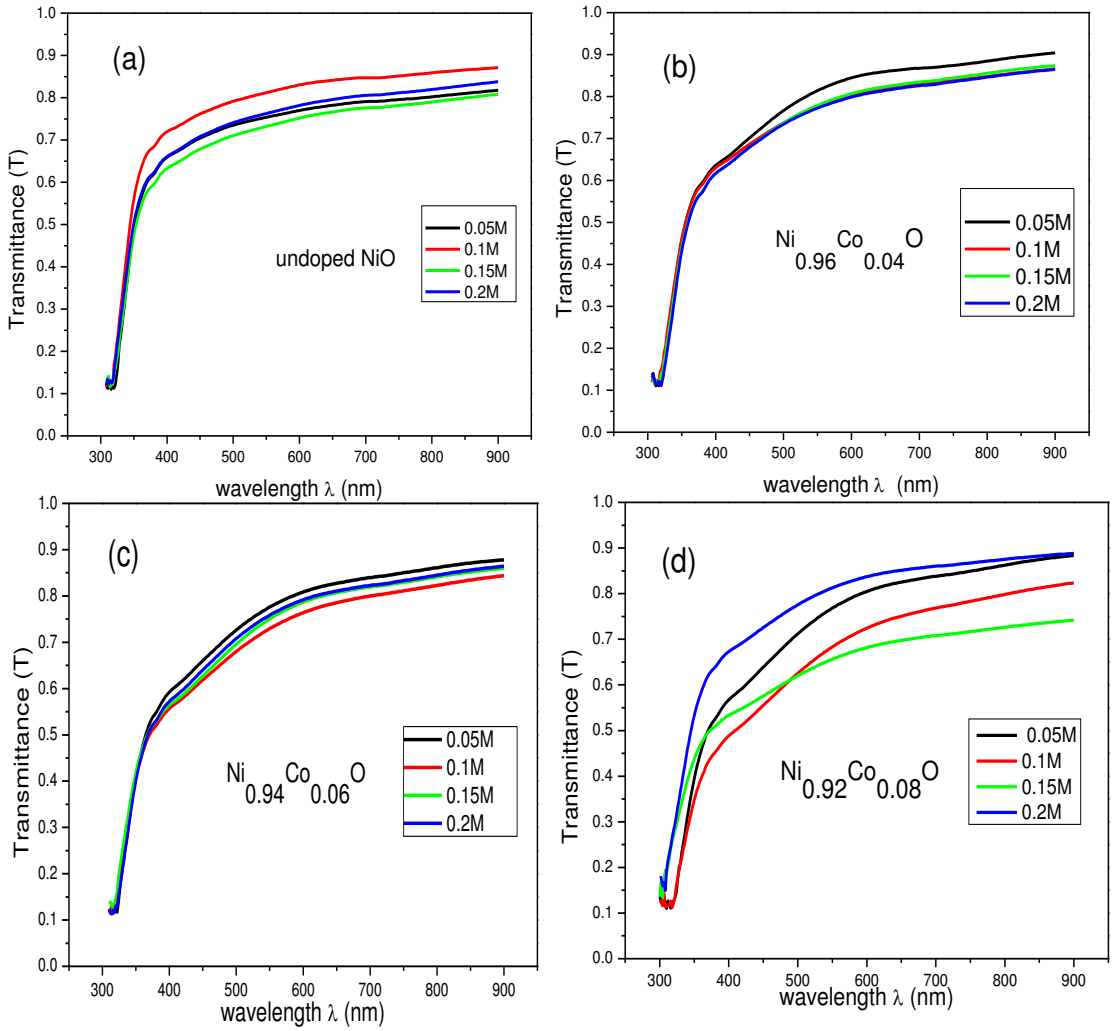

Figure (4-15): Transmittance (T) versus wavelength (λ) of Nickel-Cobalt Oxide thin films at different molarities.

4.4.2. Absorbance (A)

The variation of the absorbance spectrum with wavelength is opposite to the transmittance spectrum. The study of absorbance was in the range of (300– 900 nm). Figure (4-16) shows the relation between absorbance (A) and wavelength for Nickel-Cobalt Oxide thin films. The absorbance decreases rapidly at short wavelengths (high energies) corresponding to the energy gap of the film, (when the incident photon has an energy equal or more than the energy gap value). This evident increase of energy is due to the interaction of the material electrons with the incident photons which have enough energy for the occurrence of electron transitions, this attribute to decrease the energy gap of the film.

Nickel oxide is a high band-gap semiconductor with the absorption edge in the UV region and no absorption in the visible region. The presence of Ni^{3+} ions in the oxide lattice shows charge transfer transition, with the consequent absorption in the visible region. NiO films deposited in this study show absorption in the visible region. There may be three possible explanations for the above process. The first one is that the main stoichiometry of the film is NiO, and Ni_2O_3 is present as a minority phase that could not be detected by XRD. The second possibility is that two adjacent divalent nickel ions become Ni^{3+} due to charge transfer process caused by presence of nickel vacancy. Third possibility is that the stoichiometry of the film is NiO, but excess oxygen together with the hydrogen may be present in the film as OH groups which may show a significance absorption in the visible region of the spectrum [27].

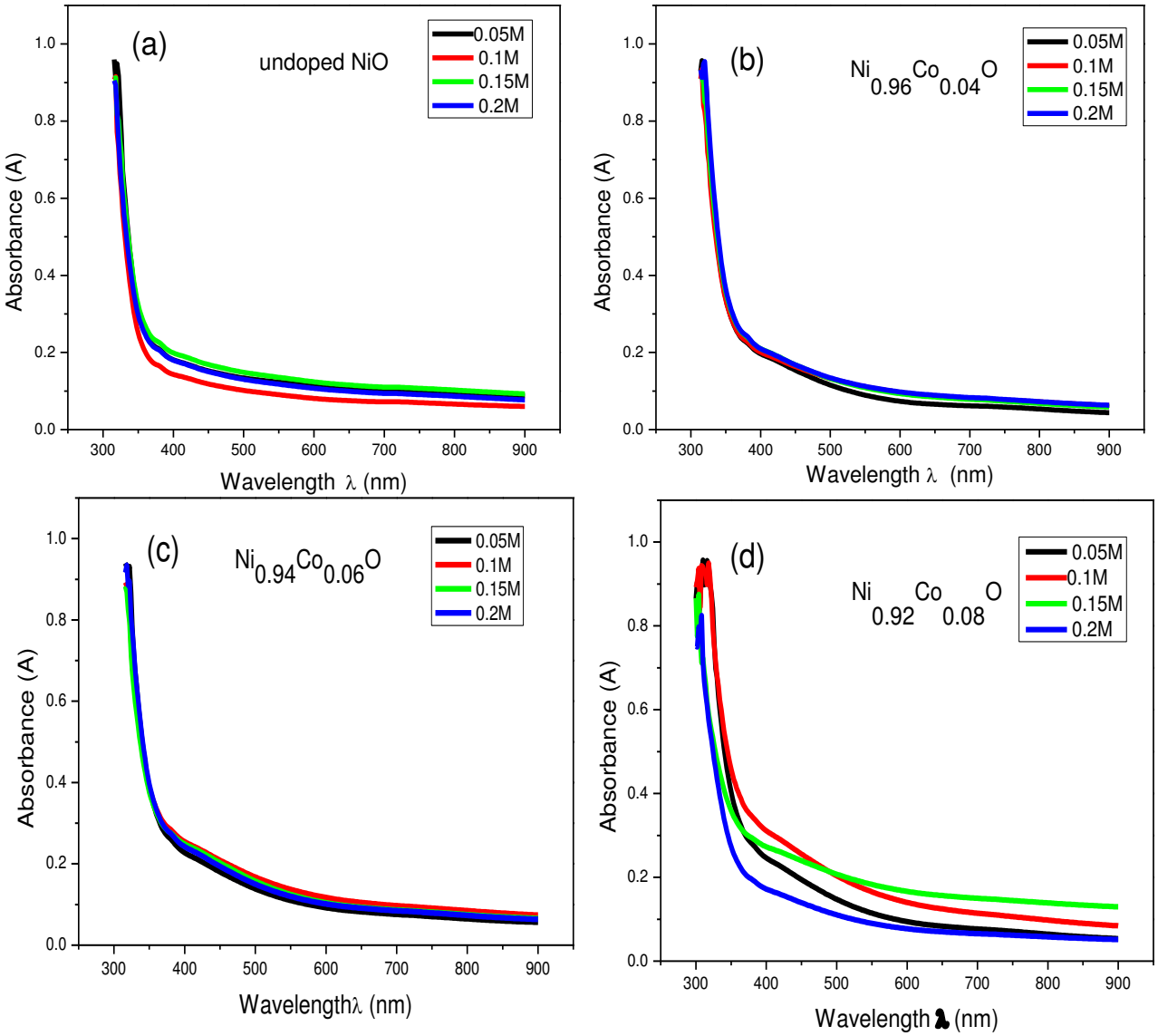

Figure (4-16): Absorbance (A) versus wavelength (λ) of Nickel-Cobalt Oxide thin films of different molarities.

4.4.3. Absorption Coefficient (α)

The absorption coefficient was calculated using equation (2-22). It have been noticed that all the prepared thin films have high absorption coefficient in visible range of the spectrum, and this could be seen in figure (4-17) which shows the relation between the absorption coefficient (α) with photon energy (hυ) of Nickel-Cobalt Oxide thin films. The absorption coefficient increases with increase in photon energy (hυ). The absorption coefficient value depends on absorbance. Nickel-Cobalt Oxide thin films

has a value of absorption coefficient ($\alpha > 10^4$ cm^{-1}) which causes the increase of the probability of the occurrence of direct transitions.

The absorption coefficient increases with increasing molarity for x= 0, 0.04 and 0.06 while it decreases with increasing molarity for x= 0.08.

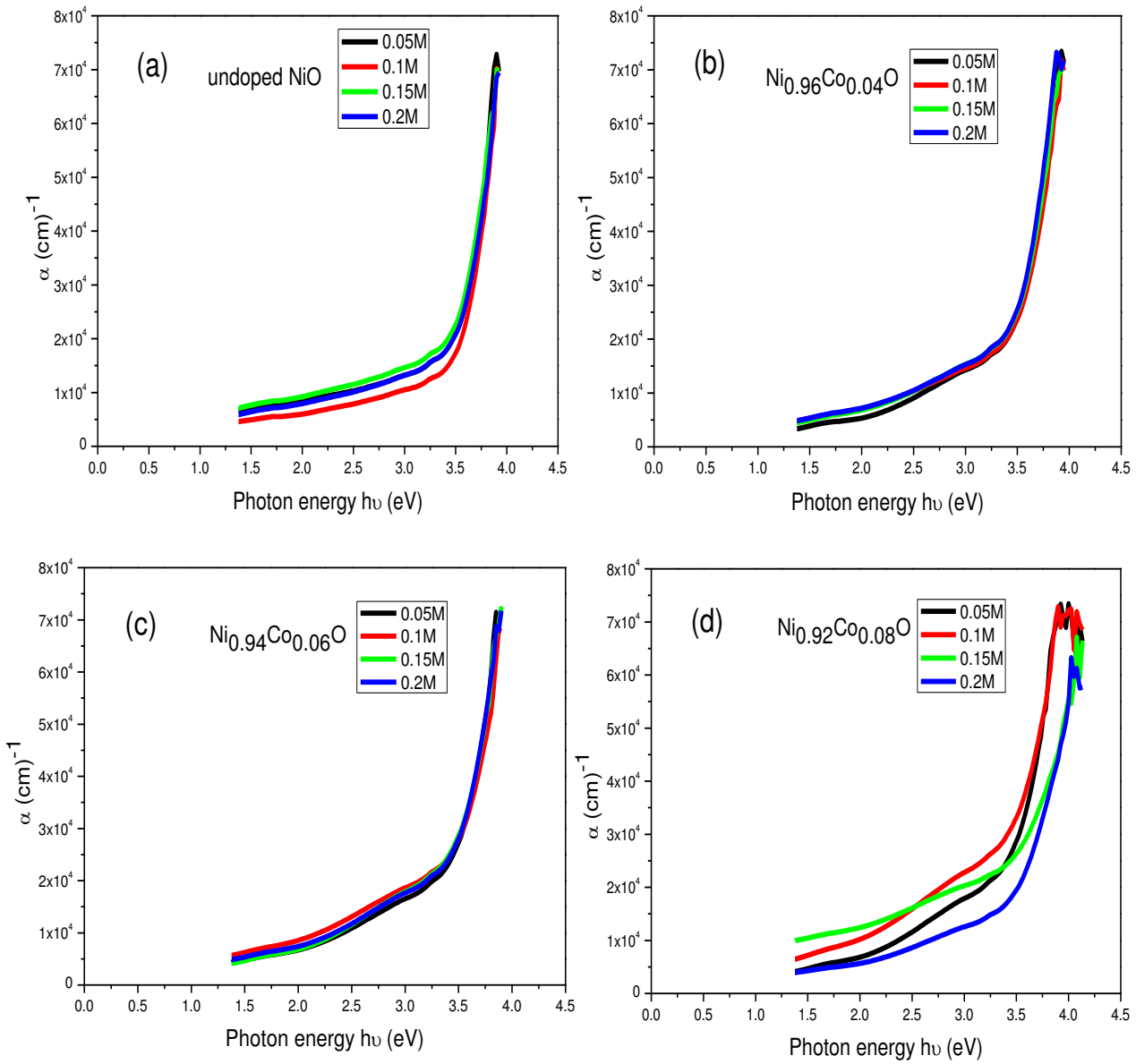

Figure (4-17): The relation between absorption coefficient and photon energy of Nickel-Cobalt Oxide thin films at different molarities.

4.4.4. Optical Energy gap (Eg)

The energy gap values depend in general on the films crystal structure, the arrangement and distribution of atoms in the crystal lattice, also affected by crystal regularity. The optical energy gap (E_g) was derived assuming allowed direct transitions between the edge of the valence and conduction band.

The energy gap was calculated using equation (2-12) where r=1/2 for allowed direct transitions for Nickel-Cobalt Oxide thin films, by plotting a graph between $(\alpha h\nu)^2$ and $(h\nu)$ in eV, a straight line is obtained which gives the value of the direct band gap. The extrapolation of the straight line to $(\alpha h\nu)^2 = 0$ gives value of the direct band gap of the material, and this could be seen in figures (4-18), (4-19), (4-20) and (4-21). Ones notice that the band gap value decreases when the molarity increases, which is in agreement with other reports [43]. This decrease in the band gap can be related to the structural modification of the films with higher molarity. However, many reports reported that the change in the optical band gap energy with molarity may be attributed to the changes in homogeneity and crystallinity of the film, caused by difference in experimental conditions, mainly the amount of spraying solution, spray rate and cooling of the substrates during deposition [42]. The allowed direct band gap values range between 3.71eV to 3.54 eV [37, 40] for the prepared samples, as shown in table (4-14). Figure (4-22) represents the variation of energy gap as a function of molarity for all the deposited thin films in this study and figure (4-23) represents the variation of energy gap as a function of Cobalt concentration for all the deposited thin films in this study. as shown in table (4-14).

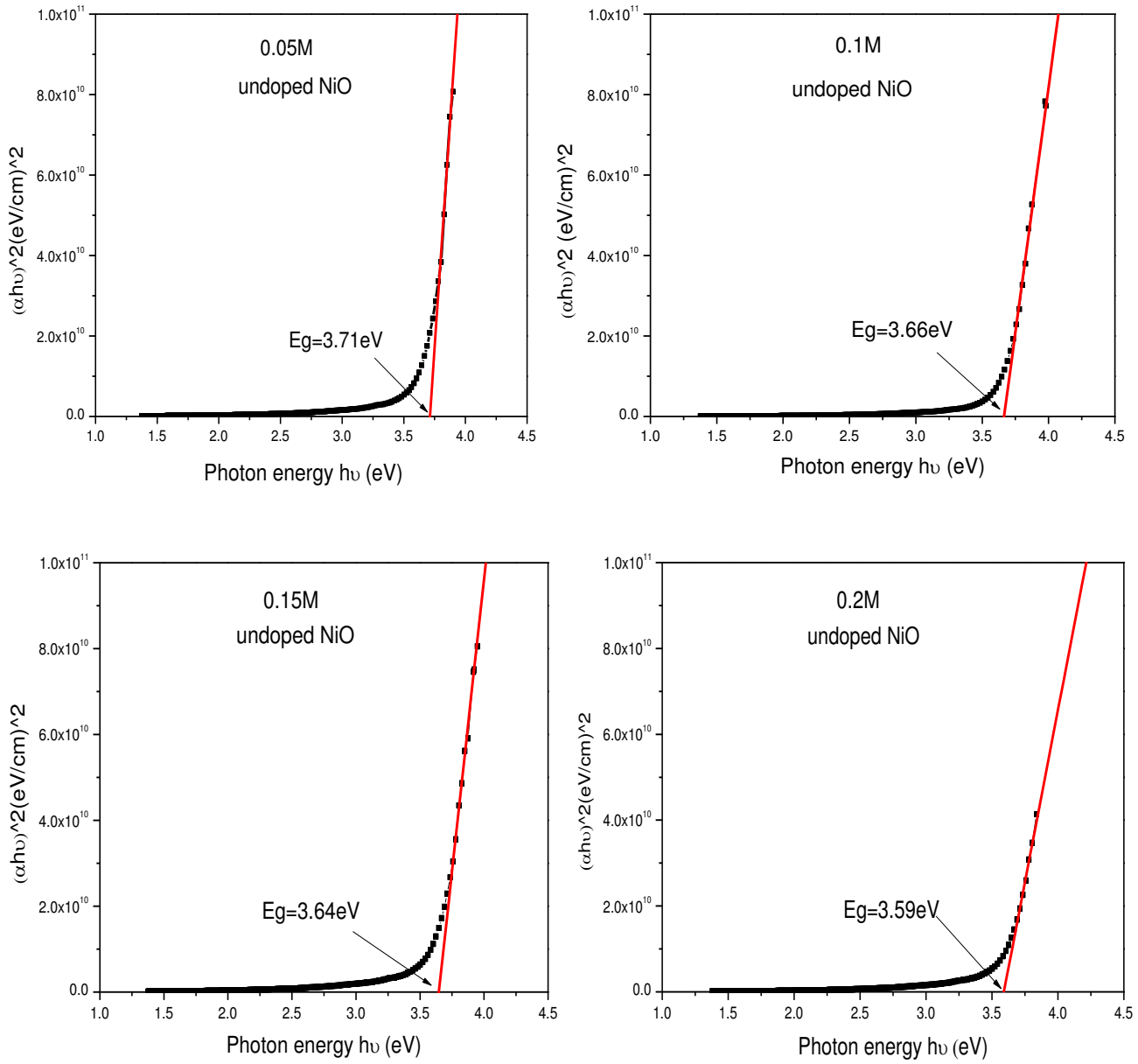

Figure (4-18): The relation between $(\alpha h\upsilon)^2$ and $(h\upsilon)$ of undoped NiO thin films at different molarities.

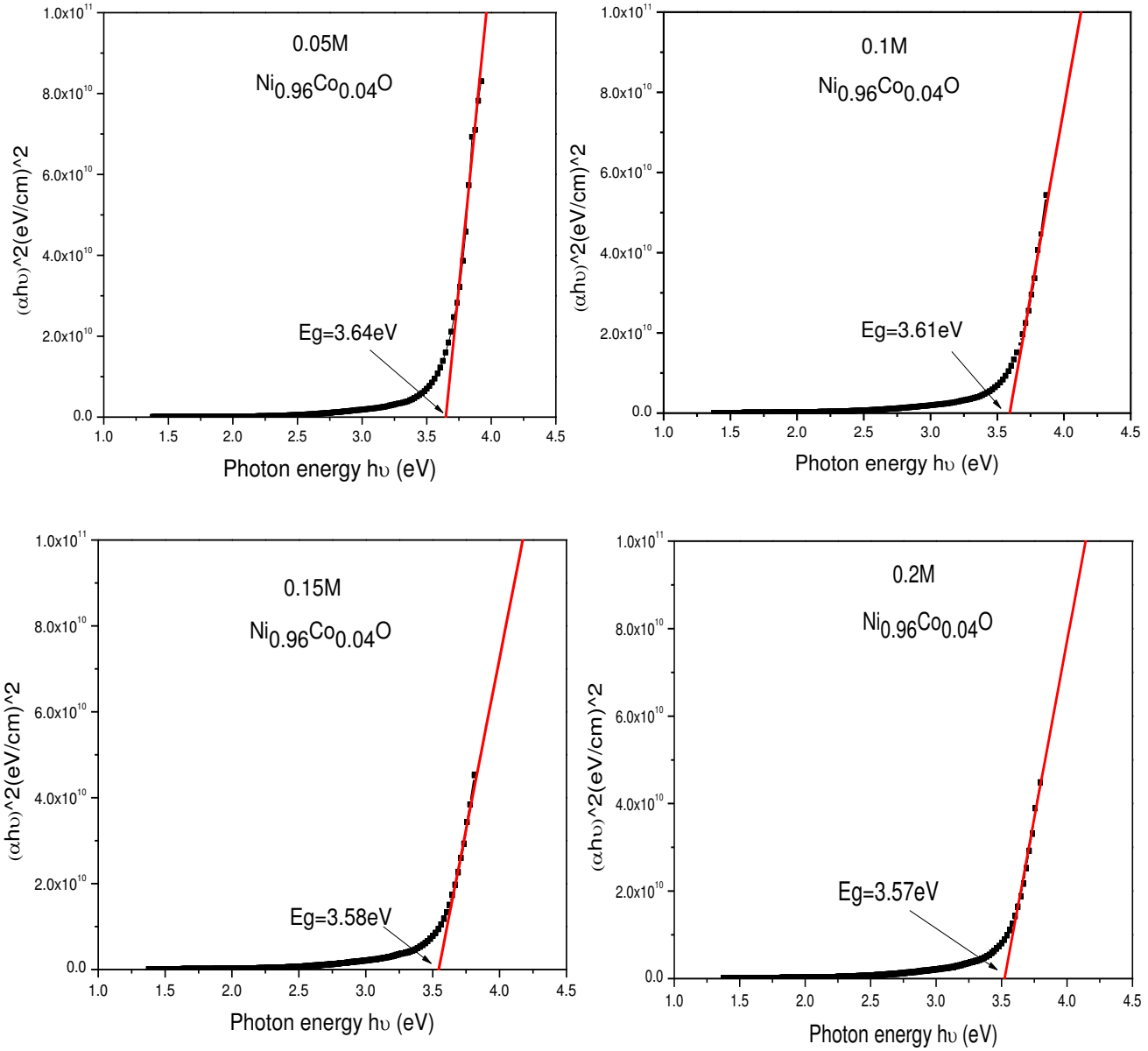

Figure (4-19): The relation between $(\alpha h\upsilon)^2$ and $(h\upsilon)$ of $Ni_{0.96}Co_{0.04}O$ thin films at different molarities.

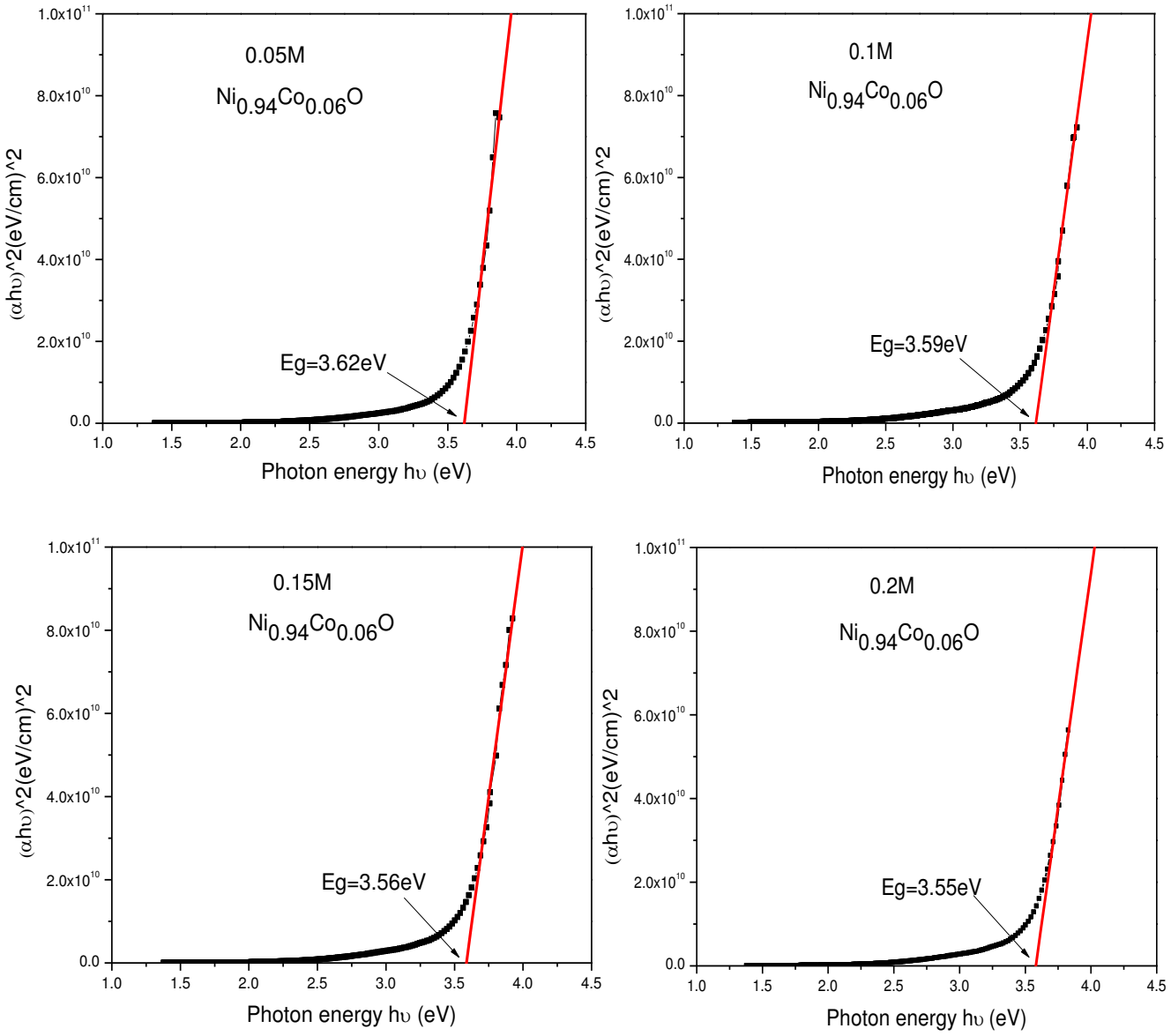

Figure (4-20): The relation between $(\alpha h\upsilon)^2$ and $(h\upsilon)$ of $Ni_{0.94}Co_{0.06}O$ thin films at different molarities.

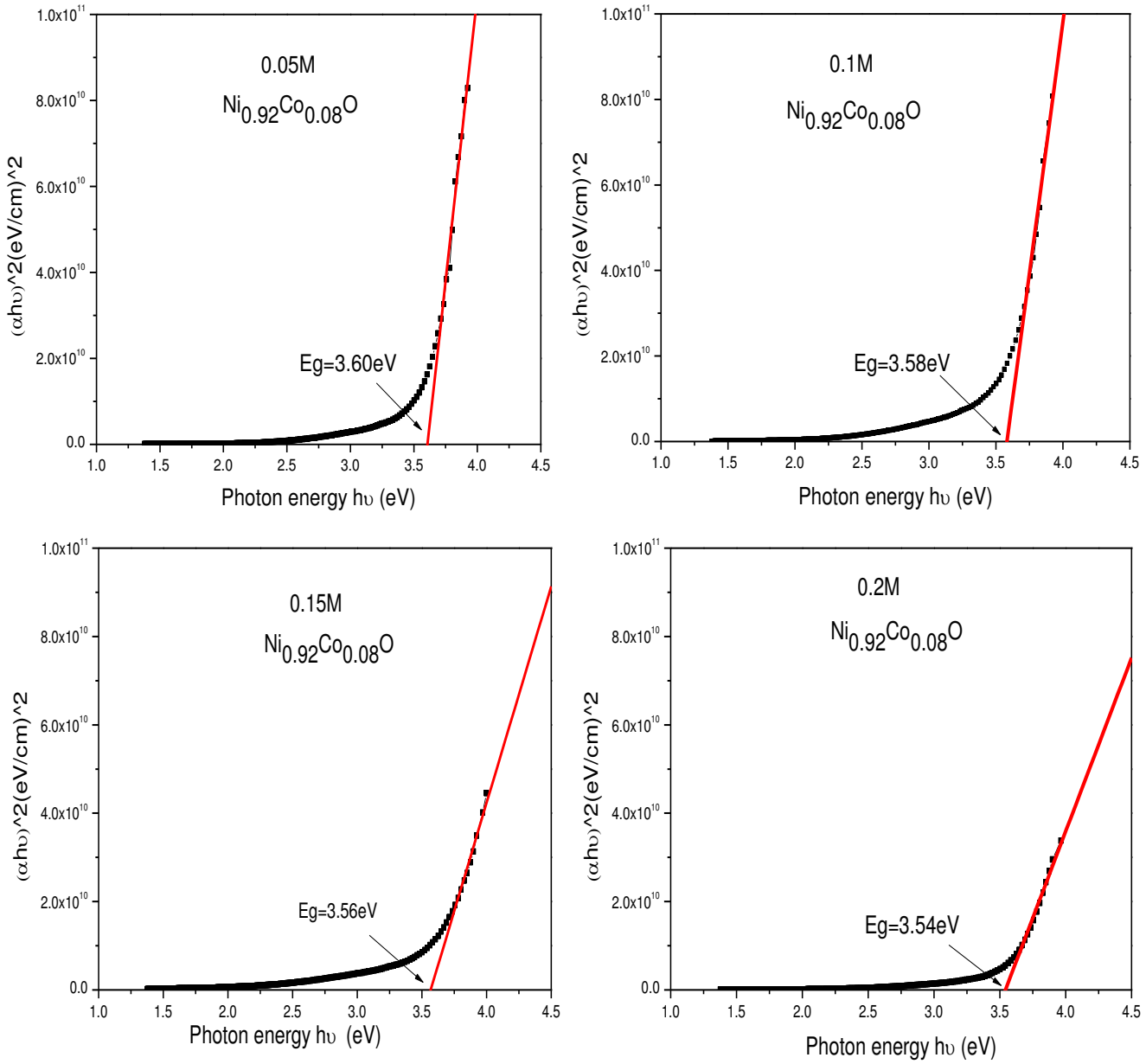

Figure (4-21): The relation between $(\alpha h\upsilon)^2$ and $(h\upsilon)$ of $Ni_{0.92}Co_{0.08}O$ thin films at different molarities.

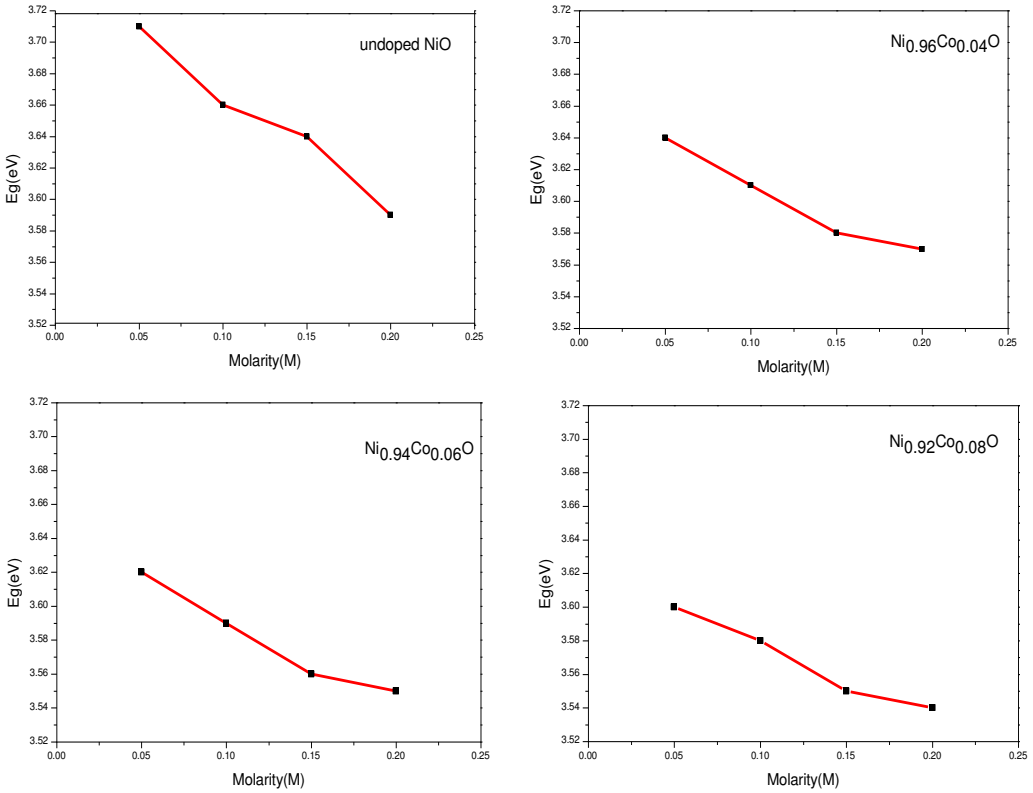

Figure (4-22): The variation of energy gap as a function of molarity for Nickel-Cobalt Oxide thin films.

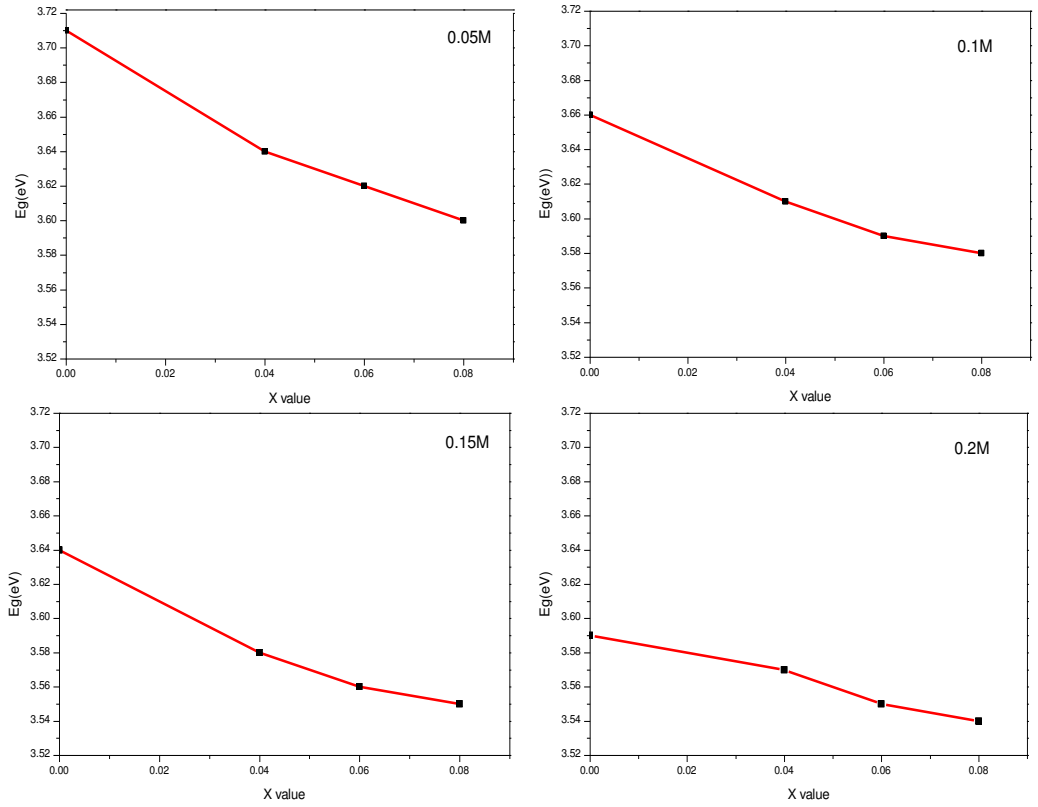

Figure (4-23): The variation of energy gap as a function of concentration for Nickel-Cobalt Oxide thin films.

Table (4-14): Energy gap of Nickel-Cobalt Oxide thin films at (0.05, 0.1, 0.15 and 0.2M).

Samples	Molarity (M)	Eg(eV)
undoped NiO	0.05	3.71
	0.1	3.66
	0.15	3.64
	0.2	3.59
$Ni_{0.96}Co_{0.04}O$	0.05	3.64
	0.1	3.61
	0.15	3.58
	0.2	3.57
$Ni_{0.94}Co_{0.06}O$	0.05	3.62
	0.1	3.59
	0.15	3.56
	0.2	3.55
$Ni_{0.92}Co_{0.08}O$	0.05	3.60
	0.1	3.58
	0.15	3.55
	0.2	3.54

4.4.5. Urbach Energies (E_u)

The Urbach energy can be calculated using equation (2-25). Figure (4-24), shows Urbach plots of the undoped NiO thin films. The values of (E_u) was obtained from the inverse of the slope of (lnα) versus (hυ).

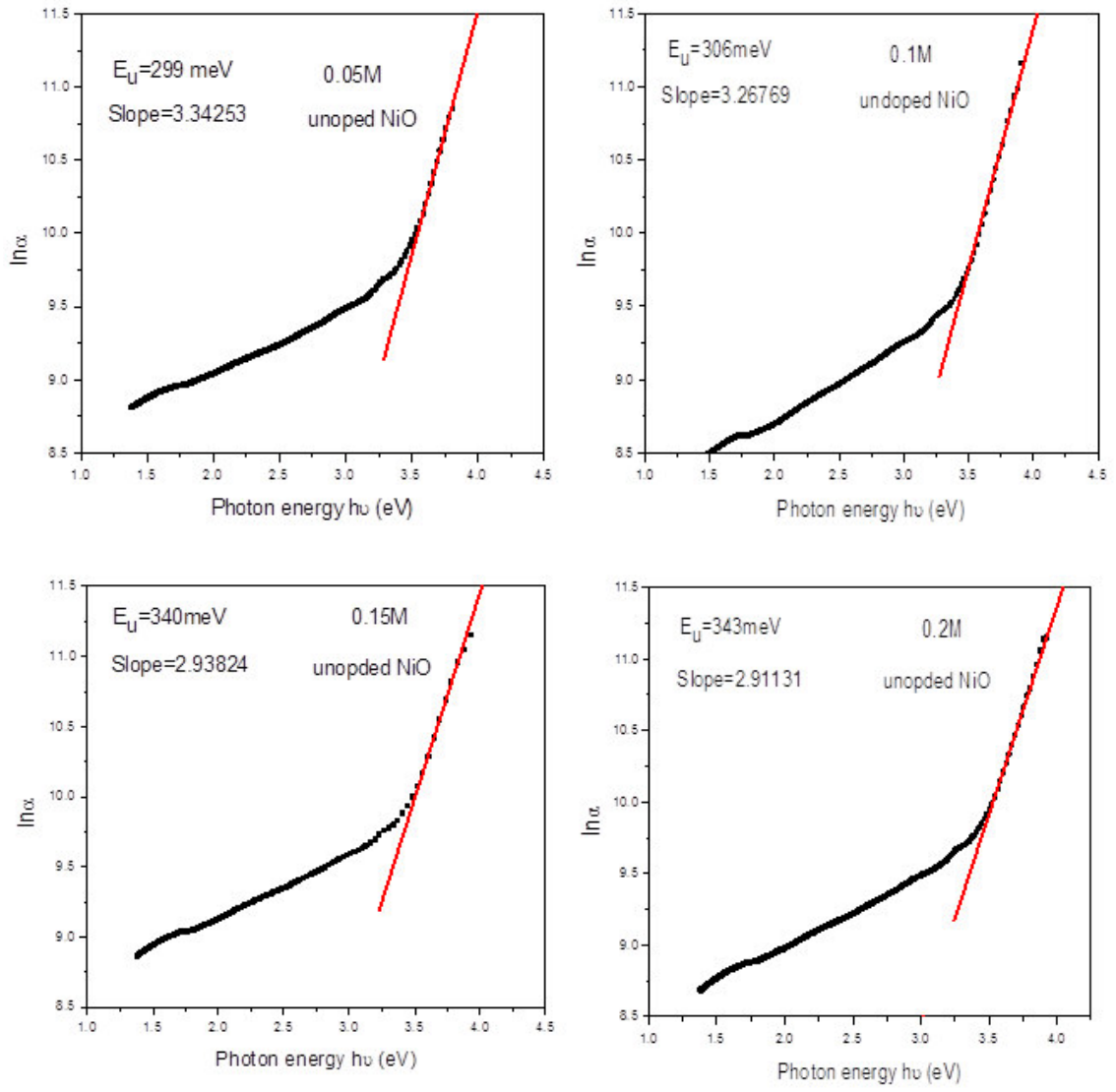

Figure (4-24): The Urbach plots of the undoped NiO thin films at different molarities.

Similar plots were done to the rest of samples and the results are shown in table (4-15). It is observed that the urbach energy increases as the molarity increasing. as shown in figure (4-25). The urbach energy increases as the concentration increasing, as shown in figure (4-26). Urbach energy values change inversely with optical band gap [96]. as shown in table (4-15).

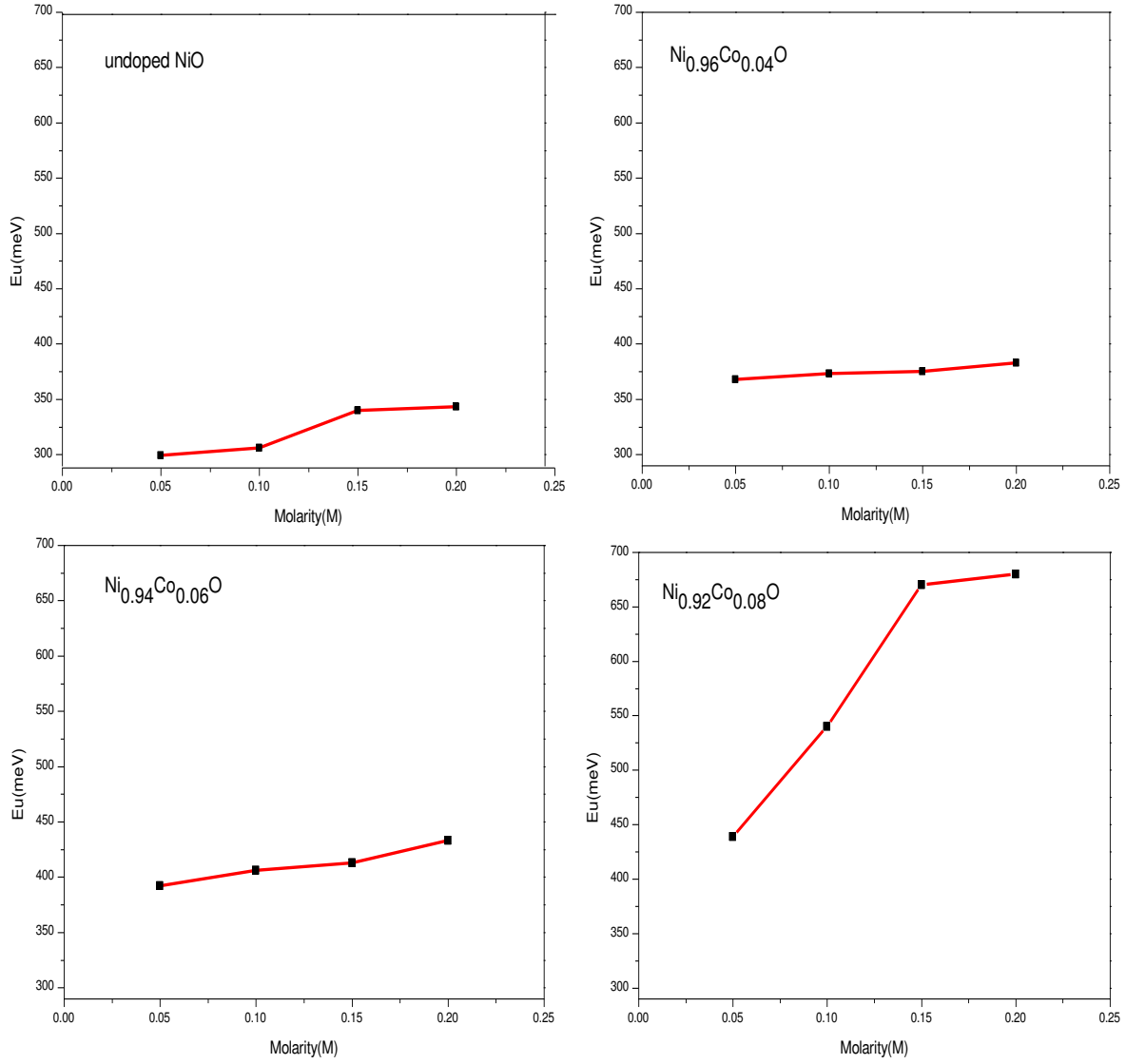

Figure (4-25): The variation of urbach energy as a function of molarity for Nickel- Cobalt Oxide thin films.

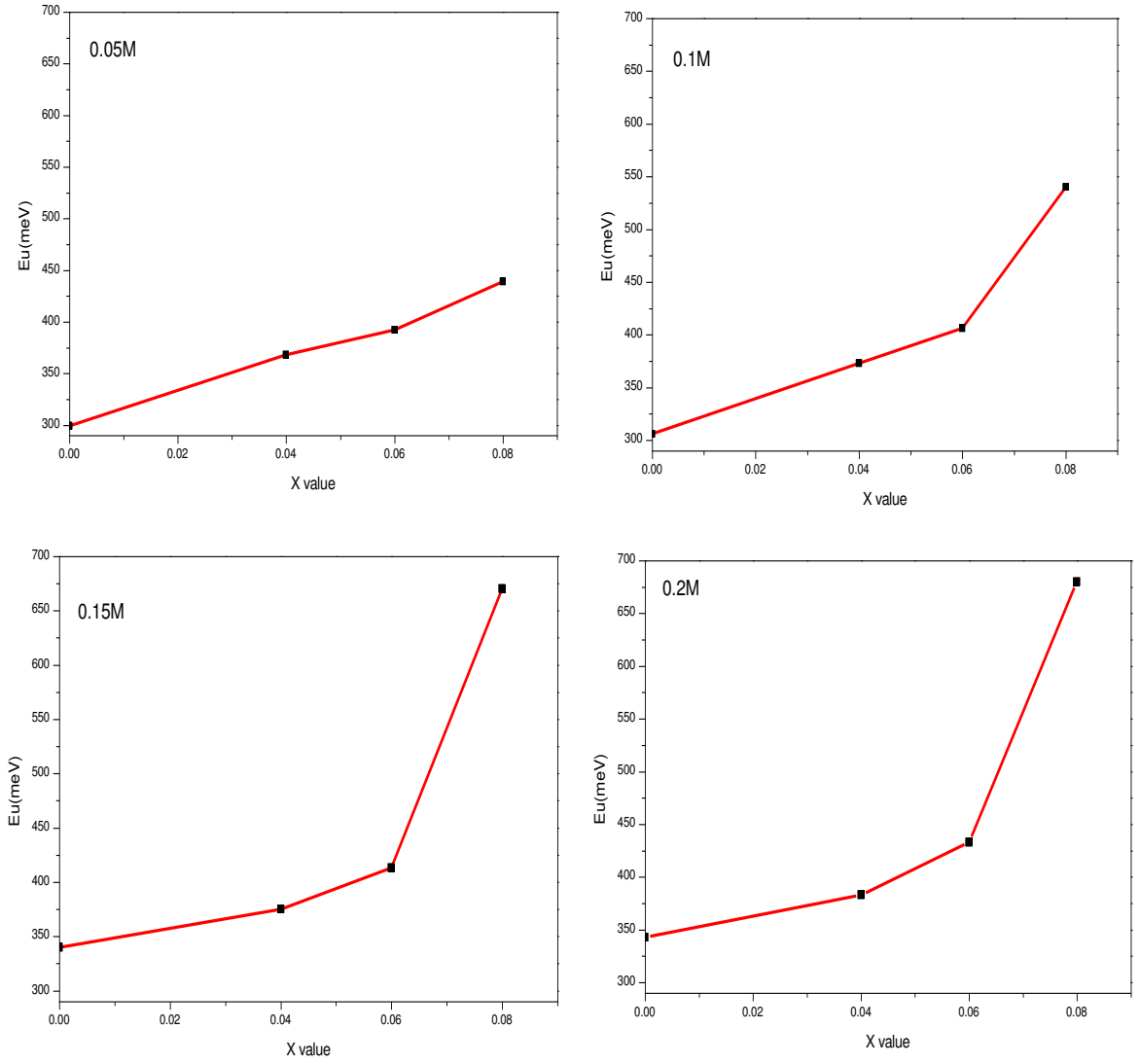

Figure (4-26): The variation of urbach energy as a function of concentration for Nickel-Cobalt Oxide thin films.

Table (4-15): Urbach Energies (E_u) of Nickel-Cobalt Oxide thin films at (0.05, 0.1, 0.15 and 0.2M).

Samples	Molarity (M)	Urbach Energy (E_u) (meV)
undoped NiO	0.05	299
	0.1	306
	0.15	340
	0.2	343
$Ni_{0.96}Co_{0.04}O$	0.05	368
	0.1	373
	0.15	375
	0.2	383
$Ni_{0.94}Co_{0.06}O$	0.05	392
	0.1	406
	0.15	413
	0.2	433
$Ni_{0.92}Co_{0.08}O$	0.05	439
	0.1	540
	0.15	670
	0.2	680

4.4.6. Refractive Index (n)

Refractive index (n) is calculated by using relation (2-27). The relation between refractive index and wavelength for spectrum range (300-900) nm of Nickel-Cobalt Oxide thin films is shown in figure (4-27). It can be seen that there is a peak for the refractive index, its value increases towards the long wavelengths. The behavior of these figures reflects the typical dispersion relation in higher wavelength. The change in refractive index with the solution molarity was not systymatic. Results show that the refractive index values of prepared films have values in the range of (1.59-2.64) [35, 38].

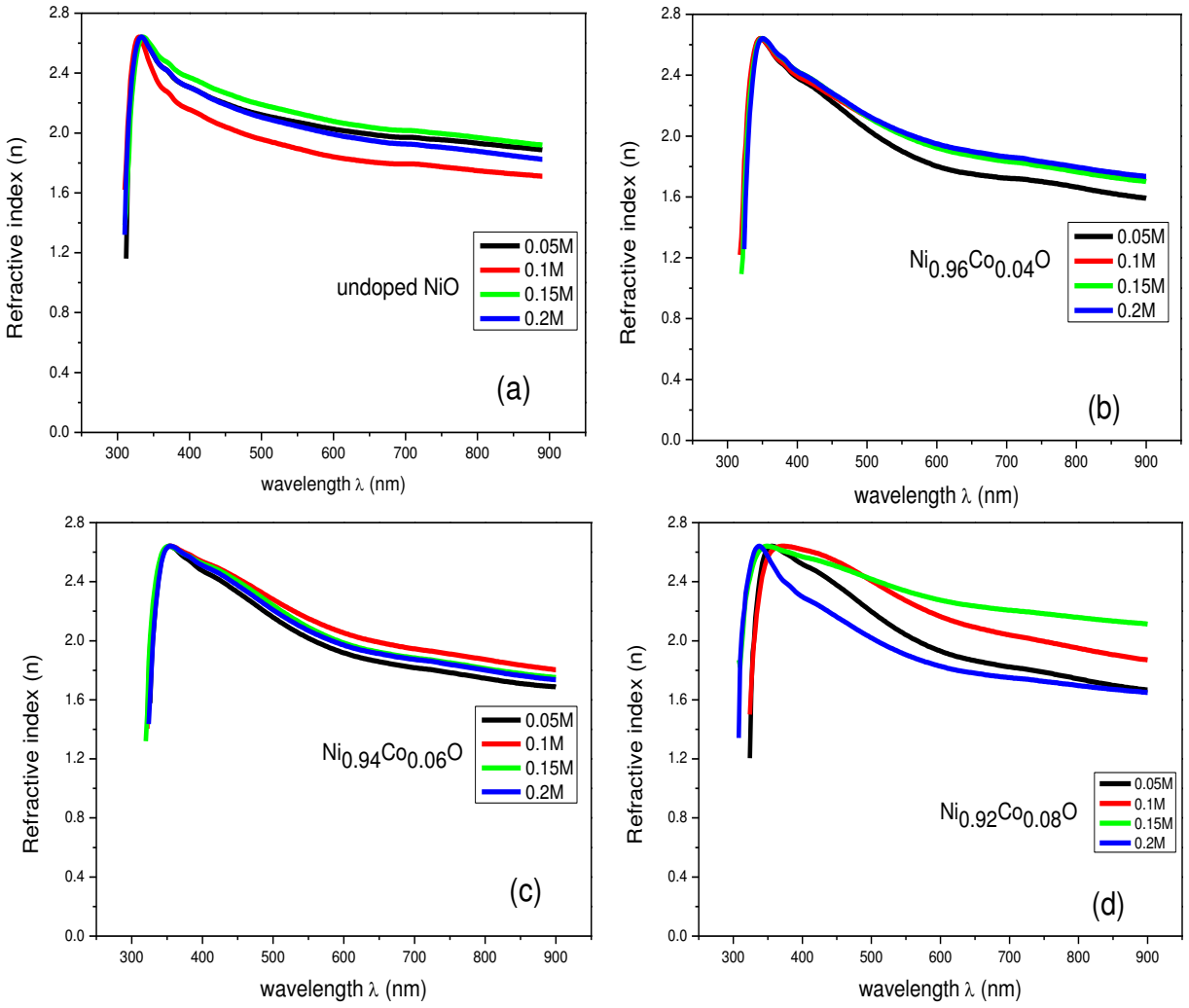

Figure (4-27): The relation between the refractive index and wavelength for Nickel-Cobalt Oxide thin films for different molarities.

In order to investigate the dispersion behavior of the prepared thin films two terms of Cauchy's equation (2-28) was applied to the n- λ data and the static refractive index (n_o) was calculated for all the prepared samples.

The correlation coefficient (R^2) of the fitted dispersion relation was more than 0.99 for all the prepared samples. Figure (4-28) shows the two terms Cauchy's equation fitted to the refractive index data for the undoped NiO thin films at different molarities. Similar analysis was done to the result of

samples and the static refractive index (n_o) was in the range of (1.403-2.002) as shown in table (4-16).

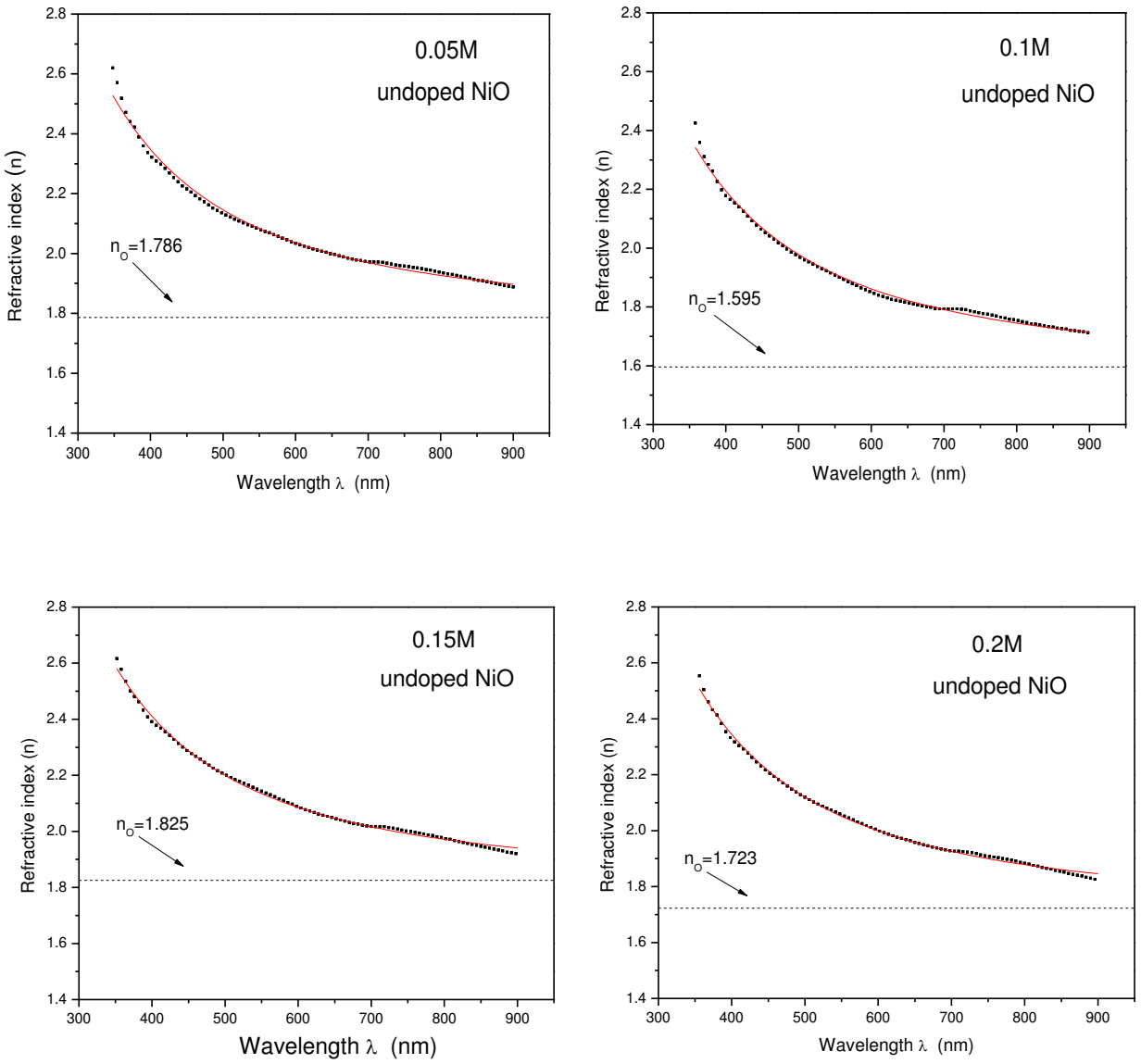

Figure (4-28): Fitting the refractive index data using two terms Cauchy's equation for undoped NiO thin films at different molarities.

Table (4-16): The static refractive index values of Nickel-Cobalt Oxide thin films at (0.05, 0.1, 0.15 and 0.2M).

Samples	Molarity (M)	n_o
undoped NiO	0.05	1.786
	0.1	1.595
	0.15	1.825
	0.2	1.723
$Ni_{0.96}Co_{0.04}O$	0.05	1.403
	0.1	1.582
	0.15	1.538
	0.2	1.579
$Ni_{0.94}Co_{0.06}O$	0.05	1.500
	0.1	1.631
	0.15	1.553
	0.2	1.557
$Ni_{0.92}Co_{0.08}O$	0.05	1.465
	0.1	1.675
	0.15	2.002
	0.2	1.482

4.4.7. Extinction Coefficient (K_o)

The extinction coefficient (K_o) was calculated using relation (2-29). The study of extinction coefficient (K_o) was in the range of (300 - 900)nm. Figure (4-29) shows the extinction coefficient as a function of wavelength for Nickel-Cobalt Oxide thin films. The extinction coefficient (K_o) decreases rapidly at short wavelengths (300-400)nm and after that the value of (K_o) remains constant. The rise and fall in the value of (K_o) is directly related to the absorption of light. The lower value of (K_o) in the wavelength range (400–900) nm implies that these films absorb light in this region very easily [44]. The change in extinction coefficient with the solution molarity was not systymatic. Results show that the extinction coefficient values of prepared films are in the range of (0.024 - 0.18) which is in agreement with other report [44].

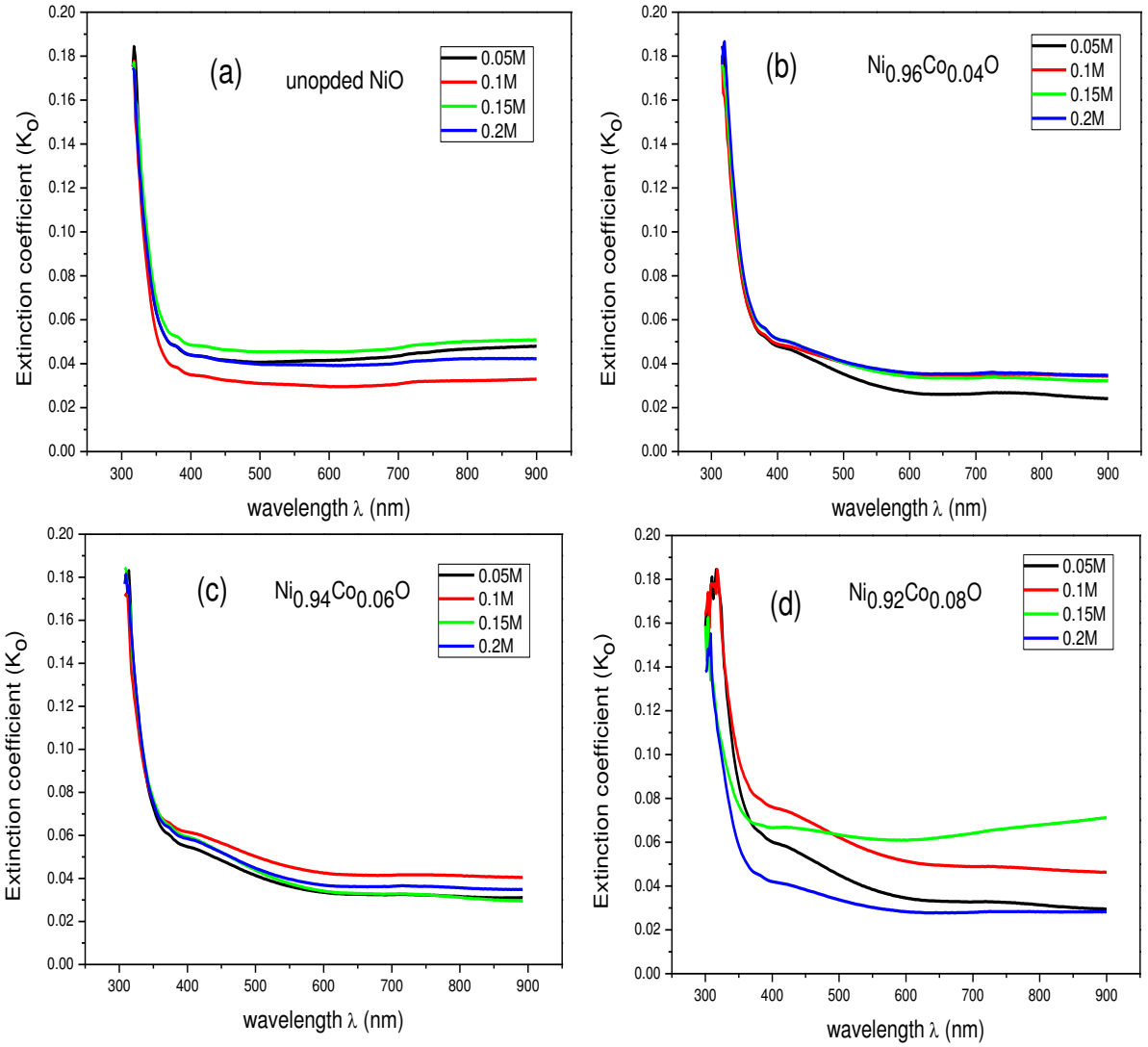

Figure (4-29): The relation between the extinction coefficient and wavelength for Nickel-Cobalt Oxide thin films at different molarities.

4.4.8. Dielectric Constant (ε)

Complex dielectric constant (ε) consists of real dielectric constant (ε_1) and imaginary dielectric constant (ε_2) where real part (ε_1) is the normal dielectric constant and imaginary part (ε_2) represents the absorption associated with free carriers. The values of (ε_1) and (ε_2) are calculated using relations (2-31) and (2-32) respectively. The relation between real and imaginary parts of dielectric constant and photon energy for Nickel-Cobalt Oxide thin films are show in figures (4-30) and (4-31). It can be seen that both the real and imaginary parts of the dielectric constant increases as photon energy increases (1.25-3.5)eV and after that the value of the real and imaginary

parts decreases. The change in real and imaginary parts of the dielectric constant with the solution molarity was not systymatic.

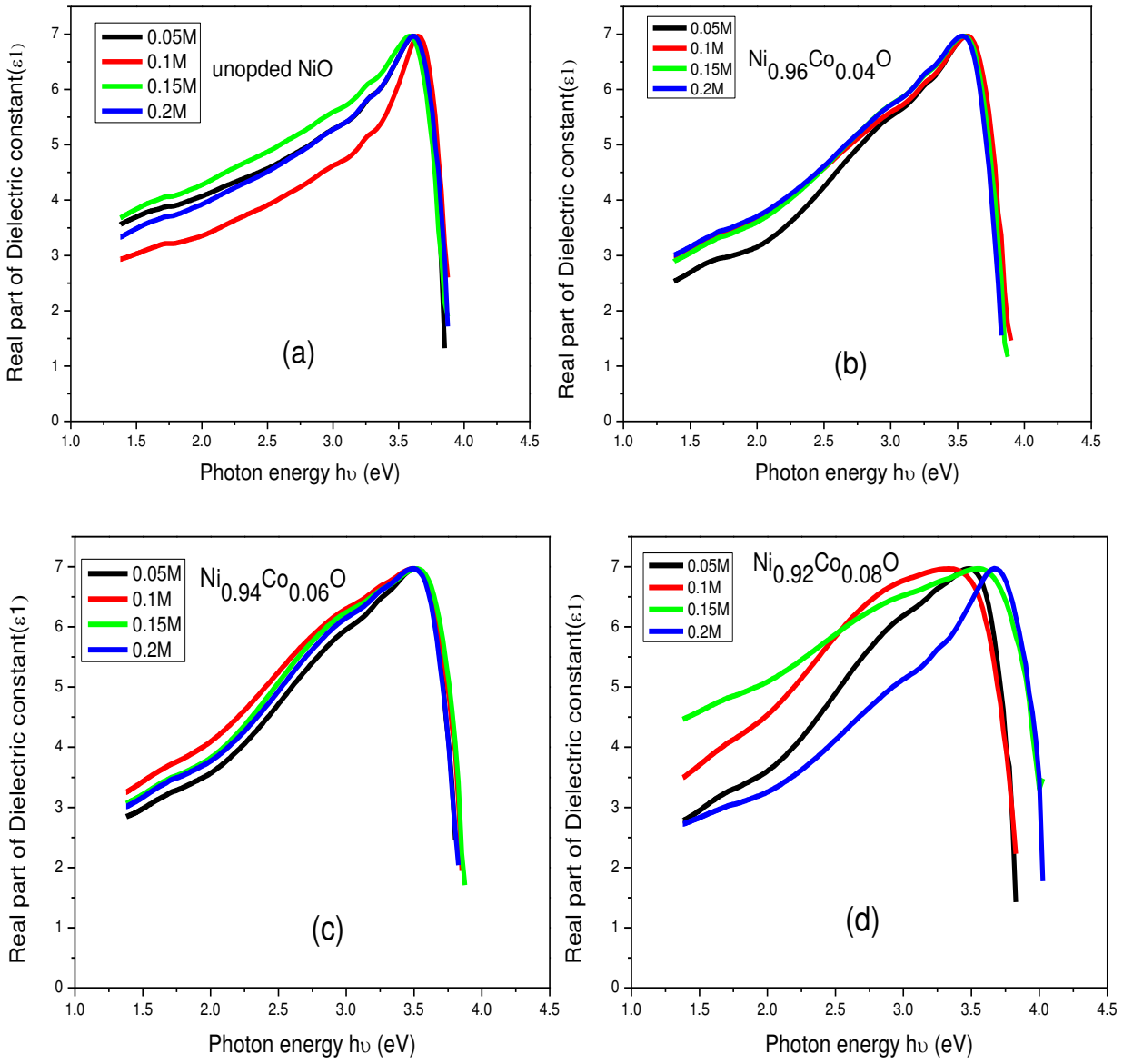

Figure (4-30): The relation between the real part of dielectric constant (ε_1) and photon energy for Nickel-Cobalt Oxide thin films at different molarities.

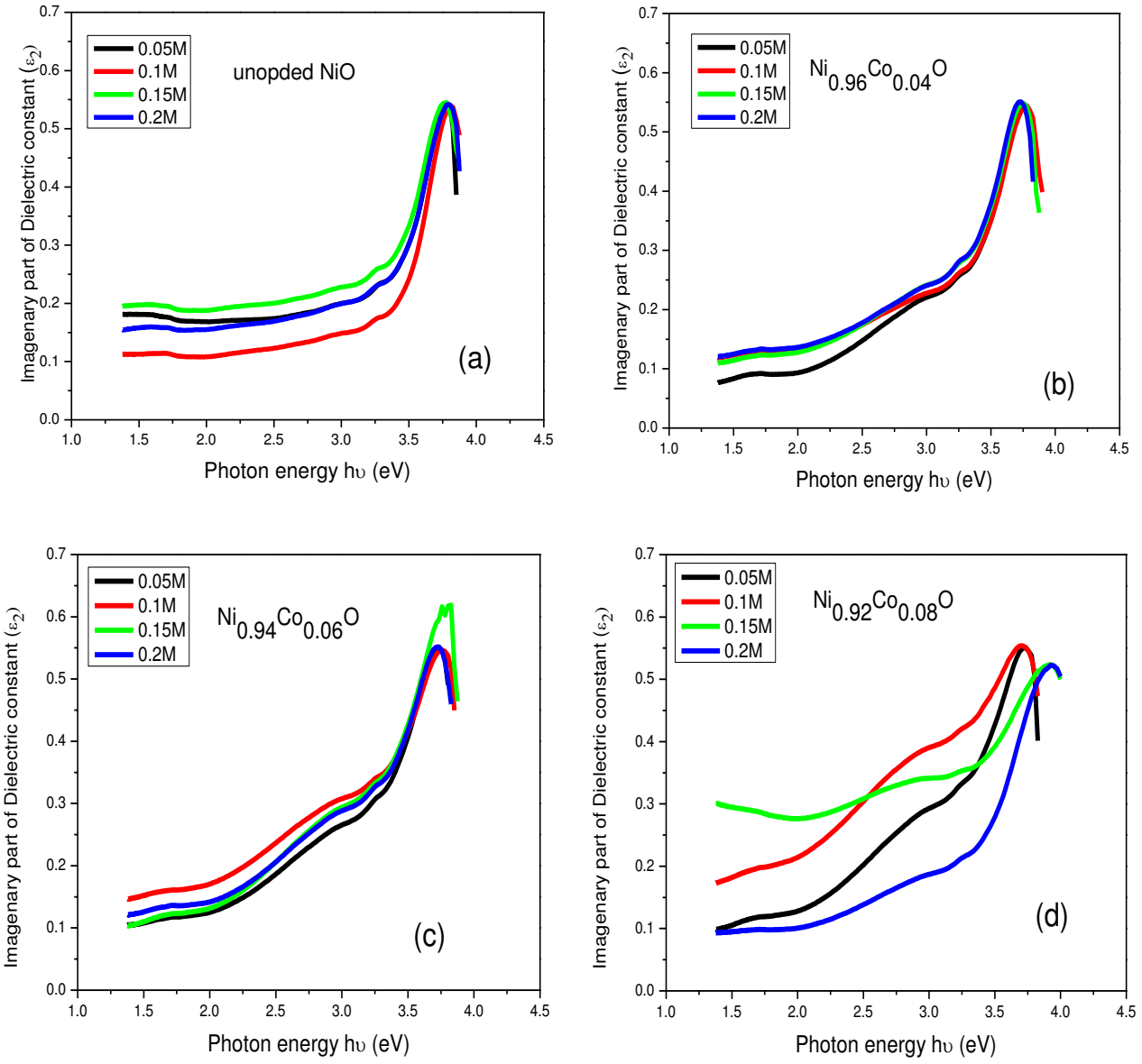

Figure (4-31): The relation between the imaginary part of dielectric constant (ε_2) and photon energy for Nickel-Cobalt Oxide thin films at different molarities.

4.5. Conclusions

1. The XRD results showed that all films are polycrystalline in nature with a cubic structure and the preferred orientation was along the (111) plane for all films. The maximum crystallite size obtained in this study was about 51.16 nm for the undoped NiO thin films at 0.1M solution molarity.

2. The transmittance for all thin films increases rapidly as the wavelength increases in the range (300- 350 nm), and then increases slowly at higher wavelengths.

3. The band gap decreases when the molarity and cobalt concentration increase and the band gap values range between 3.71eV and 3.54 eV.

4. The Urbach energy increases as the molarity and cobalt concentration increase and the Urbach energy values range between 299 meV and 680 meV.

4.6. Future Works

According to the results of this study, the following future studies are suggested :

1. Studying the electrical properties for Nickel-Cobalt Oxide thin films at different molarities.

2. Studying the structural properties (Surface morphological studies) of Nickel-Cobalt Oxide thin films by Scanning Electron Microscopic.

3. Preparation of Nickel-Cobalt Oxide thin films by another technique like thermal evaporation technique.

4. Studying the effect of annealing of Nickel-Cobalt Oxide thin films on the structural, electrical and optical properties.

References

References

[1] K. L. Chopra, I. J. Kaur, "Thin Film Device Applications", Plenum Press, New York, (1983).

[2] K.L Chopra , "Thin Films phenomena " , Mc Graw Hill Inc, USA (1969).

[3] V. Dimitrov, S. Sakka, "linear and nonlinear optical properties of Simple oxides ", J. Appl. Phys., vol. 79 (3), p. 1736 (1996).

[4] S. Major , A. Bonerjee , K. L. Chopra , " Annealing studies of un doped and Indium doped films of Zinc Oxide " ,Thin Sold Films, vol. 122 (15), pp. 31-43, (1984) .

[5] J. Szczyrbowski , A. Czapla, "Optical absorption in D.C sputtered In As films ", Thin solid Films, vol. 46, pp.127-137, (1977).

[6] K. L.Chopra, Lawreuce L. Kazmevski, "Polycrystalline and Amorphous Thin Films and Devices ", Academic Press New York, (1980).

[7] I. Giouroudi, J. Kosel, C. Scheffer, " Recent Developments and Patents on Thin Film Technology ", Recent Patents on Materials Science, vol.1 pp. 200-208, (2008).

[8] P. S. Patil, " Versatility of chemical spry pyrolysis technique", Material Chemistry and Physics vol. p.59, (1999).

[9] D. A. Neaman, "Semiconductor physics and Devices", Basic principles, Richard D. Irwin Inc, London, (1992).

[10] E. Fujii, A. Tomozawa, H. Torii, R. Takayama," Preferred Orientations of NiO Films Prepared by Plasma Enhanced Metalorganic Chemical Vapor Deposition ", Jpn. J. Appl. Phys. vol.35, pp. 328- 330, (1996).

[11] H. Sato, T. Minami, S. Takata,T. Yamada," Transparent conducting p-type NiO thin films prepared by magnetron sputtering ", Thin Solid Films, vol. 236 pp.27-31, (1993).

[12] J. C. Vigine, J. Spitz , J. Electrochem, "Chemical Vapor Deposition at Low Temperatures", Soc, vol. 15, pp. 122, 585, (1975).

[13] G. Slewah, "Study of Electrical and Optical Properties of Thin Film of CdS and CdS: In Prepared by Spray Pyrolysis Technology ", M.Sc. Thesis, College of Sciences, University of Basrah, (1990).

[14] K. D. Leaver, B.N Chapman, "Thin Films ", Wykeham publications (London) Ltd .(1971).

[15] Pradniak, Pradyot, Publications," Handbook of Inorganic Chemicals", (2002).

[16] Greenwood, Norman N, Earnshaw, Alan, " Chemistry of the Elements", Oxford, Pergamon Press, (1984)

[17] K. Lascelles, L. G. Morgan, D. Nicholls, D. Beyersmann, " Nickel Compounds", in Ullmann's Encyclopedia of Industrial Chemistry Wiley-VCH, Weinheim, (2005).

[18] E. J. M. O' Sullivan and E. J. Calvo, " Reactions at Metal Oxide Electrodes Comprehensive Chemical Kinetics", Elsevier, New York, (1987).

[19] C. M. Lambert and G. Nazri, P. C. Yu, " Spectroscopic and Electrochemical Studies of Electrochromic Hydrated Nickel Oxide Films", Solar Energy Materials, vol. 16, pp.1-17, (1987).

[20] N. Shaigan, D.G. Ivey and W. Chen, "Metal Oxide Scale Interfacial Imperfections and Performance of Stainless Steels Utilized as Interconnects in Solid Oxide Fuel Cells", Journal of The Electrochemical Society, vol. 156 pp.765-770, (2009).

[21] K. K. Purushothaman, G. Muralidharan, " Nanostructured NiO Based All Solid State Electrochromic Device", Journal of Sol-Gel Science and Technology, vol. 46, pp.190-197, (2008).

[22] I. Hotovy, J Huran, L Spiess, S Hascik, V Rehacek," Preparation of nickel oxide thin films for gas sensors applications ", Sensors and Actuators B: Chemical, vol. 57, pp. 147–152, (1999).

[23] R. Cerc Korosec, P. Bukovec, B. Pihlar, A. Surca Vuk, B. Orel and G. Drazic, "Preparation and Structural Investigations of

Electrochromic Nanosized NiO_x Films Made via the Sol-Gel Route", Solid State Ionics, vol. 165, pp.191-200, (2003).

[24] B. Sasi and K. G. Gopalchandran, "Nanostructured Mesoporous Nickel Oxide Thin Films", Nanotechnology, vol. 18, pp.115613-115617, (2007).

[25] H. Kamel, E. K. Elmaghraby, S. A. Ali, K. Abdel- Hady, " The Electrochromic Behavior of Nickel Oxide Films Sprayed at Different Preparative Conditions", Thin Solid Films, vol. 483, pp.330-339, (2005).

[26] S.U. Offiah, A.C. Nwanya, S.C. Ezugwu B.T. Sone, R.U. Osuji, Maaza Malik, C. D. Lokhande , F. I. Ezema, " Chemical Bath Synthesis and physico-chemical Characterizations of NiO-CoO Composite Thin Films for Supercapacitor applications", Int. J. Electrochem, vol. 9, pp.5837 – 5848, (2014).

[27] P. S. Patil, L. D. Kadam, " Preparation and characterization of spray nickel Oxide (NiO) thin films", Applied surface science, vol. 199, p. 211, (2002).

[28] Hao-Long Chen1, Yang-Ming Lu and Weng-Sing Hwang, " Effect of Film Thickness on Structural and Electrical Properties of Sputter-Deposited Nickel Oxide Films", Materials Transactions, vol. 46(4), pp. 872 - 879.(2005).

[29] B.A. Reguig, A. Khelil, L. Cattin, M. Morsli, J.C. Bernède, " Properties of NiO thin films deposited by intermittent spray pyrolysis process" ,Applied Surface Science vol. 253(9), pp, 4330–4334, (2007).

[30] F. E. Ghodsi, S. A. Khayatiyan, " Preparation and determination of optical properties of NiO thin films deposited by dip coating technique ", Surface Review Letters (SRL), vol. 14(02), pp. 219-224, (2007).

[31] F. I. Ezema, A.B.C Ekwealor, R.U. Osuji, " Optical properties of

chemical bath deposited nickel oxide (NiO_x) thin films", Superficies y Materials, val. 21(1), pp. 6-10, (2008).

[32] Amit Kumar Srivastava, Subhash Thota, Jitendra Kumar, " Preparation, Microstructure and Optical Absorption Behaviour of NiO Thin Films", Journal of Nanoscience and Nanotechnology vol. 8, pp. 4111–4115, (2008).

[33] H.U. Igwe, O.E. Ekpe, E.I. Ugwu," Effects of Thermal Annealing on the Optical Properties of Nickel Oxide Thin Films Prepared by Chemical Bath Deposition Technique", Journal of Science and Technology. vol. 10(2), pp.806-811, (2009).

[34] F. Saadati, A. R. Grayeli , H. Savaloni, " Dependence of the optical properties of NiO thin films on film thickness and nanostructure ", Journal of Theoretical and Applied Physics, vol. 4(1), pp.22-26, (2010).

[35] Nibras F. Al.Shammary, " Optical characteristics of NiO thin film on glass formed by Chemical spray pyrolysis", Journal of kufa- Physics vol.2 (1),p. 20, (2010).

[36] Vikas Patil, Shailesh Pawar, Manik Chougule, Prasad Godse, Ratnakar Sakhare, Shashwati Sen and Pradeep Joshi, " Effect of Annealing on Structural, Morphological, Electrical and Optical Studies of Nickel Oxide Thin Films" , Journal of Surface Engineered Materials and Advanced Technology, vol.1, pp. 35-41, (2011).

[37] Mark Guziewicz, Jakub Grochowski, Michal Borysiewicz, Eliana Kaminska, Jaroslawz, Z. Domagal,Witold Rzodkiewicz, Bartlomiej S. Witkowski, Krystyna Golaszewka, Renata Kruszka, Mark Ekielski, Annaplotrowska, " Electrical and optical properties of NiO films deposited by magnetron sputtering", Optica Applicata, vol. (2), p. 431 (2011).

[38] André Venter, Johannes R. Botha, " Optical and electrical properties of NiO for possible dielectric applications", S Afr J Sci. vol.107(1/2),

p.268, (2011).

[39] A. Thayumanavan, A. R. Balu, S. Sriram, "Design and Development of Automated Liquid Flow Deposition method for thin film formation" Archives of Applied Science Research, vol.3(2), pp.438-447. (2011).

[40] Safwat A. Mahmoud, Shereen Alshomer, Mou'ad A. Tarawnh, " Structural and Optical Dispersion Characterisation of Sprayed Nickel Oxide Thin Films", Journal of Modern Physics, vol. 2, pp. 1178-1186 (2011).

[41] Y. Ashok Kumar Reddy, A. Mallikarjuna Reddy, A. Sivasankar Reddy, P. Sreedhara Reddy, " Preparation and Characterization of NiO Thin Films by DC Reactive Magnetron Sputtering", Journal of nano-and Electronic Physics vol. 4 (4), p.04002, (2012).

[42] A.R. Balu, V. S. Nagarethinam, N. Arunkumar, M. Suganya, " Nanocrystalline NiO thin films prepared by a low cost simplified spray technique using perfume atomizer ", Journal of Electron Devices, vol. 13, pp. 920-930. (2012).

[43] Raid A. Ismail . Sa'ad Ghafori . Ghada A. Kadhim, " Preparation and Characterization of nanostructured nickel oxide thin films by spray pyrolysis" , Appl Nanosci, vol. 3, pp.509–514, (2013).

[44] S. Sriram, A. Thayumanavan, " Structural, Optical and Electrical Properties of NiO Thin Films Prepared by Low Cost Spray Pyrolysis Technique" , International Journal of Materials Science and Engineering vol. 1(2), p.118, (2013).

[45] J. C. Osuwa and G. I. Onyejiuwa, " Structural and Electrical properties of annealed Nickel Oxide (NiO) thin films prepared by chemical bath deposition " , Journal of Ovonic Research, vol. 9(1), pp. 9 –15, (2013).

[46] K.J. Patel, M. S. Desai, C.J. Panchal, P.K. Mehta, I.M. Pazukha, I.Yu. Protsenko, " Effect of Substrate Temperature on the Electrochromic Properties of Nickel Oxide Thin Films by e-Beam Evaporation

Method", Proceedings of the international conference nanomaterials: Applications and Properties vol. 2 (1), pp. 1-30, (2013).

[47] Arwaa Fadil Saleh, " Structural and morphological studies of NiO thin films prepared by Rapid thermal oxidation method ", International Journal of Application or Innovation in Engineering & Management (IJAIEM) vol. 2(1), p.16, (2013).

[48] Heba Salam Tareq," Study the Effect of Rapid Thermal Annealing on Thin Films Prepared by Pulse Laser Deposition Method", Eng. &Tech. Journal, vol. 32(3), p.444, (2014)

[49] L. L. Kazmerski, " Polycrystalline and Amorphous Thin films and Devices" Acadmic Press, New York (1980).

[50] S.O. Pillai, "Solid state physics", Revised and Enlarged Edition New age international (P) Limited Publishers (1997).

[51] M.H. Brodsky, "Topics in Applied Physics Amorphous Semiconductors", p. 36 , New York (1979) .

[52] Guray Tas, Priya Mukundhan, Timothy A. Johnson and Selezion A. Hambir, Rudolph Technologies, Flanders, N.J, Brian Howard, Spectra-Physics Semiconductor Lasers, Mountainview, Calif. Semiconductor International, (2001).

[53] يحيى نوري الجمال ، " فيزياء الحالة الصلبة " جامعة الموصل ، كلية العلوم، (١٩٩٠) .

[54] William, D. Callister , Jr , "Materials Science and Engineering An Introduction ", (2003).

[55] C. Kittle, Introduction to solid state physics, (5^{th}) edition, John Willy & sons In. (1976).

[56] Nasa," X-Rays", Retrieved, (2012).

[57] D. C. Altamirano, G. Torres, R. Castanedo, O. Jimeuz, J. Marquez, S. Jimenez, "Influence of the Al content on the optical properties of ZnO thin films obtained by the sol-gel technique", Superficies, vol. 13, P. 66, (2001).

[58] E. S. R, "Physics of Amorphous Materials", Longman Group limited (1983).

[59] احمد امين سليمان، احمد فؤاد باشا وشريف احمد خيري،" فيزياء الجوامد"، مطبعة الفكر العربي(2000) .

[60] N. A. Donald, "Semiconductor Physics and Devices", University of New Mexico,(1992).

[61] K. Alexander, "X-ray Diffraction Procedures for Polycrystalline and Amorphous Material", John wiley and Sons, (1974).

[62] S. Mondal, K. P. Kanta, P. Mitra, " Preparation of Al- doped ZnO (AZO) Thin Film by SILAR", Journal of Physical Sciences, vol. 12, P. 221, (2008).

[63] R. Yogamalar, R. Srinivasan, A. Vinu, K. Ariga, A.C. Bose, X-ray peak broadening analysis in ZnO nanoparticles, Solid State Commun. vol. 149, pp. 1919-1923, (2009).

[64] M. Caglar, S. Ilcan, Y. Caglar, "Influence of Substrate Temperature on Structural and Electrical Properties of ZnO Films ", J. Sci, vol. 7(2), p. 153, (2006).

[65] Y. T. Prabhu, K. Venkateswara Rao, V. Sesha Sai Kumar and B. Siva Kumari, " X- ray Analysis of Fe doped ZnO Nanoparticles by Williamson-Hall and Size-Strain Plot", vol. 2(5), (2013).

[66] VD Mote, Y Purushotham and BN Dole, "Williamson-Hall analysis in estimation of lattice strain in nanometer-sized ZnO particles", Journal of Theoretical and Applied Physics, vol. 6, p.6, (2012).

[67] Yendrapati Taraka Prabhu, Kalagadda Venkateswara Rao, Vemula Sesha Sai Kumar, Bandla Siva Kumari," X-Ray Analysis by Williamson-Hall and Size-Strain Plot Methods of ZnO Nanoparticles with Fuel Variation", World Journal of Nano Science and Engineering, , vol.4, pp. 21-28, (2014).

[68] C. Barret , and Massalki T. B. , " Structure of Metals ", Oxford Pergamon , (1980).

[69] M. Mazhdi, P. Hossein Khani, " Structural characterization of ZnO and ZnO:Mn nanoparticles prepared by reverse micelle method", Int. J. Nano, vol. 2(4), pp. 233-240, (2012).

[70] A. Moses Ezhil Raj, L.C. Nehru, M. Jayachandran, C. Sanjeeviraja, " Cryst.Res.Technol. " , vol. 42 (9), p. 867, (2007).

[71] رياض كمال الحكيم، عادل خضير حسين،" اسس الهندسة الالكترونية"، مطبعة وزارة التعليم العالي ، بغداد(1980) .

[72] Lang, K. M. D. A. Hite, R. W. Simmonds, R. McDermott, D. P. Pappas, John M. Martinis, " Conducting atomic force microscopy for nanoscale tunnel barrier characterization", Review of Scientific Instruments vol.75(8), pp. 2726–2731, (2004).

[73] عبد المجيد البلخي،"كيمياء العناصر الأنتقالية"، جامعة دمشق،(1993)

[74] مؤيد جبرائيل يوسف، "فيزياء الحالة الصلبة"، مطبعة جامعة بغداد،ج ٢ (١٩٨٩) .

[75] S. M. Sze,"Semiconductors Devices", John Wiley, Sons, Ins, (2002).

[76] N. F. Mott And E. A. Davis, "Electronic processes in noncrystalline materials" Clarendon press Oxford, (1971).

[77] B.G. Stereeman, "Solid State Electronic Devices", (2nd Ed), Practice Hall, Inc. Engle wood Cliffs, N. J. (1980).

[78] J.I.Pankove, " Optical Process in Semiconductors ", Dover Publishing, Inc., New York. (1971).

[79] C.F.K.Lingshirn, "Semiconductor Optics", Springer Verlag, Berlin Hridelberg, (1st ed.), (1997).

[80] R. A. Smith, "Semiconductors", Cambridge press, (2nd.ed), (1987).

[81] M.A.Omer, " Elementary of Solid State Physics ", Addison Wesley Publishing, Co. London, (1975).

[82] Hoffman, M. Martin, S. Choi, W. & Bahnemann, D. "Environmental applications of semiconductor photo catalysis"

Chemical Review, vol. 95, pp. 69-96, (1995).

[83] J.Tauc "Amorphous and Liquid Semiconductors", Ed. by J. Tauc. Plenum Press, London, (1974).

[84] S.S Al-Rawi,S.J.Shakir and Y N. Husan,"Solid State Physics", publishing of Mousal University Arabic Version (1990).

[85] F.A. Jenkins and H.E. White, ″ Fundamentals of Optics", 4th ed., McGraw-Hill, Inc. (1981).

[86] Sudad S. Ahmed, Eman K. Hassan, Ghuson H. Mohamed," Investigation of Optical Properties of $NiO_{0.99}Cu_{0.01}$ Thin Film by Thermal Evaporation Technique", International Journal of Advanced Research, vol. 2(2), pp.633-638, (2014).

[87] مصطفى عامر حسن ، " تأثير عمليتي الاشابة والتلدين في بعض الخصائص الفيزياوية لغشاء Cu_2S المحضر بطريقة التحلل الحراري " رسالة ماجستير ، الجامعة التكنولوجية ، قسم العلوم التطبيقية ،(٢٠٠٦).

[88] G. Shugar and J. Ballinger, "Chemical Technicians Handbook", New York, (1996).

[89] S.Ben "Solid State Electronic Devices" Hall International, Inc, U.S.A,

(1990) .

[90] G. Busch, H. Schade, "Lectures on Solid State Physics", Pergaman Press, London, (1976).

[91] Wolfang Brockener, Claus Ehrhardt and Mimoza Gjikaj, "Thermal decomposition of Nickel nitrate hexahydarate , $Ni(NO_3)_2.6H_2O$, in Compariosion to $Co(NO_3)_2.6H_2O$ and $Co(NO_3)_2.4H_2O$, Thermochemical Acta,vol.456, pp.64-68, (2007).

[92] R. Ueda, J. B. Millin, "Crystal Growth and Characterization", Mc Graw- Hill, (1975).

[93] J. Daniel Bayan, Daniel R. Gametin, " Doped semiconductor nanocrystals: synthesis, characterization, physical properties and

applications", Progress in Inorganic chemistry, vol.47, p.126, (2005).

[94] Suryanarayana, C, Grant Norton, M, "X-ray Diffraction A Practical Approach", Springer, New York (1998)

[95] Adachi, S, "Handbook on Physical Properties of Semiconductors", Springer, New York (2004).

[96] S. S. Chiad, N. F. Habubi, M. H. Abdul- Allah, " Determination the dispersion parameters and urbach tail of iron chromate doped PMMA films", Iraqi Journal of Physics, vol. 10(17), PP. 12-17, (2012).

وجد انها تقل بزيادة المولارية وتتراوح قيمها (3.54 eV- 3.71 eV). وقد وجد ايضا ان طاقة اورباخ تزداد بزيادة المولارية فكانت تتراوح بين (299 meV و680 meV). و تم حساب الثوابت البصرية للأغشية المحضرة التي تتضمن (معامل الامتصاص وثابت العزل بجزئيه الحقيقي والخيالي) كدالة لطاقة الفوتون ومعامل الانكسار ومعامل الخمود كدالة للطول الموجي.

الخلاصة

في هذا البحث، حضرت بنجاح أغشية أوكسيد النيكل- كوبالت ($Ni_{(1-x)}Co_xO$) حيث x تغطي القيم (0, 4, 6 and 8 %) وبتراكيز مولارية مختلفة (0.05, 0.1, 0.15 & 0.2M) المرسبة على قواعد زجاجية بطريقة التحلل الكيميائي الحراري بدرجة حرارة (400 ± 5^oC) وبسمك ($300\pm10nm$) تقريبا. درست الخواص التركيبية والبصرية لهذه الأغشية بأستخدام حيود الاشعة السينية (XRD) ومجهر القوة الذرية AFM ومطياف الاشعة فوق البنفسجية – المرئية -وتحت الحمراء القريبة.

أظهرت نتائج فحوصات الأشعة السينية أن الأغشية المحضرة كانت ذات تركيب متعدد التبلور ومن النوع المكعب وبالاتجاه السائد (111) . وتم حساب معدل الحجم الحبيبي بطريقة شيرر وتم الحصول على اعلى قيمة للحجم الحبيبي لجميع الأغشية المحضرة (51.16nm) عند المولارية 0.1M لأغشية أوكسيد النيكل غير المشوبة واقل قيمه له (8.22nm) عند المولارية نفسها لأغشية أوكسيد النيكل- كوبالت المشوبة $Ni_{0.94}Co_{0.06}O$ و كانت هذه النتائج مطابقة تقريباً مع نتائج الحجم الحبيبي المحسوبة من طريقة وليامسون- هول. وقد تم حساب معدل الحجم الحبيبي ومعدل الخشونة و قيمة جذر مربع المعدل (RMS) لأغشية أوكسيد النيكل- كوبالت بأستخدام مجهر القوة الذرية AFM .

وتمت دراسة الخصائص البصرية للأغشية من خلال تسجيل طيفي النفاذية والامتصاصية ولمدى الأطوال الموجية nm (300- 900) ، وقد وجد أن النفاذية تزداد بشكل حاد بزيادة الطول الموجي في المدى nm (300- 350) وتزداد ببطئ في الاطوال الموجية العالية، والامتصاصية تقل بشكل حاد عند الاطوال الموجية الواطئة (طاقات عالية) المقابلة لفجوة الطاقة في الأغشية المحضرة .

وقد تم حساب معامل الأمتصاص لجميع الأغشية المحضرة ولان قيمته كانت اكبر من ($10^4 cm^{-1}$) لذلك تم الاستنتاج بأن الأغشية المحضرة جميعها ذات حزم مباشرة للطاقة. وقد تم حساب فجوة الطاقة البصرية للانتقال الإلكتروني المباشر المسموح باستخدام معادلة (Tauc) وقد

جمهورية العـــــــــــــراق
وزارة التعليم العالي والبحث العلمي
جـــــــــامعة ديالـــــــــــى
كلـــــــــــية العـــــــــــلوم

تأثير مولارية المحلول على الخواص التركيبية والبصرية لأغشية أوكسيد النيكل- كوبالت الرقيقة المحضرة بطريقة التحلل الكيميائي الحراري

رسالة مقدمة إلى

مجلس كلية العلوم - جـــامعة ديـــالـــــــــــــــى
وهي جزء من متطلبات نيل درجة ماجستير علوم في الفيزياء
من قبل

أحمد محمد شنو العسكري

(بكلوريوس علوم في الفيزياء ٢٠١٢)

بإشراف

أ.د. نبيل علي بكر

١٤٣٦ هـ ٢٠١٤ م